MULTIEQUILIBRIA OF OLIGOMERIC THERMOPHILIC DNA REPLICATION POLYMERASES

by

Hsiang-Kai Lin

[Master degree, National Taiwan University, 2005]

Submitted to the Graduate Faculty of

The Kenneth P. Dietrich School of Arts and Sciences

in partial fulfillment of the requirements for the degree of

Doctor of Philosophy

University of Pittsburgh

2013

UNIVERSITY OF PITTSBURGH

THE KENNETH P. DIETRICH SCHOOL OF ARTS AND SCIENCES

This dissertation was presented

by

Hsiang-Kai Lin

It was defended on

August 6, 2013

and approved by

Linda Jen-Jacobson, Professor, Department of Biological Sciences

Sunil Saxena, Associate Professor, Department of Chemistry

Seth Horne, Assistant Professor, Department of Chemistry

Dissertation Advisor: Michael Trakselis, Assistant Professor, Department of Chemistry

MULTIEQUILIBRIA OF OLIGOMERIC THERMOPHILIC DNA REPLICATION POLYMERASES

Hsiang-Kai Lin, Ph.D

University of Pittsburgh, 2013

MULTIEQUILIBRIA OF OLIGOMERIC THERMOPHILIC DNA REPLICATION POLYMERASES

Hsiang-Kai Lin, PhD

University of Pittsburgh, 2013

DNA polymerases are essential enzymes in all domains of life for both DNA replication and repair. We examined the thermodynamics and enzymatic activity related to the oligomerization of hyperthermophilic archaeal *Sulfolobus solfataricus* (*Sso*) primary DNA replication polymerase (Dpo1) and lesion bypass polymerase (Dpo4). Both Dpo1 and Dpo4 bind to DNA with initial high affinity monomeric binding followed by sequential binding of additional molecules at higher concentrations of the enzyme. Gel filtration, chemical crosslinking, isothermal titration calorimetry (ITC) and fluorescence anisotropy experiments all show a stoichiometry of three Dpo1 and two-four Dpo4 molecules bound to a single DNA substrate. In particular, oligomeric Dpo1-DNA complexes significantly increase both the kinetic rate and processivity of DNA synthesis.

Differentiation of binding accurate DNA replication polymerase Dpo1 over error prone DNA lesion bypass polymerase Dpo4 is essential for the proper maintenance of the genome. Binding discrimination between these polymerases on DNA templates is complicated by the fact that multiple oligomeric species are influenced by concentration and temperature. Fluorescence anisotropy experiments were used to separate discrete binding events for the formation of trimeric Dpo1 and dimeric Dpo4 complexes on DNA. The associated equilibria are found to be temperature-dependent, generally leading to more favorable binding at higher temperatures for both polymerases. At high temperatures, DNA binding of Dpo1 monomer is slightly favored

over binding of Dpo4 monomer, but binding of Dpo1 trimer is strongly favored over binding of Dpo4 dimer, thus providing thermodynamic selection.

The results from ITC showed an unusually strong temperature dependence of the change in heat capacity (ΔC^{o}_{p}), which switches from positive to negative values with increasing temperature. The observed sign change in ΔC^{o}_{p} does not derive from temperature-dependent changes in structure, protonation, or electrostatics. Rather, we propose that temperature affects the coupled equilibria between self-associations of free Dpo1 or Dpo4 and their binding to DNA. Taken together, *Sso* differentiates between Dpo1 and Dpo4 binding to DNA by integrating molecular and cellular principles including concentration, temperature, oligomerization, and coupled equilibria to maintain uninterrupted, rapid, and high fidelity DNA replication.

TABLE OF CONTENTS

LIST OF TABLES

LIST OF FIGURES

PREFACE

I would like to thank sincerely my advisor, Dr. Michael Trakselis, for his guidance and support throughout my PhD study. He is a role model to me in research. His diligence, efficiency, and prudence taught me how to work hard and smart. He is the best advisor you can expect. Thank you very much for your patience, help, and motivation. If I can be a professor in my career, I wish I can be a professor like him.

I also want to express my gratitude to Dr. Jen-Jacobson for her thorough attitude, generous help, and passion for our collaboration. She showed me what quality a research should have to be a successful scientist. I will benefit from what I learned from her in the future as a researcher.

I am also thankful to my defense committee, Dr. Horne and Dr. Saxena, for their advice, insightful comments, and constructive criticisms. I really appreciate your help throughout my proposal and my defense.

My research would not be complete without the contributions from our collaborators. I would like to give thanks to Dr. Thomas M. Laue and Susan F. Chase at University of New Hampshire for training and working with me on the analytical ultracentrifuge; Dr. Preeti Mehta for the training and consulting on isothermal titration calorimetry.

Special thanks to my group mates, Rob, Brian, Beth, Sean, Andrey, and Zhongfeng, all of you have been so helpful and caring. I would like to extend my gratitude as well to all the chemistry staff, my life is happier with all of you, thank you. Also to my friends in Pittsburgh outside the department, without you, I will not be able to survive my foreign life here is US. To my family and friends back home in Taiwan, thank you for your love and support from thousands of miles away. I am also thankful to my relatives here in US for the make me feel at home from time to time.

I am very grateful to my mom and dad, to whom this work is dedicated. I own you all the support and caring through all of my education and life. Without your motivation and support, I will not realize my dream to become a doctor. I greatly appreciate my brother who accompanied and cared for mom and dad during these years. I also want to thank my fiancée, Jing, for her company and support when we are running on the road of religion, academics, love, and our life.

And lastly, I would like to give thanks to God, for being with me all the time.

1.0 INTRODUCTION

1.1 DNA REPLICATION

DNA replication is an essential biological process for all living organisms to pass their genome to their next generation. In DNA replication, a parent DNA duplex is duplicated into two identical daughter DNA duplexes, with each of them containing one single strand of the parent. Therefore DNA replication is regarded as a semiconservative process, which was hypothesized first by Watson and Crick,(*2*) and later proven by the Meselson-Stahl experiment.(*3*) The DNA replication process involves the coordination of multiple enzymes in several steps. First, a helicase unwinds a DNA duplex at a replication fork resulting in single-strand DNA, a template for DNA replication, which is then stabilized by single-strand binding protein (SSB). SSB prevents the re-annealing of the single-strand DNA and helps the loading of primase on specific priming initiation sites. Then, the primase catalyzes the synthesis of a short RNA strand complementary to the DNA priming initiation site. The RNA primer has a free 3'-hydroxyl group and can be handed off to a DNA polymerase to begin replication.(*4*) Upon the hydrolysis of deoxyribonucleoside 5'-triphosphates, DNA polymerase incorporates the hydrolyzed deoxyribonucleoside mono-phosphates to the free 3'-hydroxyl group on RNA primer. The new synthesized DNA strand is complementary to the DNA template. Because of the absolute requirement of free 3'-hydroxyl group, DNA polymerase has to elongate the two parental single-

strand DNAs, which are the leading and the lagging strand, in different directions. While DNA can be synthesized continuously on the leading strand (3'→5') in the direction of 5'→3' without interruption, the synthesis of DNA on the lagging strand is discontinuous. The lagging strand DNA polymerase also synthesizes DNA in the direction of 5' → 3' but occurs opposite to the direction of the progressing replication fork. Thus, the lagging strand has to recruit or recycle the DNA polymerase at newly synthesized RNA primers, creating small pieces of DNA fragments, known as Okazaki fragments. Meanwhile, the RNA primers on the completed Okazaki fragments are removed by an endonuclease, leaving gaps that are later filled by a DNA polymerase. Finally, these DNA fragments on the lagging strand are jointed together by DNA ligase. A model of the DNA replisome is demonstrated in Figure 1-1.

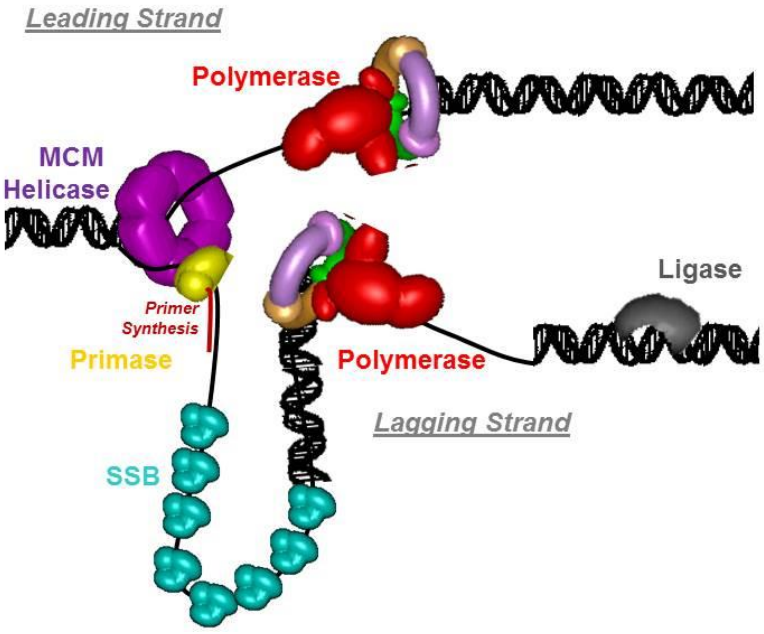

Figure 1-1. The DNA replication replisome.

1.2 DNA REPLICATION IN THE ARCHAEAL DOMAIN

The fundamental process of DNA replication is conserved in all three domains of life, but the enzymatic details vary. While bacteria tend to use a simpler replication machinery involving fewer enzymes, eukaryotic organisms control the DNA replication mechanism with a meticulous and complicated collaboration of enzymes used primarily for regulation. Intriguingly, the third domain of life, Archaea, shares some similarity with both bacteria and eukaryotes.(*5*) Archaeal organisms are prokaryotes and lack a nucleus like bacteria, however, their DNA replication machinery is more homologous to that of eukaryotes.(*6-8*) In fact, Archaea seem to possess a simpler ancestral core group of enzymes compared with eukaryotes. These similarities allow us to investigate DNA replication mechanisms from archaea that are relevant to the homologous but more complex eukaryotic system.

This work reported here attempts to understand the functions of Archaeal DNA replication proteins alone or in complexes as molecular machines. This information will be used to decipher Archaeon DNA replication mechanisms on both the leading and lagging strands as a model system to give a better perspective on eukaryotic DNA replication. Deficiencies in DNA replication have been linked to neurological diseases or cancer.(*9*) This information will be used to determine or suggest causes of aberrant DNA replication in cancer cells within a dynamic DNA molecular machine.

There are two main protein complexes involved in DNA replication: primosome and the DNA polymerase holoenzyme. While the primosome, including helicase and primase, initiates DNA replication, the DNA polymerase holoenzyme incorporates a complementary deoxynucleotide to the parent strand for elongation of a newly synthesized daughter strand. Within the replisome, the DNA polymerase holoenzyme is comprised of the polymerase and its accessory factors, PCNA (clamp or processivity factor) and RFC (clamp-loader). PCNA forms an oligomeric ring encircling DNA and serves as a moving platform for replication processing proteins.(*10-14*) In all three domains of life, clamps share morphological similarities, constructing toroidal conformers that must be opened and closed on to DNA and then slide along DNA to increase the speed and processivity of DNA replication.(*15-17*)

Compared to other sliding clamps, the homodimeric bacterial β-clamp is not orthologous to the trimeric archaeal/eukaryal PCNA but is functionally analogous. The PCNA clamp in *Sulfolobus solfataricus* is one of the most unique replication complexes due to the heterotrimeric arrangement consisting of three separate subunits.(*10*) *Sulfolobus* and a related creanarchaeal, *Aeropyrum pernix*, are the only organisms to date that possess three different but highly homologous proteins.(*18*) The *Sulfolobus* PCNA heterotrimer has a consistent stereochemistry and assembles first as a dimer of PCNA1 and 2. Then, the PCNA1/PCNA2 heterodimer can then bind to PCNA3.(*10*)

Three different PCNA subunits imply that each may have preferred interacting protein partners. Indeed, three separate publications of crystal structures of PCNA complexes show PCNA heterotrimer alone,(*17*) PCNA1-PCNA2 heterodimer with Flap endonuclease 1 (Fen1, responsible for removing RNA primers in replication fork),(*12*) and PCNA heterotrimer with DNA ligase respectively.(*13*) *Sso*PCNA heterotrimer, but not individual monomers, can

stimulate the activities of Fen1 and ligase.(*10*) More specifically, PCNA1 interacts with either Fen1 or Dpo4 (the Y-family lesion bypass polymerase); PCNA2 interacts with the polymerase (Dpo1); and PCNA3 interacts with the DNA ligase.(*13, 19*) Also, the DNA repair nuclease (XPF) interacts with PCNA1 and PCNA3 to perform its endonuclease activity,(*14*) and uracil DNA glycosylase (UDG1, a family of enzymes involved in base excision repair) can interact with PCNA3.(*11*) An ensemble representation of the DNA polymerase holoenzyme based on the individual crystal structure complexes is shown in

Figure 1-2. PCNA interacts with many proteins and holds them in close proximity to the replication fork, which may increase the processivity of polymerase holoenzyme, regulate DNA repair, and control ligation on the lagging strand.

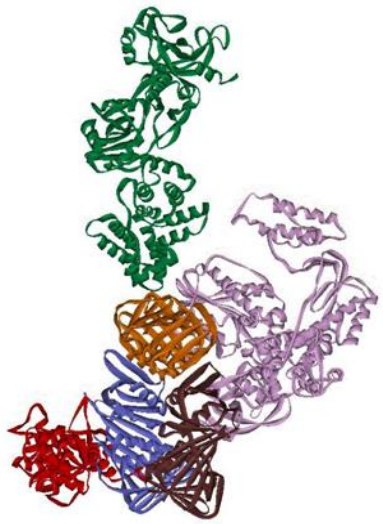

Figure 1-2. Model of the protein interactions arranged by *Sso*PCNA123 (PDB ID 2hii). The polymerase (lavender) (PDB ID 1s5j) interacts with PCNA2 (brown). The DNA ligase (green) (PDB ID 2hiv) interacts with PCNA3 (orange). The flap endonuclease (red) (PDB ID 2izo) interacts with PCNA1 (blue).

PCNA subunits not only have specific interaction partners, but also display differential interactions with the clamp loader, RFC.(*10*) *Sulfolobus* RFC contains one large (RFCL) and

four small (RFCS) subunits. The homotetramer of RFCS interacts with the PCNA1 + PCNA2 dimer and RFCL interacts with PCNA3.(*10*) Again, three different subunits of PCNA have their preference to different RFC subunits inferring an unique PCNA-loading mechanism to DNA among all domains of life.(*20*)

1.3 *SULFOLOBUS SOLFATARICUS* DNA POLYMERASE

DNA polymerases can be classified into seven different families: A, B, C, D, X, Y, and RT based on different sequence homology.*(21, 22)* Family A contains both replicative mitochondrial DNA polymerase γ and repairing *E. coli* DNA pol I. Family B contains mostly replicative DNA polymerases, including eukaryotic DNA polymerases α, δ, ε, and *E. coli* DNA pol II. The B-family of DNA polymerases has remarkable accuracy during replication, and many of them have strong 3'-5' exonuclease proofreading activity. Family C polymerases are the primary bacterial chromosomal replicative enzymes which include *E. coli* DNA Polymerase III. Family D polymerases are still not well characterized and only found in the *Euryarchaeota* subdomain of Archaea but are thought to be primarily responsible for replication in the phyla.*(23)* Family X contains the short-patch base excision repair eukaryotic polymerase pol β, as well as other eukaryotic polymerases such as pol σ, pol λ, pol μ, and terminal deoxynucleotidyl transferase (TdT). The Y-family polymerases have low fidelities on undamaged templates and are unique for their abilities to bypass damaged DNA sites. The reverse transcriptase (RT) family uses an RNA template to synthesize the DNA strand, containing retroviruses and several eukaryotic polymerases.

Crenarchaeal *Sulfolobus* contains three B-type DNA polymerases (Dpo), Dpo1, Dpo2, Dpo3 and one Y-type Dpo4 in its genome.*(24, 25)* The B family polymerases have been classified as the primary replication polymerases and have similar structures across organisms that include fingers, thumbs, and palm domains which cradle DNA in the correct conformation for catalysis by using conserved aspartates as the active site residues.*(26-32)* In Figure 1-3a, a partial crystal structure of Dpo1 demonstrates a typical right handed conformation of the B-type polymerase with an extended fingers domain proposed to be involved in conformational changes associated with catalysis or protein-protein interactions.*(33)* On the other hand, as shown in Figure 1-3b, the structural domains of Y-family Dpo4 share most of structural feature with B-family polymerase, but also includes a little finger domain. It is suggested that the extended finger domain in Dpo1 and the little finger domain in Dpo4 can directly interact with each other for coupled uninterrupted lesion bypass during DNA replication.*(34)* At sites of DNA damage, Dpo1 interacts with a Dpo4 in a proposed polymerase-switching mechanism on the damaged DNA strand.

The respective affinities of the polymerase accessory proteins are expected to be different for B-family-polymerase Dpo1, 2, and 3 and to date are only shown to interact with Dpo1.*(10, 19)* Polymerase accessory proteins PCNA, RFC are known to increase the processivity of Dpo1.*(35-37)* Dpo1 and Dpo4 have been found to specifically interact with PCNA2 and PCNA1, respectively, through a PCNA interacting peptide (*PIP*) *motif.(19, 38, 39)* Specificities for replication enzymes, including Dpo1 and Dpo4, for simultaneous binding to PCNA hold these enzymes at high local concentrations at the replication fork in a common tool-belt model to maintain the speed and fidelity of DNA replication.*(40)* PCNA binds to all the other interacting

enzymes through an unique PIP interaction domain suggesting a requirement of switching of enzymes at this PIP motif to fulfill a variety of actions of DNA replication.*(41)*

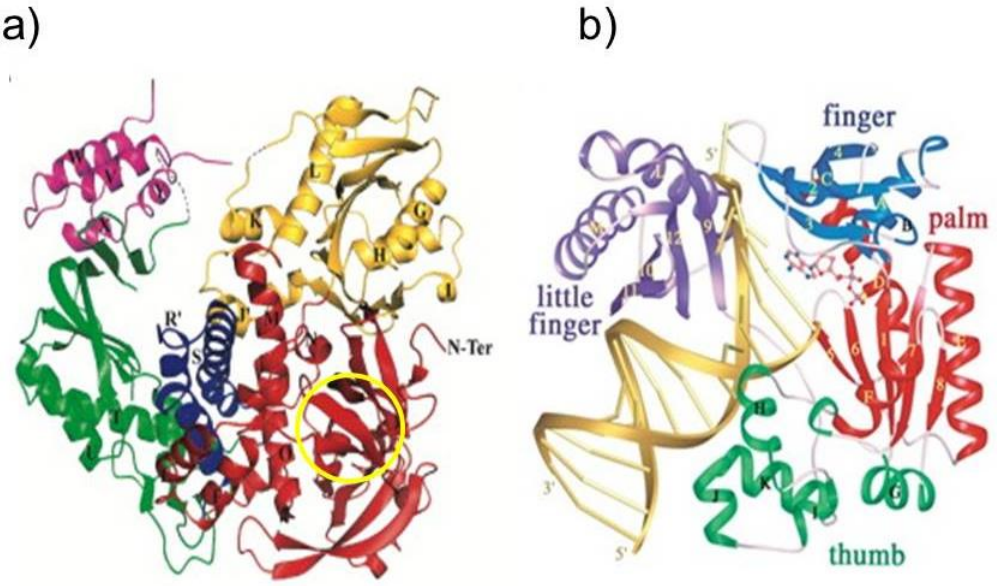

Figure 1-3. a) Overall Structure of *Sso* Dpo1. The Dpo1 structural domains are demonstrated in red (N-terminal subdomain), yellow (exonuclease subdomain), green (palm), blue (fingers), magenta (thumb).*(42)* The extended finger on N-terminal subdomain is circled in yellow. b) Overall structure of *Sso* Dpo4-DNA complex, DNA bases shown as rods, and the incoming nucleotide and the Ca^{2+} ion in a ball-and-stick model. The Dpo4 structural domains are demonstrated in red (palm), green (thumb), blue (finger), and purple (little finger); the DNA is in gold.*(43)*

1.4 OLIGOMERIZATION OF *SSO* DNA POLYMERASES

Oligomeric proteins, assemblies of two or more protein subunits, are found frequently in all domains of life. Protein oligomerization may be an evolutionary product, which have the advantages of increasing access, higher order complexity in a regulatory control.*(44)* Many primitive species use either homo-oligomeric or hetero-oligomeric proteins to support their

physiological function. On the other hand, higher order species, containing more variety of regulatory proteins, may use a specific enzyme to coordinate the formation of oligomeric complex. In this work, we focus on interactions, oligomerization, and thermodynamics of archaea replication and repair polymerases on DNA. Understanding the strategy and the mechanism in archaea *Sso* DNA replication system infers the evolutionary path for polymerase oligomerization and serves as an important and relevant model for detailing and comparing their eukaryotic counterparts.*(45-47)*

Protein oligomerization is necessary for coordinated DNA replication at replication fork. Ishmael et al. showed the interaction of two DNA polymerases from bacteriophage T4 in a crosslinking assay.*(48)* The utility of this dimeric complex is illustrated by studying the catalytically inactive mutant of T4 DNA polymerase, which was shown to shut down ongoing DNA replication, suggesting a dynamic polymerase-switching mechanism during DNA replication.*(49)* In *E. coli*, polymerase oligomerization is medicated through the tau subunit of the clamp-loader complex.*(50)* This oligomerization is important in maintaining efficient Okazaki fragment processing as shown in Figure 1-4. The illustrations demonstrate the *E. coli* replication fork containing a triple polymerase Pol III3-τ3-δδ′χψ complex.(1) Other DNA polymerases such as Klenow,*(51)* human pol β,*(52)* an African swine fever virus polymerase X have all been found to in a dimeric complex with DNA.*(53)* HIV reverse transcriptase (RT) also forms a dimer as the functional unit although one of the subunits (p55) is inactivated in favor of the active (p66) subunit.*(54)* Effects of polymerase oligomerization either alone or in concert with the accessory factors may have important implications in in maintaining high processivity and specificity, as well as coordinated DNA synthesis between the leading and lagging strands, and molecular switching between replication and repair polymerases.

In this work, affinities and stoichiometries of binding Dpo1 and Dpo4 to DNA has been examined using a number of techniques, including fluorescence anisotropy, analytical gel filtration, crosslinking assays, electrophoretic mobility shift assays, analytical ultracentrifugation, and isothermal titration calorimetry. Enzymatic evidence showing greater processivities for Dpo1 and Dpo4 at higher temperatures and protein concentrations promote DNA polymerase assembly, stability, and kinetics at the replication fork. Overall, our results indicate that the binding specificities of multiple oligomeric archaeal DNA polymerases are regulated by changes in cellular concentrations and temperature for efficient DNA binding recognition and synthesis.

Figure 1-4. The illustrations demonstrate the *E. coli* replication fork containing a triple polymerase Pol III_3-τ_3-$\delta\delta'\chi\psi$ complex.*(1)*

2.0 A TRIMERIC DNA POLYMERASE COMPLEX INCREASES THE NATIVE REPLICATION PROCESSIVITY AND THERMODYNAMICALLY STABLIZE DNA DUPLEX[1]

DNA polymerases are highly conserved enzymes found in all domains of life, and depending on the type, are primarily responsible for DNA replication or repair activities. Many of the structural and mechanistic features of these polymerases are shared across a broad range of organisms, but slight differences have been identified with regards to substrate specificity, template sensing, as well as coordinating polymerase and exonuclease activities.(*55-58*) The genome of *(Sso)* contains DNA polymerase members from both the DNA replication B-family as well as a lesion bypass polymerase from the Y-family.(*59, 60*) The B-family DNA polymerase (*Sso*Dpo1) has been shown to have the necessary enzymatic and kinetic properties to be the replicative polymerase in *Sulfolobus*.(*61-66*) A crystal structure of *Sso*Dpo1 has been solved showing a typical right-handed conformation of the polymerase with an extended fingers domain hypothesized to be involved in either conformational changes involved in catalysis or protein–protein interactions.(*42*) Under normal DNA replication conditions, *Sso*Dpo1 is thought to interact with the heterotrimeric *Sso*PCNA complex to maintain a high degree of processivity and

[1] Text from this chapter is reprinted with permission from Andrey L. Mikheikin, Hsiang-Kai Lin, Preeti Mehta, Linda Jen-Jacobson and Michael A. Trakselis. *Nucleic Acids Research* 2009, 37, 7194-7205 Copyright 2009 Oxford and Zhongfeng Zuo, Hsiang-Kai Lin, and Michael A. Trakselis. *Biochemistry* 2011, 50, 5379-5390. Copyright 2011 American Chemical Society.

possibly with the Y-family DNA polymerase, *Sso*Dpo4, to bypass DNA lesions.(*67-70*) This common tool belt model of protein interactions has been suggested to be important in increasing the local concentrations of proteins, especially DNA polymerases, at the replication fork to maintain the speed and accuracy needed for successful DNA replication.(*71*) This is even more evident with the many other known stable interactions with proliferating cell nuclear antigen (PCNA) within the cell.(*72*)

Polymerase–polymerase interactions either directly or indirectly are also necessary for coordinated DNA replication on both the leading and lagging strands. Direct evidence of a polymerase interaction was detected by protein crosslinking in bacteriophage T4.(*73*) In addition, a dominant negative form of the T4 polymerase was shown to shut down DNA replication in a coordinated replisome, suggesting the utilization of a dynamic polymerase-switching mechanism during DNA replication.(*74*) In *E. coli*, polymerase coupling is mediated through the tau subunit.(*50*) In fact, a trimeric polymerase complex in which three copies of tau are incorporated into the clamp loader complex has been shown to be fully active on both the leading and lagging strands and may be an important factor in maintaining efficient Okazaki fragment processing.(*75*) In higher eukaryotes, it is currently unknown how the replication polymerases, ε and δ, are coordinated on the leading and lagging strands, respectively,(*76*) but they are thought to have specific yet unknown plastic interactions with accessory proteins and themselves to maintain the replication fork.(*77*)

Because of a large distance between the polymerase and exonuclease active sites in most DNA polymerases, it has been suggested that there may be multiple polymerase-bound conformations. Co-crystal structures of *E. coli* Klenow polymerase and the homologous version in *Thermus aquaticus* bound to primer/template DNA identify separate polymerization and

editing modes of binding.(*78-80*) A recent report shows that Klenow can bind to primer/template DNA as a monomer or dimer, but the dimer form is more prevalent in the polymerization mode.(*81*) Effects of polymerase multimerization either alone or in concert with accessory factors may have important implications in maintaining high processivity as well as coordinated DNA synthesis between the leading and lagging strands.

We have used a variety of biochemical techniques to investigate the stoichiometry of *Sso*Dpo1 on DNA and show that the oligomeric state influences the mechanism of polymerization. We have determined that *Sso*Dpo1 binds to a DNA primer/template initially as a monomer and cooperatively forms a trimeric polymerase complex with increasing concentrations. This trimeric complex can increase both polymerase kinetic activity and processivity. The organization of this multimeric polymerase is discussed with regard to binding conformation and effect on polymerization kinetics and has important implications for DNA replication mechanisms. In the later work, we also show that Dpo1 has a remarkable ability to stabilize weak base pairing interactions to replicate a template strand at high temperatures. This annealing activity is not recognized for either *Thermus aquaticus* pol I (Taq) or *Pyrococcus furiosus* B-family DNA polymerase (*Pfu*-Pol), suggesting a relationship with the oligomeric state of Dpo1.

2.1 MATERIALS AND METHODS

Materials. Oligonucleotide substrates were purchased from Integrated DNA Technologies (IDT) (Coralville, IA). Gel purification of the DNA strands was performed as

previously described.(*82*) Primer/template and duplex substrates were prepared by mixing each strand in 1:1 ratio in a buffer containing 20 mM Tris (pH 7.5) and 200 mM NaCl. The annealed complex was heated at 95 ℃ for 2 min and allowed to cool down slowly for at least 2 hours in the heat block. M13mp18 was purchased from USB Corporation (Cleveland, OH). All radiochemicals were purchased from MP Biochemicals (Santa Ana, CA). Commercial enzymes were from NEB (Ipswich, MA). All other chemicals were analytical grade or better.

*Sso*Dpo1 was amplified from genomic *S. solfataricus* P2 (ATCC, Manassas, VA.) using *Pfx*50 polymerase (Invitrogen, Carlsbad, CA). Initial ligation of the PCR product into pGMET (Promega, Madison, WI) was performed using standard T-cloning. Standard QuikChange protocol (Stratagene, La Jolla, CA) was used to create an exonuclease mutant of SsoDpo1 (D231A/D318A). Specific restriction sites *AseI* and *XhoI* contained in the primers were used to clone *Sso*Dpo1 into pET30a digested with *NdeI* and*XhoI* (Novagen) to include a C terminal His tag. The *Sso*Dpo1 exonuclease mutant (D231A/D318A) was used hereafter in all studies described in this manuscript. DNA sequences were verified by the Genomics and Proteomics Core Laboratories at the University of Pittsburgh.

SsoDpo1 expression and purification. pET30a-*Sso*Dpo1 exo$^-$ was transformed into BL21(DE3) Rosetta 2 (Stratagene) and grown at 37 ℃. Cells were induced with 0.5 mM IPTG at OD_{600} between 0.5 and 0.6. The cells were lysed by sonication and heat treated at 70 ℃ for 30 min followed by centrifugation. The lysate supernatant was purified further by Ni-NTA agarose, heparin and SP sepharose columns (GE Healthscience). Final cleanup and size selection was performed using a Superdex 200 26/60 gel filtration column. The extinction coefficient for *Sso*Dpo1 was calculated to be 118,282 $M^{-1}cm^{-1}$.(*83*)

Analytical gel filtration. Superdex 200 10/30 column (GE Healthscience) was used at a flow rate of 0.2 ml min^{-1} in Buffer A [20 mM HEPES-NaOH (pH 7), 240 mM NaCl, 5% Glycerol, 10 mM $Mg(OAc)_2$, 0.2 mM DTT] and protein elution was monitored at 280 nm. Binding and kinetic experiments were performed using identical buffer conditions (Buffer A) unless indicated otherwise. The molecular ruler standards Thyroglobin (165 kDa, Sigma), Conalbumin (75 kDa, GE Healthscience), Albumin (43 kDa, Sigma), Myoglobin (17.6 kDa, Sigma) and Vitamin B12 (1.4 kDa, Sigma) were run to create a standard log curve fit by linear least squares. One hundred microliters *Sso*Dpo1(100 µM) in the absence or presence of DNA substrates at concentrations of 20 µM was injected with the internal standard, vitamin B12, added for monitoring any elution shift. The molecular weight of the eluting species was calculated from the standard log plot.

Electrophoretic mobility shift assay. Electrophoretic mobility shift assays (EMSAs) were performed in a 10 µl reaction volume containing Buffer A with 4 nM DNA probe labeled at the 5′-end using a standard polynucleotide kinase reaction and ^{32}P-γ-ATP, and the indicated amount of *Sso*Dpo1. Binding reactions were allowed to equilibrate for 10 min followed by directly loading onto a gradient 4–15% polyacrylamide/TBE ReadyGel (BioRad, Hercules, CA). Gels were run for 1 h at 13 volts cm^{-1} followed by drying and imaging using a Storm phosphorimager (GE Healthscience). Quantification of the fraction of band shift was performed using the ImageQuant software (v5.0).

Data were fit using non-linear least squares analysis using Kaleidagraph (Synergy, Reading, PA) to an equivalent multiple site binding model defined by:

$$y = \frac{f_{\max} \times [P]^n}{K_d^n + [P]^n} \qquad \text{(Equation 2-1)}$$

where f_{max} is the maximum fraction shifted, P is the *Sso*Dpo1 concentration, K_d is the dissociation constant and n is the Hill coefficient which defines cooperativity.

Fluorescence anisotropy. Fluorescence anisotropy measurements were performed in Buffer A. A fluorescently labeled DNA hairpin 5′-Cy5-TTTTTTTTTTTTTTTCGAATGGCGCTTTGCCTGGTTTTTACCAGGCAAAGCGCCATTCG that was HPLC purified (IDT) was used in all anisotropy experiments. Before measurements, the hairpin was heated to 95 ℃ and then allowed to anneal slowly to room temperature over at least 1 h. Measurements were performed on FluoroMax-3 spectrofluorimeter (HORIBA Jobin Yvon). Fluorescence was excited at 645 nm, and the emission was monitored at 675 nm during 1-s integration times and represents an average of 10 consecutive readings. The absolute fluorescence intensity at 675 nm did not change with addition of a high concentration of *Sso*Dpo1 ruling out the possibility that *Sso*Dpo1 binds specifically to the Cy5 fluorophore. The fluorescence anisotropy, r, was calculated using the equation:

$$r = \frac{I_{VV} - GI_{VH}}{I_{VV} + 2I_{VH}} \qquad \text{(Equation 2-2)}$$

where I is the polarized fluorescence intensity with subscripts V and H identifying either vertical or horizontal polarized light, respectively. The G-factor is a correction for the difference in sensitivities of detection for horizontal and vertically polarized light, and was measured immediately before each experiment and is defined by

$$G = \frac{I_{HV}}{I_{HH}} \qquad \text{(Equation 2-3).}$$

The observed anisotropy is the sum of all the anisotropy values for each species present. In this case, only the DNA was labeled so there is no contribution from free protein. Only species containing DNA, either alone or *Sso*Dpo1-bound complexes contribute to the anisotropy, defined as

$$r = \sum_i f_i r_i \qquad \text{(Equation 2-4)}$$

where f_i is the fraction of an individual species and r_i is the associated anisotropy values. Contributions to anisotropy are therefore equal to:

$$r = r_D[D] + r_{DP}[DP] + r_{DP_3}[DP_3] \qquad \text{(Equation 2-5)}$$

where r_D, r_{DP}, r_{DP3} are the anisotropy values for the DNA alone, singly bound *Sso*Dpo1 and trimeric *Sso*Dpo1-bound complexes, respectively.

Isothermal titration calorimetry. Isothermal titration calorimetry (ITC) was performed using VP-ITC (MicroCal Inc., Northampton, MA) at 303°K for *Sso*Dpo1 binding to DNA.(*84*) Prior to the experiment, *Sso*Dpo1 and DNA were dialyzed in Buffer A. The concentrations of the dialyzed protein and DNA were determined prior to the titration. Typical titrations consisted of 30 injections of 2 – 5 µl of DNA solution (500 µM) into the overfilled (~1.4 ml) sample cell containing *Sso*Dpo1 (20 µM). To obtain the effective heat of binding, the observed heats of reaction were corrected for the heat of dilution of the DNA by subtracting the baseline heats obtained after saturation. All data were fit using Origin 7.0 (MicroCal) to the following equation,(*85*)

$$Q = \left(\frac{n[P]_t \Delta H V_0}{2}\right)\left\{1 + \frac{[D]_t}{n[P]_t} + \frac{1}{nK_a[P]_t} - \left[\left(1 + \frac{[D]_t}{n[P]_t} + \frac{1}{nK_a[P]_t}\right)^2 - \frac{4[D]_t}{n[P]_t}\right]^{1/2}\right\} \quad \text{(Equation 2-6)}$$

where V_0 is the volume of the cell, ΔH is the enthalpy of binding per mole of ligand, $[P]_t$ is the total [*Sso*Dpo1] including both bound and free fractions, K_a is the binding constant, $[D]_t$ is the total DNA concentration and n is the stoichiometry of the reaction.

Crosslinking studies. We performed all crosslinking studies in buffer A and over a range of [NaCl]. Sulfo-EGS [ethylene glycol bis(sulfosuccinimidylsuccinate)] (Pierce, Rockford, IL) was used as the crosslinker targeting free amino groups. 10 μM of *Sso*Dpo1 was incubated with primer/template DNA (similar to ITC conditions) for 1 min at various temperatures, then crosslinker was added to a final concentration of 0.5 mM and the reaction mixture was incubated for 30 min at variant temperatures. The reaction was stopped by addition of 1 M Tris–HCl (pH 7.5) to a final concentration of 50 mM and then incubating at room temperature for 15 min. Products of crosslinking reaction were analyzed using a 6% SDS–PAGE gel and stained with Coomassie dye.

Polymerase kinetics. The polymerase assay monitored the incorporation of nucleotides on primer/template 5′ [γ-^{32}P]-labeled DNA substrates. Individual primer strands were first labeled with [γ-^{32}P ATP] using a standard polynucleotide kinase reaction and then annealed to M13mp18 or 31-mer ssDNA. The reaction was started by mixing labeled DNA substrates (4 nM), dNTPs (0.05 mM), reaction buffer and *Sso*Dpo1 at various concentrations and incubating at 37 or 60℃ for various times. For single-turnover processivity experiments, *Sso*Dpo1 was preassembled on ptDNA and the reaction was initiated with dNTPs and a 5000-fold excess of

ssDNA as a polymerase trap at 37 or 60 ℃. One volume of stop solution (100 mM EDTA, 0.1% SDS, 80% Formamide, 0.1% Bromophenol Blue) was added to terminate the reaction. Aliquots were run on either a denaturing (14% Acrylamide/8M Urea/1X TBE) or alkaline agarose (0.8% agarose, 1N NaOH, 0.5 M EDTA) gel, dried and phosphorimaged. Quantification of the band intensities and lengths was performed using ImageQuant software (v5.0). The calculated rate of DNA synthesis (bp/min or fraction of full length product) as a function of *Sso*Dpo1 concentration was initially fit to a standard Michaelis–Menten equation, but a fit that included a positive cooperativity parameter (n) for allosteric enzymes according to the following equation,

$$v = \frac{V_{\max} \times [P]^n}{K_D^n + [P]^n} \qquad \text{(Equation 2-7)}$$

gave a much better fit where K_d' is the apparent catalytic dissociation constant for *Sso*Dpo1 (*P*) and V_{max} is maximal rate of synthesis. The off-rate of the polymerase for each oligomeric state can be calculated by dividing the rate of DNA synthesis (bp/min) by the average processivity (bp) to give min^{-1}.

Determination of Melting Temperatures. DNA melting temperature measurements were conducted on a Varian Cary100 Bio UV visible spectrophotometer. The UV absorbance at 260 nm was measured for 1.5 μM DNA with or without 1.5 μM Dpo1exo in assay buffer [50 mM glycine (pH 8) and 5 mM $Mg(CH_3COO)_2$] at every integral temperature point from 4 to 90 ^oC programmed at a rate of 1 ^oC/min. The melting temperature was determined from a plot of the UV absorbance versus temperature for multiple replicates and analyzed using the included software.

2.2 RESULTS

2.2.1 Analysis of *Sso*Dpo1-DNA substrate complex formation by analytical gel filtration

During the purification as detected by both preparatory and analytical gel filtration, *Sso*Dpo1 exists as a monomer (101 kDa) and eluted alone at 13.5 ml (Figure 2-1). Addition of DNA was found to shift the equilibrium of binding to a higher molecular weight species consistent with the formation of a higher-order complex. Although lower concentrations of NaCl (100 mM) gave a larger proportion of the higher-order complex (data not shown), we used 240 mM NaCl contained in buffer A in further binding and kinetic assays to reduce any potential contributions of nonspecific aggregation events.

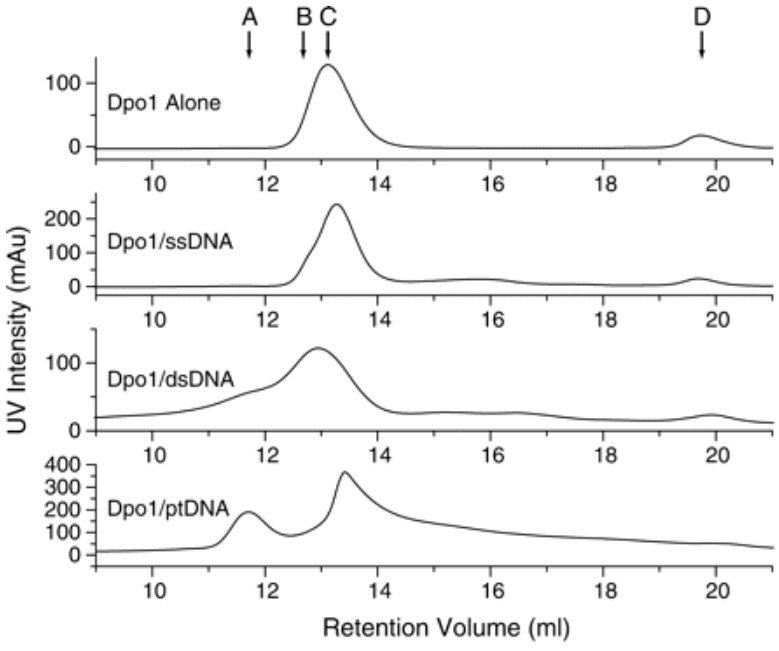

Figure 2-1. Gel filtration profile of a constant initial concentration of *Sso*Dpo1 (100 µM) and various DNA substrates (20 µM). Single strand (ssDNA) (31-mer), blunt duplex (dsDNA) (50/50-mer) and primer/template (p/tDNA) (21/31-mer) DNA are shown. Peaks identified as A, B and C represent trimer:DNA, monomer:DNA and monomer forms of *Sso*Dpo1, respectively according to fit of a standard molecular weight ruler. A constant concentration of vitamin B12 was used as an internal standard in all the experiments to account for drift in the elution profile (peak D).

To determine relative binding affinities for different DNA substrates, an identical initial loading concentration (100 µM) of *Sso*Dpo1 was incubated with separate DNA substrates and then analyzed by analytical gel filtration. The most obvious change in these elution profiles is from the complexation of *Sso*Dpo1 and p/tDNA (21/31) (Figure 2-1). This shifted peak (*bottom panel*) eluted at a position consistent with a trimeric *Sso*Dpo1 complex bound to DNA (as determined from the standard log curve with

molecular weight markers). Complexes with single strand and with blunt duplex DNA were also compared under the same conditions. In both cases, a protein–DNA complex eluted in the position (unresolved from free monomeric protein) predicted for a monomeric *Sso*Dpo1–DNA complex. Blunt duplex DNA was able to stimulate the formation of a trimeric complex, significantly more than with ssDNA but less than p/tDNA.

It is possible that higher-order complexes exist on the single and double strand substrates at the high initial concentrations prior to injection, but because of dilution during the course of gel filtration chromatography, the equilibrium is driven to the lower-order monomeric *Sso*Dpo1—DNA species. The composition of the peaks C and B (Figure 2-1) consisting of monomer and monomer bound to DNA would therefore dominate the equilibrium after elution from the column for the single and dsDNA substrates.

2.2.2 EMSA of *Sso*Dpo1/DNA complexes

EMSAs were utilized to analyze the binding of *Sso*Dpo1 to 5′ [γ-^{32}P]-labeled ssDNA, dsDNA and primer/template (p/tDNA) substrates (Figure 2-3). *Sso*Dpo1 can bind to all substrates, since in all cases, a shift in the apparent molecular weight is observed. For *Sso*Dpo1 binding to ssDNA and dsDNA, only two bands are clearly observed on the gels (Figure 2-3A): lower band corresponds to unbound DNA (at [*Sso*Dpo1] < 150 nM) and upper one (at [*Sso*Dpo1] > 1500 nM) corresponds to *Sso*Dpo1-DNA complex. There is some evidence, just above a background level, of an intermediate band from 150 to 1500 nM *Sso*Dpo1 with the dsDNA template (Figure 2-3B) consistent with either a monomer or dimer of *Sso*Dpo1 bound to DNA. This monomeric or dimeric polymerase DNA complex was not reproducible due to its low abundance with some DNA substrates. Fitting these data to a model that analyzes the percent of

DNA shifted, regardless of the complex state (Equation 2-1), identifies a cooperativity of binding leading to a stoichiometry of *Sso*Dpo1-DNA complex as 3:1 (Figure 2-2A and B). Similar global binding affinities and stoichiometries are calculated for ss- and dsDNA templates (Table 2-1). These results cannot specifically rule out preferential binding of a preformed trimeric *Sso*Dpo1 complex to either substrate due to the low abundance of an intermediate band, which could indicate either progression of *Sso*Dpo1 binding cooperatively or dimeric *Sso*Dpo1 binding directly to DNA.

Table 2-2-1. Dissociation constants (K_T) and stoichiometries (n) of *Sso*Dpo1 binding to different DNA substrates determined by EMSAs

DNA substrate	K_T[a] (nM)	Stoichiometry (n)
ssDNA(21-mer)	0.42 ± 0.02	2.8 ± 0.4
dsDNA (21/21-mer)	0.33 ± 0.02	2.7 ± 0.3
Short p/tDNA (21/31-mer)	0.27 ± 0.01	2.8 ± 0.1
Medium p/tDNA (21/40-mer)	0.23 ± 0.01	3.1 ± 0.2
Long p/tDNA (28/66-mer)	0.10 ± 0.01	3.0 ± 0.3

[a]The dissociation constant (K_T) represents the overall binding affinity of the total complex of *Sso*Dpo1 to DNA. In this analysis, it includes parameters from monomeric, dimeric and trimeric *Sso*Dpo1 binding to DNA.

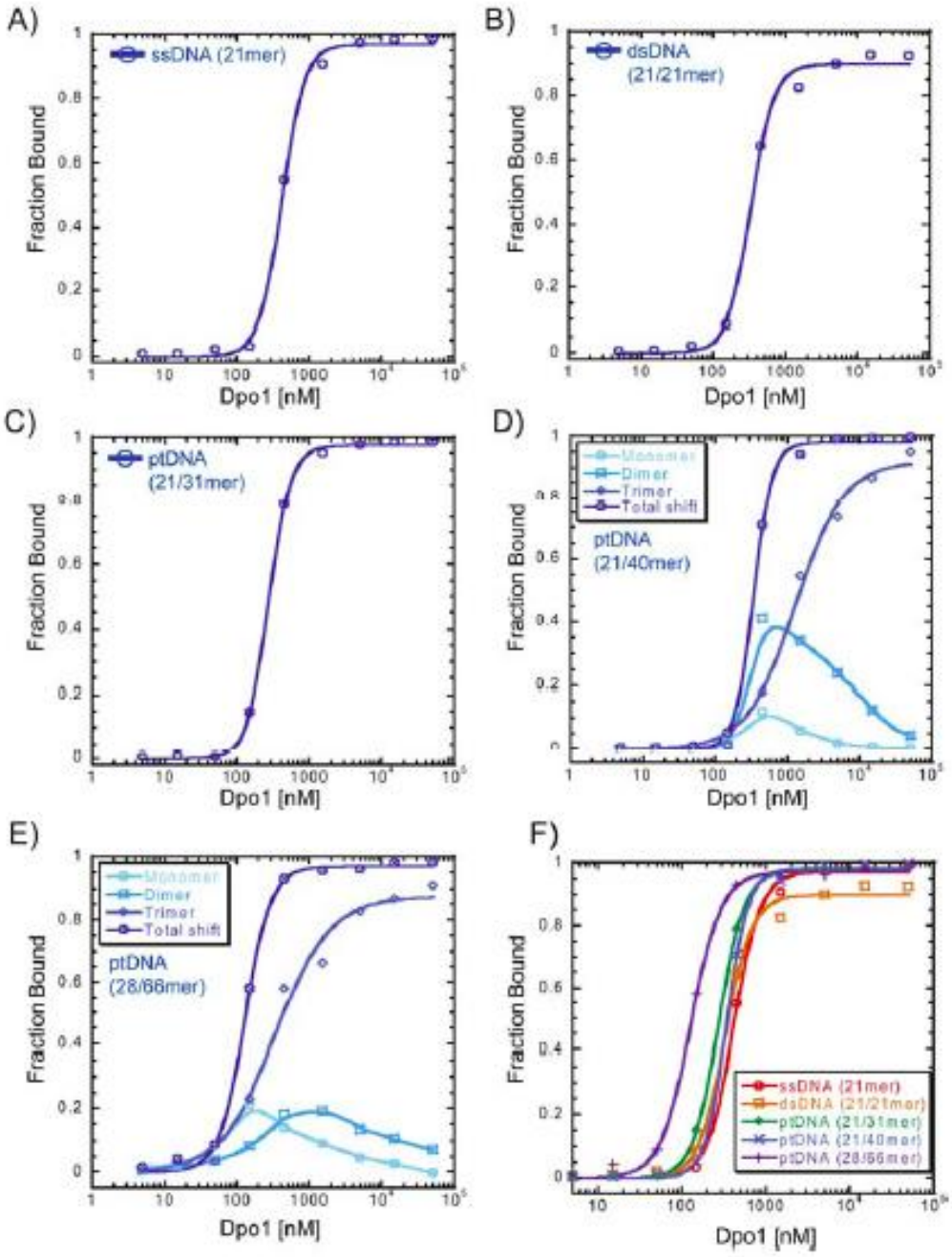

Figure 2-2. Shows the fits of EMSA for different DNA templates from Figure 2-3 according to equation 1 for A) ssDNA (21mer), B) dsDNA (21mer), C) short primer/template DNA (21/31mer), and D) medium primer/template (21/40mer), E) long primer/template DNA (28/66). When the presence of monomeric and dimeric polymerase:DNA complex was observed, the fits of the individual species are shown in D) and E). Both the stoichiometric values of n and the global dissociation constant (KT) are reported in Table 1. F) Compares the total EMSA shift between DNA substrates.

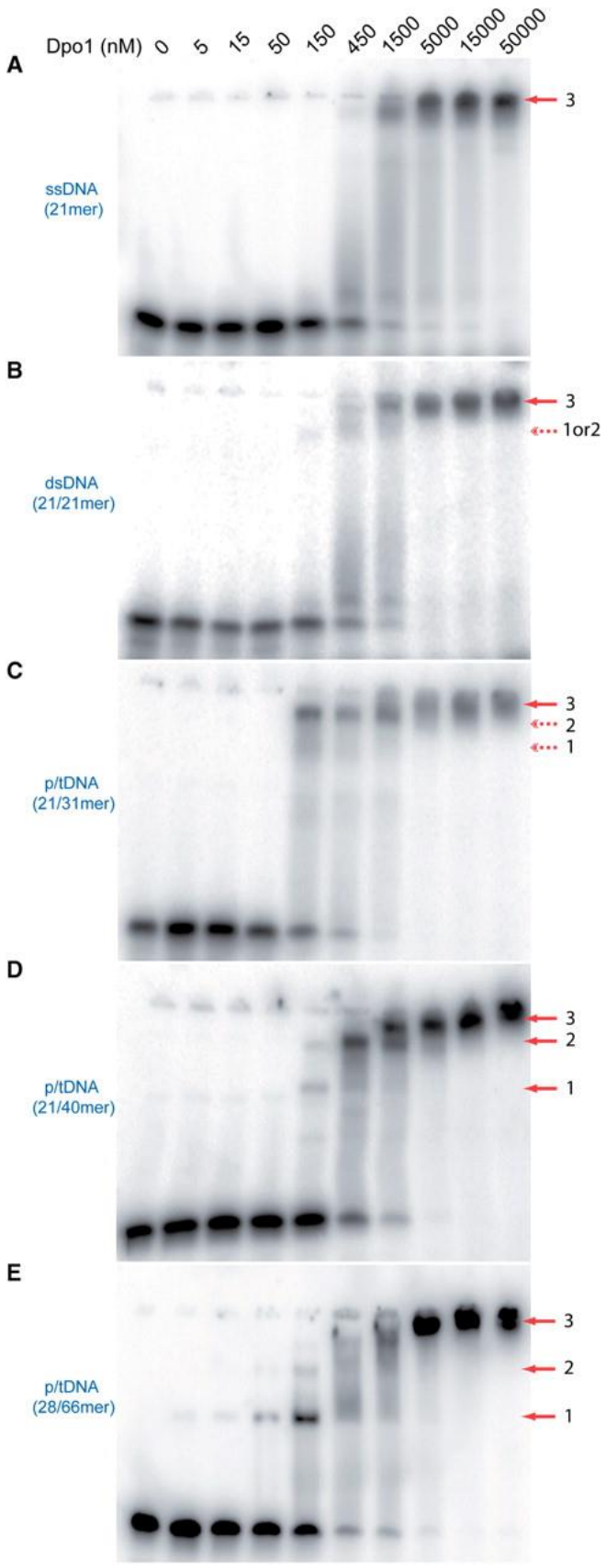

Figure 2-3. EMSA of the interaction of *Sso*Dpo1 with a variety of different DNA substrates labeled at the 5′-end with ^{32}P; (**A**) single strand (21-mer), (**B**) duplex DNA (21/21-mer), (**C**) short primer/template DNA (21/31-mer), (**D**) medium primer/template (21/40-mer) and (**E**) long primer/template DNA (28/66). The concentration of *Sso*Dpo1 was increased as shown above the gels identically for all experiments. The shift to the top of the gel identifies the trimeric polymerase complex highlighted by an *arrow* labeled with 3. The other *arrows* labeled 1 and 2 represent a monomeric and dimeric DNA complex, respectively. *Dashed arrows* represent extremely weak and faint complexes, while *solid arrows* are highly reproducible complexes. Fits of the fraction of DNA shifted are shown in Figure 2-2.

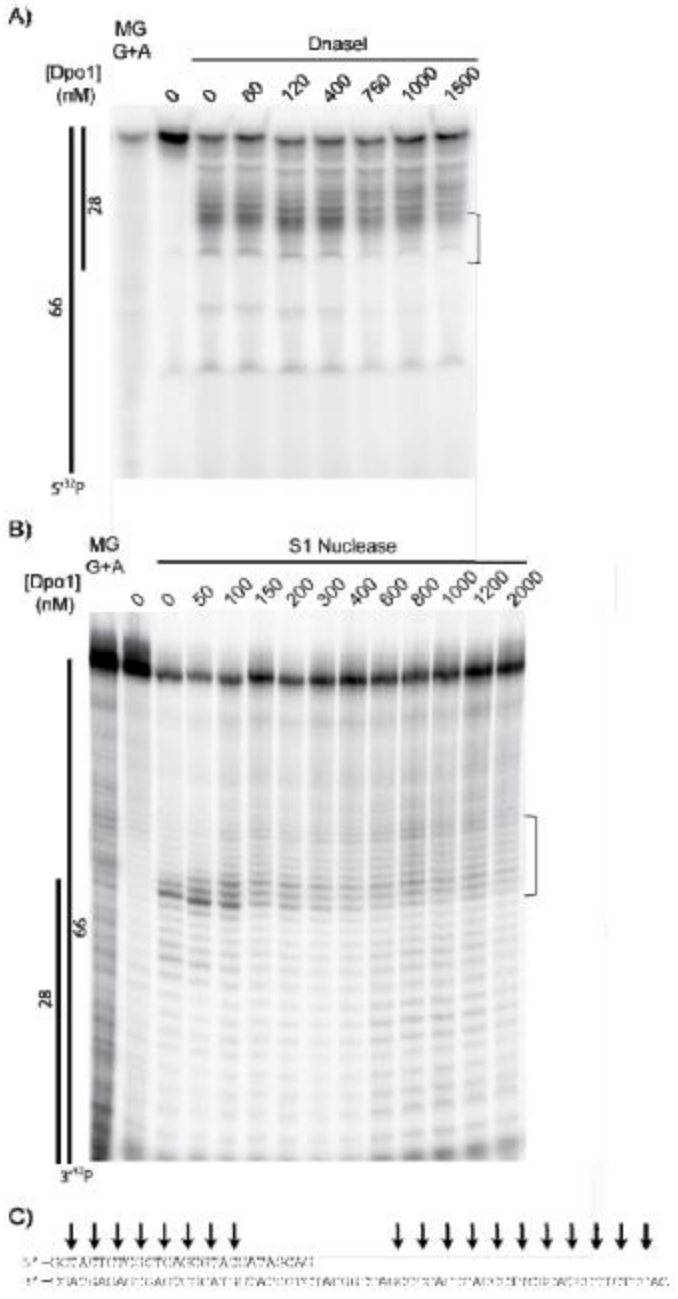

Figure 2-4. A) DNase I footprinting of *Sso*Dpo1 on ptDNA (28/66mer). The template strand (66mer) is labeled at the 5' end with ^{32}P. Increasing concentration of SsoDpo1 shows protection from eight bases from the primer template junction in the dsDNA region. B) Similar experiments with increasing concentrations of *Sso*Dpo1 designed to target primarily the ssDNA were performed with S1 nuclease. S1 nuclease primarily cleaves at a primer template junction but also cleaves ssDNA and dsDNA to lesser extents. A shift in cleavage is seen nine bases into the ssDNA template from the primer template junction with increasing concentrations of *Sso*Dpo1. C) Shows the cleavage sites (arrows) of both DnaseI and S1 nuclease on the pimer template substrate at high concentrations of *Sso*Dpo1

In contrast, four bands are observed on the gels for the complex of *Sso*Dpo1 with p/tDNA substrates with increasing size (Figure 2-3C, D and E). These additional protein DNA complexes, barely visible with the dsDNA substrate above, are more pronounced with p/tDNA and appear at lower protein concentrations. These additional bands labeled 1 and 2 are more clearly seen in the case of p/tDNA with a longer single-stranded tail (Figure 2-3D and E). Bands 1 and 2 suggest the formation of another type of *Sso*Dpo1–DNA complex with an apparent lower molecular mass than the fully shifted protein DNA complex seen in Figure 2-3A and B. The

stoichiometry of *Sso*Dpo1 binding to DNA was determined by performing an EMSA at high concentrations of DNA (7.5 μM) and stained with either ethidium bromide or coomassie blue (data not shown) and was found to be 3.5 ± 0.7 for *Sso*Dpo1:DNA.

Higher mobility of this type of complex in gel compared to the upper band 3 indicates a lower stoichiometry of this type of complex: either monomeric or dimeric (1 : 1 or 2 : 1 *Sso*Dpo1:DNA ratio, respectively). At [*Sso*Dpo1] > 150 nM, band 1 and eventually band 2 disappear and *Sso*Dpo1-DNA complex has mobility similar to the trimeric complex observed for ss- and dsDNA (see above). Fitting the percentage of DNA (fraction of total DNA) shifted above the free DNA position revealed a 3:1 *Sso*Dpo1:DNA stoichiometry (see Figure 2-2C, D and E) (Table 2-1). Since band 1 appears at a lower [*Sso*Dpo1] concentration than in either the ssDNA or dsDNA EMSA, the monomeric *Sso*Dpo1 has a higher initial affinity (~3-fold) for p/tDNA compared to ss- and dsDNA and promotes the cooperative formation of a trimeric *Sso*Dpo1/DNA complex that proceeds first through a dimeric *Sso*Dpo1/DNA complex. At high concentrations of *Sso*Dpo1 for either the 21/40-mer or 28/66-mers substrate (Figure 2-3D and E), there may be a percentage of complex that is above the molecular weight for the trimer. The resolution between trimer and higher complex states in these cases is small and difficult to differentiate. Binding of additional polymerase molecules (>3) to these longer templates at either the single strand or double strand ends may be responsible for these complexes.

To determine if this complex is binding along the length of these longer primer-template substrates or specifically at the primer-template junction, we used nuclease footprinting to map protected sites with increasing concentrations of *Sso*Dpo1 corresponding to monomer and trimer formation (Figure 2-4). A reproducible footprint is observed at roughly 9–10 bases on either side

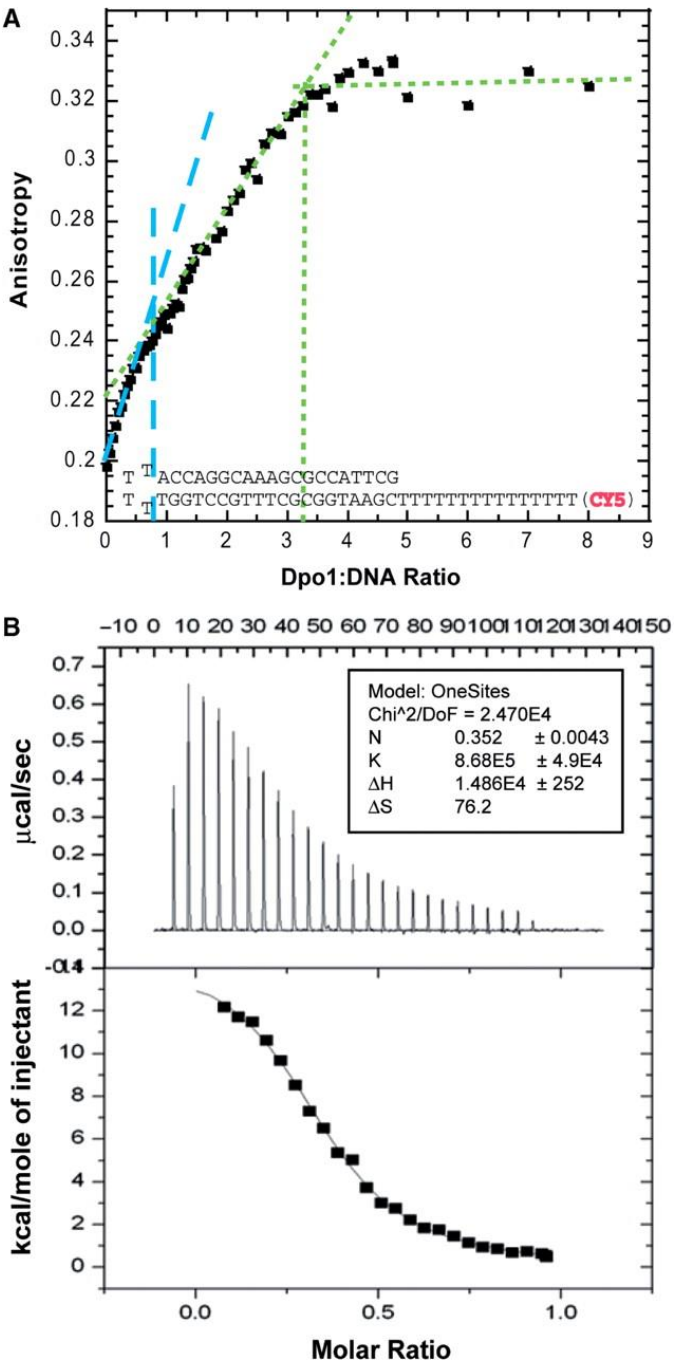

Figure 2-5. Quantifying stoichiometry of *Sso*Dpo1 binding to DNA. (A) Dependence of fluorescence anisotropy of labeled DNA hairpin (see the 'Materials and Methods' section) on *Sso*Dpo1:DNA stoichiometry. DNA concentration was fixed at 400 nM while the concentration of *Sso*Dpo1 was increased to give the stoichiometry listed on the*x*-axis. Cy5 was excited at 645 nm and an increase in anisotropy corresponding to a decrease in rotational diffusion due to *Sso*Dpo1 binding was monitored at 675 nm. Fits to the approximate limiting individual slopes are used to extrapolate the stoichiometry of the two binding phases for a monomeric-bound *Sso*Dpo1 (blue dash) and trimeric *Sso*Dpo1 complex (green dot). (B) ITC titration of primer/template (21/31-mer) DNA substrate into *Sso*Dpo1. Data was fit using Origin software and Equation (2-6) to yield thermodynamic parameter ($\Delta H°$) 14.86 ± 0.252 kcal mol^{-1}, equilibrium association constant (K_a) 8.68 × 10^5 ± 4.9 × 10^4 M and stoichiometry (n) 0.352 ± 0.043 DNA:*Sso*Dpo1.

of the primer-template junction for both monomer and trimer. A shift in the hypersensitivity of DNA cleavage by S1 nuclease upon binding of *Sso*Dpo1 identifies the free ssDNA boundary. The extreme double or single strand ends are not protected in these assays even at high concentrations of *Sso*Dpo1 (2 µM).

2.2.3 Stoichiometric fluorescence anisotropy of *Sso*Dpo1 binding to DNA

To learn more about the stoichiometry of *Sso*Dpo1-DNA complex, we monitored the increase in fluorescence anisotropy upon *Sso*Dpo1 binding to fluorophore-labeled DNA (Figure 2-5A). Fluorescence anisotropy monitors the relative rotational diffusion rates of molecules so

that an increase in molecular mass upon complex formation produces an increase in anisotropy. A ptDNA hairpin labeled with fluorescent dye, Cy5, at the 5′-end was used as a substrate (see the 'Materials and Methods' section). This hairpin eliminates a potential binding site at the double strand end known to be a binding site for some polymerases.(*86*) The concentration of this fluorescent DNA substrate used in these experiments (400 nM) is higher than normally used to measure dissociation constants (K_d) so that stoichiometry can be monitored.

Binding of *Sso*Dpo1 to DNA was monitored by the increase in anisotropy upon addition of protein. The titration curve is also characterized by a steep slope for *Sso*Dpo1:DNA ratio < 1, a more shallow slope for 1 <*Sso*Dpo1:DNA ratio < 3 followed by saturation at *Sso*Dpo1:DNA ratio > 3. Such stoichiometric titration curve behavior indicates the presence of at least two different types of *Sso*Dpo1-DNA complexes. The approximate slopes of the individual binding events are shown along with their apparent stoichiometries (Figure 2-5A). Note that changing the initial DNA concentration 2-fold does not change stoichiometry (data not shown). Based on the magnitude of anisotropy change associated with each slope before a breakpoint, we suggest that the initial complex monitors formation of a 1:1 *Sso*Dpo1:DNA ratio and the other with a 3:1 ratio (Figure 2-5A). There are not sufficient data to detect an additional slope associated with a 2:1 *Sso*Dpo1:DNA ratio. However, we were able to determine an absolute stoichiometry of *Sso*Dpo1 to DNA of 3:1 and show that formation of this complex proceeds through a higher affinity 1:1 state.

2.2.4 ITC to determine thermodynamic parameters of *Sso*Dpo1 binding

ITC was used to determine the stoichiometry and thermodynamic parameters for *Sso*Dpo1 binding to the short primer/template (21/31-mer) substrate (Figure 2-5B). From a fit

to the binding isotherm generated from titration of p/tDNA into a cell containing *Sso*Dpo1, the following parameters were calculated for the reaction at 30 ℃ according to Equation 6: an apparent equilibrium association constant (K_a) of 8.7 (±0.5) × 10^5 M^{-1} (i.e. K_d = 1.2 ± 0.1 μM), an endothermic ΔH° of 14.9 kcal mol^{-1} and a stoichiometry of 2.84 ± 0.04 *Sso*Dpo1:DNA. Based on these values, the binding free energy (ΔG° = -RT ln K_a) is −8.2 kcal mol^{-1} and TΔS° is 23.1 kcal mol^{-1}. Thus at 30℃, the binding of *Sso*Dpo1 to the 21/31 primer/template is enthalpically unfavorable and entropically favorable. However, if there is a large negative heat capacity change (i.e. strong temperature dependences for ΔH° and ΔS°) for *Sso*Dpo1 polymerase binding to DNA, we anticipate that at the physiological temperature (75 ℃) for *S. solfataricus*, the driving force for the formation of the *Sso*Dpo1-DNA complex will switch from entropy to enthalpy. This has been shown for Taq and Klentaq DNA polymerases. (*87*) For Taq and Klentaq polymerase, the minimum for ΔG° is near 50 °C, but for *Sso*Dpo1 the minimum may occur at even higher temperatures. In addition, the stoichiometry for the overall binding reaction can be measured in these experiments and is consistent with both the EMSA and anisotropy experiments showing a trimer of *Sso*Dpo1 capable of binding to primer/template DNA.

2.2.5 Protein chemical crosslinking of a *Sso*Dpo1 complex

To directly show the physical contact between *Sso*Dpo1 molecules alone and in complex with DNA, we employed chemical crosslinking. Covalent crosslinking of multimeric forms of proteins can be easily detected by SDS-PAGE.(*88*) We used a Sulfo-EGS crosslinker containing two amine-reactive groups—NHS esters, connected with a relatively short linker (16.1 Å length), so that only protein amino groups in close proximity can be covalently modified.

Crosslinking of free *Sso*Dpo1 and in presence of DNA at two *Sso*Dpo1:DNA ratios (1:1 and 3:1) produced two distinct complexes (Figure 2-6A). Whereas only one band at 101 kDa is seen for unmodified *Sso*Dpo1, addition of crosslinker leads to the appearance of the second band at roughly 303 kDa. Trimeric *Sso*Dpo1 can be captured over a range of NaCl concentrations up to 600 mM (Figure 2-6B). The molecular weight band is consistent with a trimer of *Sso*Dpo1. Surprisingly, this trimer band is also present in the absence of DNA. Because no complex of *Sso*Dpo1 in the absence of DNA was found by analytical gel filtration, we suggest that the interaction is transient at the concentrations of *Sso*Dpo1 used in the gel filtration analysis and only detectable by covalent capture of this complex. Addition of DNA significantly increases the amount of crosslinked trimer complex suggesting the presence of a more stable complex consistent with the gel filtration experiments. At the same time, there is no significant difference when crosslinking is performed at two different concentrations of *Sso*Dpo1, over a range of different temperatures, or using different DNA substrates (Figure 2-6). It should be noted that no *Sso*Dpo1 dimer—either with or without DNA—is observed possibly due to the lower relative abundance of a dimeric species as well as the detection limits of coomassie staining. It is probable that in the time and concentrations used to perform the crosslinking experiments, very little dimer is present due to the cooperative association and capture this complex into the trimeric state, effectively reducing the dissociation to zero. Alternatively, simultaneous binding of two *Sso*Dpo1 molecules to different sites on *Sso*Dpo1 may be favored in this case.

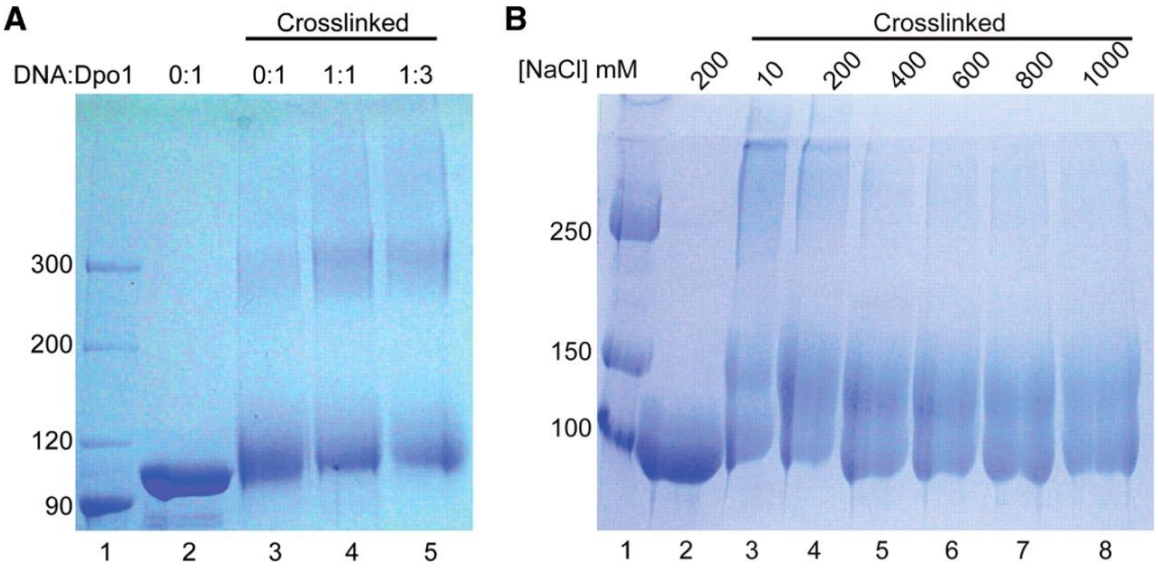

Figure 2-6. Covalent protein crosslinking of *Sso*Dpo1. (A) Performed in the absence and presence of different ratios of primer-template DNA. Lane 1: protein ladder, lane 2: *Sso*Dpo1 without modification, lane 3: *Sso*Dpo1 plus crosslinker, lane 4: *Sso*Dpo1–DNA complex plus crosslinker (1:1 *Sso*Dpo1:DNA ratio), lane 5: *Sso*Dpo1–DNA complex plus crosslinker (3:1 *Sso*Dpo1:DNA ratio). (B) Covalent protein crosslinking of 10 µM *Sso*Dpo1 performed at different concentrations of NaCl (10–1000 mM) in the presence of 100 nM ptDNA (21/31). Lane 1: protein ladder, lane 2: *Sso*Dpo1:DNA without modification, lanes 3–8:*Sso*Dpo1:DNA plus crosslinker at different [NaCl].

2.2.6 Polymerization kinetics at different oligomeric states of *Sso*Dpo1

We tested the polymerization kinetics of both monomeric and trimeric *Sso*Dpo1-DNA complexes at 60 ℃. Traditional polymerase extension assays using a primed M13 substrate were performed at different concentrations of *Sso*Dpo1, quenched after 2 min, and then separated on an alkaline agarose gel (Figure 2-7A). Quantification of the average rate of synthesis based on the size of the DNA was performed by comparing to λHindIII DNA standards in *lane* 1 using the ImageQuant software. The measured polymerization rate was vastly different at concentrations shown to be primarily monomer (<200 nM) versus those that are primarily trimer (>750 nM). A fit of the polymerization data to Equation 7 was more consistent with a cooperativity model for kinetic activity (Figure 2-7B) to give a kinetic K_d for *Sso*Dpo1 of 542 ± 5 nM and a maximal rate (V_{max}) of 422 ± 4 bp min^{-1}. A positive cooperativity constant associated with this fit was 14 ± 1. Thus, the formation of a trimeric *Sso*Dpo1 is required for maximal activity of this enzyme. This

catalytic K_d is slightly higher than the binding constant for the trimeric complex determined in our EMSAs (Table 2-1). This suggests that fully formed trimeric *Sso*Dpo1 that approaches binding saturation in Figure 2-3E is necessary for optimal kinetic activity. At higher concentrations of enzyme (>2 μM), we consistently see a decrease in the kinetic rate. We suspect this is enzyme inhibition due to binding and blocking of additional sites on the single strand region of M13. This would cause an impediment to the active polymerase complex, and although the polymerase roadblock can be removed by the active one, it requires a certain amount of time that negatively affects the overall rate of synthesis.

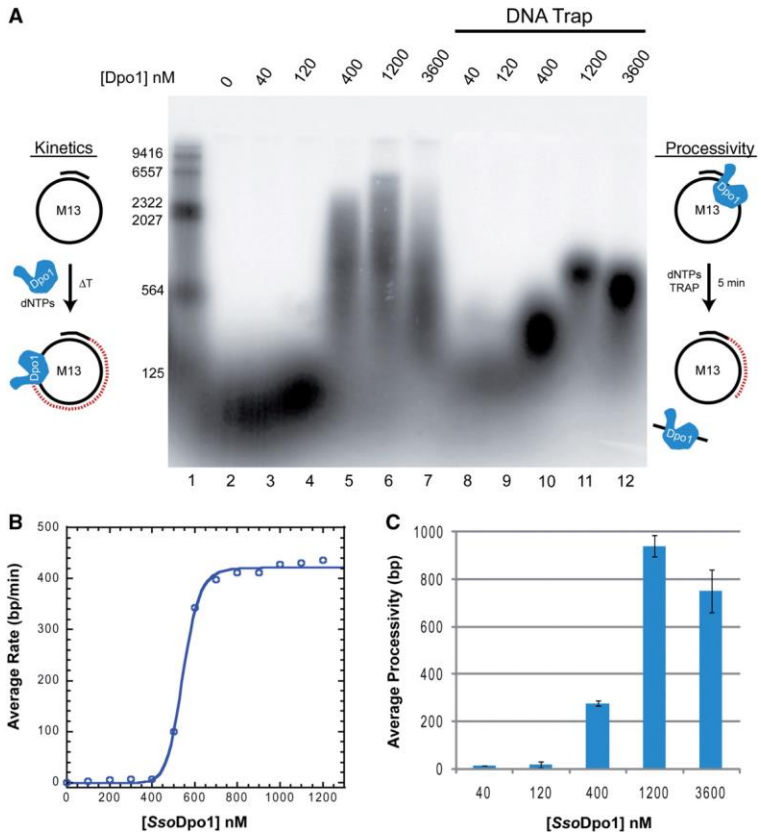

Figure 2-7. (A) Polymerase experiments were performed on primed M13 in the absence or presence of a DNA trap to monitor processivity at different concentrations of *Sso*Dpo1. A 5000-fold excess of ssDNA trap was added with dNTPs to initiate the reaction and then bind any dissociated *Sso*Dpo1 to prevent further synthesis. Experiments were quenched after 5 min and analyzed on an alkaline agarose gel for products >100 bases. Lanes 2–7 are kinetic experiments used to show the rate of DNA synthesis as a function of [*Sso*Dpo1]. Lanes 8–12 are identical to lanes 2–7 except that ssDNA trap was included to monitor processivity as a function of [*Sso*Dpo1] concentration. (B) Experiments covering a more complete range of *Sso*Dpo1 concentrations were performed and quenched at an identical 2-min time point. The rate of polymerization is calculated as the length of DNA synthesized divided by the time (bp/min) as calculate from the standard molecular weight markers (M) using ImageQuant software. Data was fit using Equation (7) for positive allostery to yield the following parameters: K_d = 543 ± 5 nM and V_{max} = 422 ± 4 bp min^{-1}. (C) The average length of DNA synthesized as a function of [*Sso*Dpo1] when DNA trap is included (lanes 8–12 in A) was calculated from the molecular weight markers using ImageQuant software.

We also performed identical kinetic assays on short ptDNA (21/31) to eliminate the possibility of binding multiple molecules laterally along the length of the DNA substrate. Due to the rate of synthesis measured above, these experiments were performed at 37 ℃ and quenched after 10 s and shown and quantified in Figure 2-8A and B. Similar kinetic constants and cooperativity curves to those fit above were also determined for the short ptDNA template confirming an active trimeric form of *Sso*Dpo1.

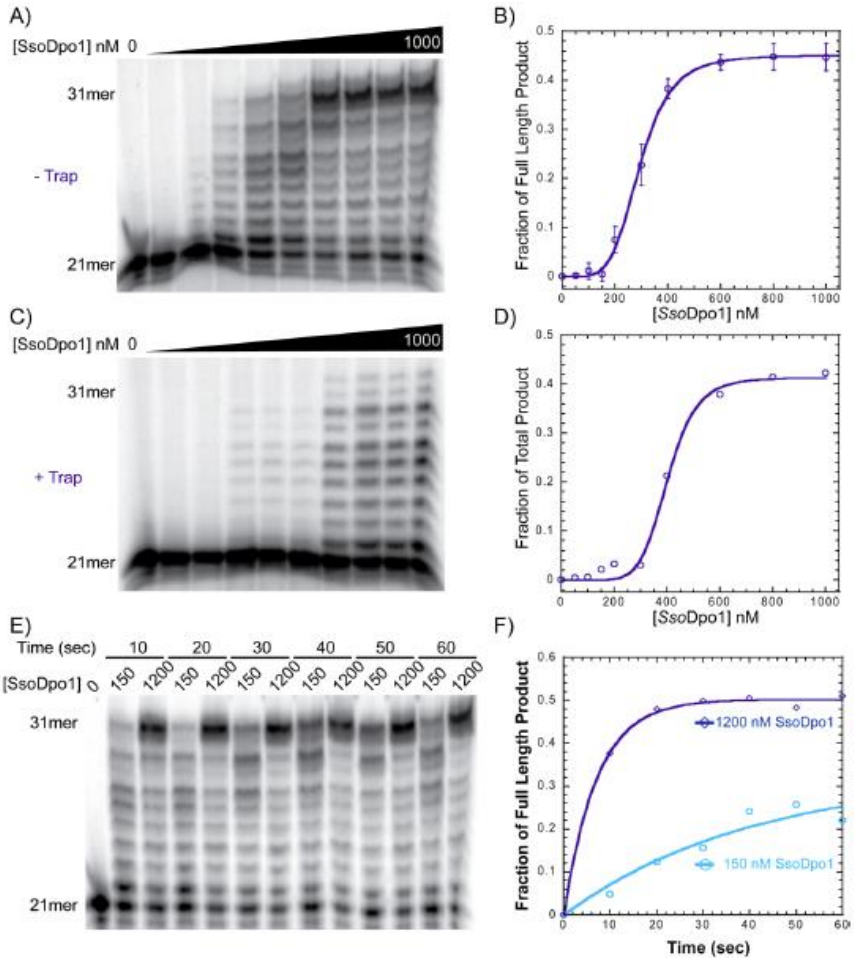

Figure 2-8. A) The degree of full length product formation synthesized from short ptDNA (21/31) at different concentrations of *Sso*Dpo1 at 37 ^{o}C after 10 seconds is shown and B) quantified. Maximal full length product occurs at concentrations greater than 400 nM and the catalytic K_d is calculated to be 292 ± 5 nM according to equation 7. As can be seen from this plot, positive cooperativity is apparent with a Hill coefficient equal to 4.9 ± 0.3. C) Processivity experiments over a range of [*Sso*Dpo1] were performed on the short ptDNA (21/31) as single turnover assays in the presence of a large excess of cold ssDNA trap as described in the Materials and Methods. D) Quantification of the single turnover products shows positive cooperativity with a catalytic K_d equal to 400 ± 10 nM and a Hill coefficient of 7.4 ± 1,4. E) A kinetic time course of product formation synthesized from short ptDNA (21/31) for two different concentrations of *Sso*Dpo1 representing primarily monomer or trimer (150 nM vs 1200 nM). F) The rates of full length product formation are fit to equation 8 and equal to 0.025 ± 0.012 sec^{-1} and 0.14 ± 0.01 sec^{-1} for 150 nM and 1200 nM, respectively.

As can be seen from Figure 2-7, concentrations of *Sso*Dpo1 that are primarily monomer have a rate of synthesis of <50 bases min^{-1}, while the trimer rate is >300 bases min^{-1}. Because we can detect the rate of synthesis from the average length of DNA products independent of the total amount of fully extended product, we are specifically examining how the oligomeric state of *Sso*Dpo1 influences the rate of synthesis and not the quantity of product formation. Under these conditions, the rate of synthesis is influenced by the off-rate and subsequent on-rate of either the monomeric or trimeric forms of *Sso*Dpo1. In these experiments, increasing the concentration of enzyme will naturally increase the re-association rate dependent on the K_d to produce longer DNA products. In order to examine the effect of monomer or trimer on the rate of DNA synthesis independent of re-association events, we utilized single-turnover experiments.

2.2.7 Polymerase processivity at different oligomeric states of *Sso*Dpo1

In these single-turnover assays, the length of DNA synthesized prior to dissociation from the DNA template is measured. Once *Sso*Dpo1 dissociates from the primed M13 template, it is trapped by binding to a high concentration of cold primer/template DNA substrate. We titrated the concentration of ssDNA trap needed to obtain a consistent processivity value and found that a 5000-fold excess of primer-template DNA was sufficient to trap all dissociated *Sso*Dpo1 as to not rebind the ^{32}P-labeled substrate and further influence our results.

Due to the range in processivity lengths that we found dependent on the concentration of *Sso*Dpo1, we separated the products on a denaturing acrylamide (short DNA fragments <100 bases) and alkaline agarose (long DNA fragments >100 bases) gels (Figure 2-9and Figure 2-7A). For concentrations of *Sso*Dpo1 that are mostly monomeric (120 nM), we measured an average processivity value of 18 ± 6 bases. This is consistent with processivity values measured for other

polymerases in the absence of accessory factors.(*89-91*) Upon increasing the concentration of *Sso*Dpo1 to promote trimer formation, the maximal processivity value increased roughly 500-fold to 942 ± 46 bases (Figure 2-7C). Similar to the kinetic data above, higher concentrations of *Sso*Dpo1 (>2 μM) show a reduction in processivity. This can be attributed to binding of additional molecules of *Sso*Dpo1 along the single strand region of M13 that can prematurely displace an active trimeric *Sso*Dpo1 complex.

As above and to test single monomeric or trimeric *Sso*Dpo1 complexes on DNA, we utilized the short ptDNA substrate (21/31) in similar single-turnover experiments at 37 ℃ and quenched after 10 s (Figure 2-8C and D). Once again, the data matched a cooperative fit similar to Figure 2-7C where the trimeric *Sso*Dpo1 is required for maximal processivity.

Due to greater processivity, the trimeric *Sso*Dpo1 complex is more stable on the DNA substrate such that the off-rate is greatly reduced. By taking the rates of DNA synthesis and the processivity values for the monomeric and trimeric *Sso*Dpo1

Figure 2-9. Polymerase experiments were performed on primed M13 in the absence or presence of a DNA trap to monitor processivity at different concentrations of *Sso*Dpo1. A 5000 fold excess of ssDNA trap was added with dNTPs to bind any dissociated *Sso*Dpo1 in prevent further DNA synthesis. Experiments shown here were analyzed on a denaturing PAGE gel to show products < 100 bases. More >100 base product can be seen for higher concentrations of Dpo1 (lanes 4 vs. 5).

(Figure 2-7), we can calculate the off-rates as 2 $min^{-1}$and 0.5 min^{-1}, respectively. A 4-fold decrease in the off-rate for the trimeric *Sso*Dpo1 over that of the monomeric form promotes both an increase in the DNA synthesis ability and processivity for the enzyme complex.

2.2.8 Thermal Stabilization Activity of Dpo1

We designed four hairpin DNA substrates (named according to their melting temperatures, T_M) with different T_M values that place the annealed bases at the 3'-end, leaving 10 thymine bases in the template strand. A stretch of thymidines in the template region was included to limit any hairpin formation to the designed site. The T_M values of the DNA substrates without and with Dpo1 were experimentally measured as described in Materials and Methods (Table 2-2). In all cases, addition of Dpo1 increased the T_M and stabilized weak base pairing interactions for the DNA hairpins. There was an average increase of 5.5 ^oC in the hairpin T_M when Dpo1 was included.

Table 2-2. DNA Sequences and Melting Temperatures

DNA NAME	Sequence	T_M (^oC)[1] DNA	DNA/Dpo1	ΔT_M (^oC)
DNA32	TTATG T ||| TTTACTTTTTTTTTT-5'	31.6 ± 1.3	37.0 ± 2.3	5.4
DNA37	TTTACG T |||| TTATGCTTTTTTTTTT-5'	37.0 ± 1.0	42.5 ± 1.4	5.8
DNA39	TTTTACG T |||| TTTATGCTTTTTTTTTT-5'	38.6 ± 1.9	44.5 ± 1.4	5.5
DNA88	TCGCCGGCCCGGG T ||||||||||||| TGCGGCCGGGCCCTTTTTTTTTT-5'	88	n/d[2]	n/d[2]

[1] Experimentally determined. [2] Not determined.

2.3 DISCUSSION

*Sso*Dpo1 is one of the four predicted DNA polymerases contained within the genome of *S. solfataricus* and has been proposed to be the main DNA replication polymerase.(*60*) Despite this, there was no detailed information about the binding thermodynamics or kinetics of this polymerase to DNA. In most respects, *Sso*Dpo1 is structurally and enzymatically similar to other DNA polymerases from the B-family except for an insertion in the fingers domain of the enzyme proposed to play a role in stabilization between the exonuclease and polymerase domains as well as a potential *Sso*Dpo4 interaction site.(*42, 70*) This unique insertion in *Sso*Dpo1 may act as a landing pad for other proteins within the context of DNA replication or repair, or it may serve to form the trimeric *Sso*Dpo1 complex described here.

In this chapter, the binding of *Sso*Dpo1 to DNA was found to induce and stabilize the formation of a trimeric DNA polymerase complex that activates polymerization. Formation of the trimeric form of the polymerase has important implications in the enzymatic activities of this enzyme complex that occur during DNA replication. Higher-affinity binding to the 3′-OH of the first polymerase followed by cooperative formation of the trimeric polymerase complex is consistent with the read-ahead function of this polymerase in detecting lesions on the template strand.(*92, 93*)

2.3.1 Monomeric, dimeric and trimeric polymerase complexes are detected on p/tDNA substrates

During protein purification and in the absence of DNA substrates, *Sso*Dpo1 exists stably and solely as a monomer as shown by the analytical gel filtration studies even at very high

concentrations (>20 μM) after elution from the column. Primer/template DNA was shown to shift the molecular mass of the complex to multiple forms consistent with a monomeric, dimeric and trimeric form of *Sso*Dpo1 bound to DNA. Initial binding of *Sso*Dpo1 to primer/template DNA depends slightly on template length, as a monomeric *Sso*Dpo1-DNA complex was not reproducibly detected by EMSA with the 21/31-mer substrate but more easily observed with a longer primer/template strand. DNA polymerases are known to bind with higher affinity to the 3′OH of the primer strand in the active site to discriminate incorporation of the next nucleotide from the template strand, so it is not surprising that *Sso*Dpo1 binds to this junction. What is surprising is the observation that an additional two molecules of *Sso*Dpo1 bind cooperatively to the initial *Sso*Dpo1/DNA complex.

The cooperative formation of a trimeric complex occurs at a higher dissociation constant than the monomeric form, but it is not outside the dissociation constant (K_d) realm of polymerase DNA interactions detected previously and is within a physiological concentration range to be biologically relevant for replication proteins held at the replication fork.(*70, 94, 95*) In support, Zhang *et al*.(*96*) has shown what we suspect to be a monomeric EMSA of *Sso*Dpo1 (300 nM) interacting with Orc/Cdc6 homologs while also reporting alterations in *Sso*Dpo1 activity at trimeric concentrations (900 nM). This shows that both monomeric and trimeric forms of *Sso*Dpo1 can have specific interactions with other proteins that modulate its activity.

2.3.2 Specific protein-protein interactions within *Sso*Dpo1 are responsible for trimerization on a variety of DNA substrates

A stoichiometry of three molecules of *Sso*Dpo1 to one molecule of DNA was observed for binding to different DNA substrates in four independent assays including: analytical gel

filtration, EMSA, fluorescent anisotropy and ITC experiments. Although trimeric polymerase complexes form with single stranded, double stranded and primer/template substrates, the trimer of *Sso*Dpo1 has the highest affinity for the primer/template substrate due to the presence of a 3′-OH at the primer/template junction. The relative global binding affinities of this trimeric polymerase complex for other DNA substrates varied little (Table 2-1), highlighting a possible non discriminating binding mode resulting from specific protein-protein interactions of the second and third polymerase with the first. The first molecule of *Sso*Dpo1 differentiates between DNA substrates (ss-, ds- versus p/t) due to the identification of a monomeric *Sso*Dpo1 shift in our EMSA experiments with p/tDNA at lower concentrations. Cooperative formation of the trimeric complex then occurs at higher concentrations. Both the detection and quantification of trimeric *Sso*Dpo1 on short p/tDNA (21/31) where only a single molecule of *Sso*Dpo1 can bind laterally to the DNA as well as the restricted binding to the primer-template junction even at high concentrations of *Sso*Dpo1 as detected by nuclease footprinting is consistent with preferential binding to the primer-template junction and subsequent *Sso*Dpo1 binding directly to the primary polymerase.

In support of this binding model, protein crosslinking identified the presence of a complex consisting of primarily a trimeric *Sso*Dpo1. Because our gel filtration results were never able to detect a complex larger than a monomer in the 'absence of DNA', we suspect that the K_d for the oligomerization in the absence of DNA is much higher, such that the off-rate is large. Protein crosslinking was able to capture this transient complex through the formation of a covalent bond between molecules. We were also never able to detect a polymerase complex larger than a trimer for shorter ptDNA substrates where only a single polymerase can be bound

laterally on DNA. This is consistent with our gel filtration studies which also did not detect the presence of complexes >300 kDa.

Taken together, these findings allow us to propose a model for the trimeric complex of *Sso*Dpo1 bound to the primer-template substrate that encircles the DNA (Figure 2-10). In this model, one polymerase molecule is bound to DNA substrate in an active conformation while the two others have little or no contacts with DNA. In this model, one, two or all three *Sso*Dpo1 molecules can be accessible to binding cofactors such as PCNA. In fact, this proposed circular representation of the trimeric polymerase complex is reminiscent of the structure of the processivity factor, PCNA, known to increase processivity for monomeric *Sso*Dpo1 along with a variety of other DNA polymerases,(*68, 97*) and is most likely responsible for the increase in processivity that we detect with the trimeric complex. We have arranged our model in this fashion due to the absence of any species greater than a trimer as well as a means to explain the enhanced processivity of the trimeric species.

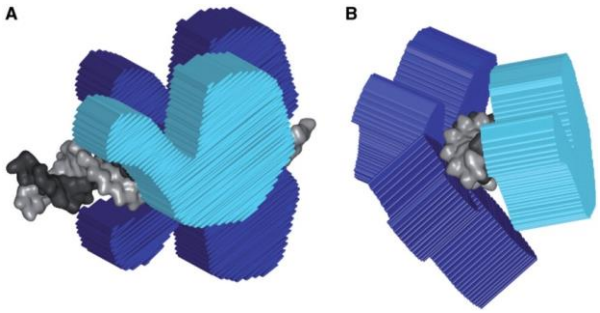

Figure 2-10. Hypothetical model of the *Sso*Dpo1 trimeric complex bound to the primer-template DNA substrate. (A) is rotated 90° to the right to obtain (B). The trimeric polymerase complex is shown to encircle the DNA substrate (gray). The active polymerase is in light blue, while the other two molecules are in darker blue and are not directly bound to the DNA template.

2.3.3 The monomeric and trimeric *Sso*Dpo1 complexes contribute differently to the kinetic proficiency of the polymerase

This is not the first example of a higher-order DNA polymerase complex, but it is the first trimeric-specific DNA polymerase complex of which we are aware. In *E. coli*, when three subunits of tau are incorporated into the gamma complex (clamp loader), a replisome can be constructed with three polymerases,(*75*) but these are not specific polymerase-polymerase interactions. Instead, each polymerase is held in the replisome by specific interactions with the tau subunit. We determined the effect of having a monomeric or trimeric *Sso*Dpo1 complex assembled on DNA with the associated kinetic activity of both polymerization and processivity. Both the kinetic rate constant for polymerization as well as the processivity are increased with the trimeric *Sso*Dpo1. In fact, the kinetic rate data with increasing concentration of *Sso*Dpo1 also showed a cooperativity term similar to the binding data. Maximal DNA synthesis is achieved by the formation and associated activity of a trimeric *Sso*Dpo1. Therefore, depending on the concentration of the polymerase at the replication fork and accessibility of binding in the context of the entire replisome, the DNA synthesis ability can be controlled. This concentration dependence on the kinetics of polymerization is unlike that shown for other B-family DNA polymerases from T4 or *E. coli*.(*74, 98, 99*)

Single-turnover experiments that monitor how long a polymerase stays associated with the DNA template before dissociating clearly show that the trimeric *Sso*Dpo1 complex has a much greater processivity than that of the monomeric form. Therefore, the trimeric polymerase represents a dynamic complex able to promote the formation of longer DNA products before dissociation. Based on our model for binding (Figure 2-10), the active sites of the three polymerases are in a close enough proximity to the DNA template that they could easily

exchange binding to the DNA template. We hypothesize that this mode of polymerase binding and active site switching is responsible for the increased processivity that we have observed. Transient dissociation from a DNA substrate by an individual molecule of *Sso*Dpo1 would allow for proximal binding of one of the other two molecules in the complex. Data presented here provide a general mechanism to increase polymerase processivity in the absence of cofactors due solely by polymerase oligomerization.

We have shown previously, that the DNA polymerase from bacteriophage T4 utilizes dynamic processivity mechanism to recruit additional molecules of the polymerase from solution to the replication fork during coupled leading and laggings strand synthesis.(*74*) *Sulfolobus* may utilize a similar form of dynamic polymerase processivity in the absence of PCNA. We propose that multiple polymerases at the replication fork could also allow for alternative binding to the DNA substrate in the polymerase or exonuclease active sites to more effectively process the DNA substrate. The polymerase used in these experiments is devoid of exonuclease activity to allow for thermodynamic-binding measurements, so, we were unable to examine the exonuclease activities for the monomeric or trimeric forms. This ability to switch between polymerase and exonuclease active sites is essential in maintaining the high proofreading ability of this class of enzymes.(*100*) *E. coli* Klenow and rat polymerase β show stoichiometries of two and four, respectively, on their DNA substrates.(*81, 101*) In the case of Klenow, binding of a dimeric complex in the polymerization mode is favored and may play a role in coordinating high-fidelity DNA synthesis.

The existence of multiple polymerase oligomeric forms allows for the possibility of differential functions of these complexes. This may be influenced and/or modified by the presence or absence of accessory factors, such as *Sso*PCNA, known to interact with *Sso*Dpo1. A

trimeric polymerase complex may also build up in response to specific states of DNA conformations or in response to roadblocks, such as lesions, to DNA replication. Because of the lack of nucleotides in all our binding assays, we are simulating a stalled DNA polymerase so that we can measure the thermodynamics of binding to different DNA substrates. Within the cell, both thermodynamics and kinetics of binding conformation will determine the activities and states of complexes (either monomer or trimer); for example, in response to a lack of nucleotides, RNA primer handoff from the primase, DNA damage on the template strand or physical blocks to *Sso*Dpo1.

Theoretically, only two *Sso*Dpo1 molecules are necessary for a switch to occur between polymerase and exonuclease active sites. In addition to increasing processivity, the third DNA polymerase found in our complex may have a role in coordinating DNA synthesis on the lagging strand. In *E. coli* PolIII, the tau subunit acts to coordinate synthesis on the leading and lagging strands;(*75*) however, the protein component or motif required for coupled DNA synthesis in eukaryotes and archaea has yet to be determined. The identification of this trimeric polymerase complex in *Sso* may be the first evidence for a polymerase complex capable of highly processive replication in the absence of accessory factors. Additionally, upon formation of the lagging strand holoenzyme, it is possible that another trimeric polymerase complex may also be associated with each Okazaki fragment. In any case, efficient processing of DNA in response to nucleotide selection, dNTP concentration pressures, proofreading and replication blocks, requires a dynamic polymerase complex capable of efficiently handling each scenario. The trimeric polymerase complex found in *Sso* may be an effective model system to study the coordination of these events.

2.3.4 Dpo1 thermodynamically stabilizes DNA

Severe destabilizing thermodynamic forces that persist at high physiological temperatures for *Sso* would make maintaining annealed dsDNA templates during replication difficult. It is thought dsDNA is stabilized by specific DNA binding proteins, which is necessary to protect the integrity of the genome at high temperatures. *Sso*Dpo1 has the inherent ability to stabilize thermodynamically weak base pairing interactions to facilitate template dependent DNA polymerization. Surprisingly, *Sso*Dpo1 is also found to have robust terminal transferase activity that proceeds by two independent mechanisms: a loop-back annealing template-dependent polymerase activity and a slower template independent TdT activity.(*102*) The loop back mechanism utilizes *Sso* Dpo1's annealing mechanism to synthesize DNA using internal strand hybridization. These annealing and transferase activities have not been noted for any other DNA replication polymerase within this family and may provide a mechanism for efficient replication and repair at high temperatures.

2.4 CONCLUSION

In this chapter, we were able to detect the stepwise assembly of monomeric, dimeric, and trimeric complexes of Dpo1 associating with DNA by EMSA in a basic reaction condition (pH~8.5). While the trimeric and monomeric complexes will be compared and discussed in the following chapters, the dimeric complex cannot be reproducible observed by other techniques under a neutral environment. Most likely, the second and third molecules of *Sso*Dpo1 bind cooperatively giving two predominate species, monomer and trimer on DNA. Therefore, we will not discuss the dimeric complex of Dpo1 with DNA further in other chapters.

Furthermore, we used DNA foot-printing assays to demonstrate that the trimeric Dpo1 complex binds solely at the primer-template junction. Therefore, we proposed a hypothetical model of the *Sso*Dpo1 trimeric complex encircling DNA (Figure 2-10). However, we also detected the association between the trimeric Dpo1 complex and ssDNA or dsDNA at similar concentration range by EMSA (Figure 2-3). In order to eliminate the additional association between Dpo1 and the single-strand or double strand part along with the association with the primer/template DNA, we used a shorter DNA hairpin substrate (10 bps of single-strands and 12 bps of double-strands, about the size of Dpo1) allowing for a single association between polymerases and DNA in the following chapters.

The relative physiological roles of these Dpo1 complexes in DNA replication are still unclear, but we were able to demonstrate that the trimeric complex has a better kinetic proficiency than the monomeric Dpo1-DNA complex in the DNA replication. Assumed protein occupies 20% weight of cell,(*103*) and *Sso* cell has diameter of 1 μm, the concentration of Dpo1 in *Sso* cell is roughly 2.2 μM based on quantitative immunoblot analysis.(*104*) This concentration lies in the concentration range of the trimeric Dpo1 complex formation. We will demonstrate that the DNA binding affinity of Dpo1 is higher and the free energy is lower at *Sso's* physiological temperature (~ 75 ^{o}C) than its lesion bypass partner Dpo4 in the following chapters, showing that Dpo1 is playing a primary role at DNA replication fork.

3.0 DIFFERENTIAL TEMPERATURE-DEPENDENT MULTIMERIC ASSEMBLIES OF REPLICAITON AND REPAIR POLYMERASES ON DNA INCREASE PROCESSIVITY[2]

Over the past two decades, a multitude of DNA polymerases have been discovered and classified into at least six separate families.(*105*) Many organisms have multiple DNA polymerases with humans having fifteen.(*106*) Most traditional B-family DNA polymerases are involved in faithful copying of our genome, while Y-family DNA polymerases have more flexible active sites allowing for synthesis across locations of DNA damage in an effort to maintain uninterrupted DNA synthesis during replication. Binding and recognition of normal or damaged DNA bases require that each DNA polymerase has a precise specificity with the appropriate DNA template to maintain fidelity of replication or repair directed by interacting proteins at the replication fork. Specificity is increased through interactions with shared accessory proteins for DNA replication and repair polymerases at the site of catalysis. Alternatively, the repeated shuttling between polymerization and exonuclease states of B-family DNA polymerases at sites of damage may locally destabilize binding, allowing a Y-family polymerase to bind more specifically to bypass the lesion.(*107*) Therefore, a question arises as to how each polymerase is regulated with regards to binding the correct DNA substrate.

[2] Text from this chapter is reprinted with permission from Hsiang-Kai Lin, Susan F. Chase, Thomas M. Laue, Linda Jen-Jacobson, and Michael A. Trakselis. *Biochemistry* 2012, 51, 7367-7382. Copyright 2012 American Chemical Society.

DNA polymerases Klenow,(*51*) T4 gp43,(*48*) human pol ,(*108, 109*) and African swine fever virus polymerase X have all been found to form 2:1 complexes with DNA.(*53, 110*) Other DNA polymerases appear at the replication fork as multimers during DNA replication through interactions with their accessory proteins.(*111*) Interestingly, DNA replication polymerases have also been found to exchange freely from solution during active replication, suggesting that either direct interactions between polymerases or indirect interactions through accessory proteins provide mechanisms for switching enzymes at the site of catalysis.(*112, 113*) Therefore, it is likely that the high concentration of DNA polymerases within or around replisome complexes is a common mechanism for coordinated DNA synthesis, increased kinetics, and coupled replication and repair to maintain the genomic integrity of the cell.

DNA replication in archaea serves as an important and relevant model system for detailing the molecular mechanisms of DNA polymerases homologous to their eukaryotic counterparts.(*114-116*) Contained within the archaeal *Sulfolobus solfataricus* genome are DNA polymerases from both the B-family replication (Dpo1) and Y-family lesion bypass (Dpo4) families. Both individual DNA polymerases have been structurally characterized,(*33, 117, 118*) have similar specificities for DNA,(*119, 120*) and robust kinetics,(*121-123*) but differ in their fidelities for nucleotide incorporations.(*121, 124-126*) Dpo4's lower fidelity, as well as the ability for *Sulfolobus* to survive in the absence of this protein,(*127*) highlights a nonessential role in DNA replication. Direct interaction between Dpo1 and Dpo4 has also been noted and is thought to be important for uninterrupted lesion bypass during DNA replication.(*34*) We have also shown that Dpo1 can form a trimeric complex in the presence of DNA,(*120*) suggesting that homo and heteroligomeric DNA polymerase complexes exist.

Quantification of binding various DNA polymerases to DNA has been examined using a number of techniques to characterize this single binding event. The resulting temperature dependent thermodynamic binding parameters can provide insight into the specificity of the binding process through determination of the heat capacity change (ΔC^o_p).(*128, 129*) Although a strongly negative ΔC^o_p has been shown to be the thermodynamic signature of sequence-specific binding,(*129*) the non-sequence specific binding to primer template DNA by the A-family DNA polymerases from *Thermus aquaticus* (Taq) and *Escherichia coli* (Klenow) is also associated with large and negative ΔC^o_p values.(*128, 130-134*). Even though there is no sequence specificity, the negative ΔC^o_p is consistent with the high structural complementarity of the DNA polymerase binding to the primer template junction, visualized in a variety of crystal structures.(*118, 128, 135, 136*). The inherent thermostability of proteins from *Sso* (where the growth temperature is ~75 ^oC) allows us to fully investigate the energetic constraints of DNA polymerase binding to DNA. Access this broad temperature range results in a more complete thermodynamic characterization of the differences in binding B and Y-family polymerases to an undamaged DNA primer-template. These thermodynamic differences can be evaluated directly by determining the affinities (K_d), free energies (ΔG^o), heat capacity changes (ΔC^o_p), and stoichiometries (n) for binding each polymerase.

Here, we use chemical crosslinking, isothermal calorimetry (ITC), and analytical ultracentrifugation (AUC) to show that Dpo4, like Dpo1, can also form an oligomeric complex on DNA. Using AUC, we have found both a strong concentration dependent and modest temperature dependent shift in the reaction boundaries, highlighting changes in Dpo4 monomer-dimer and Dpo1 monomer-trimer equilibria. Temperature dependent equilibrium fluorescent anisotropy binding experiments were used to separate the free energy (ΔG^o) of binding either

monomer or higher order oligomeric DNA polymerases (Dpo1 or Dpo4) states. For both polymerases, we have detected an initial higher affinity monomeric binding site followed by sequential binding of additional polymerase molecules to form either trimeric Dpo1 or dimeric Dpo4 complexes on DNA. Separation and quantification of these individual binding events reveal that a Dpo1 monomer binds to DNA with only slightly greater affinity than Dpo4 up to 50 ^{o}C. This binding affinity difference is exaggerated at the highest temperatures, suggesting that binding of Dpo1 to undamaged DNA templates is favored at physiological growth conditions for *Sso*. The free energy associated with trimer Dpo1 binding to DNA is significantly more favorable than that associated with dimer Dpo4 DNA binding, and this difference increases strongly with increasing temperature. Enzymatic evidence showing greater processivities for Dpo1 and Dpo4 at higher temperatures and protein concentrations is used to explain the role of temperature and oligomeric state in promoting DNA polymerase assembly, stability, and kinetics at the replication fork. Collectively our results indicate that the binding specificities of multiple oligomeric archaeal DNA polymerases are regulated by changes in cellular concentrations and temperature for efficient DNA binding recognition and synthesis.

3.1 MATERIALS AND METHODS

Materials. Oligonucleotide substrates including the 37 nucleotide (nt) DNA hairpin, 5'-fluorescein or 5'-Cy3 labeled DNA were purchased from Integrated DNA technologies (IDT, Coralville, IA). The sequence of the 37 nucleotide DNA hairpin was 5'-TTTTTTTTTTCCCGGGCCGGCGTTTCGCCGGCCCGGG, which included a 12 base-pair

duplex region, a three residue loop, and a ten residue single strand template. DNA was dissolved in annealing buffer [20 mM HEPES (pH 7) and 200 mM NaCl], heated to 95 ^{o}C for 15 minutes, and then cooled to room temperature by turning off the hot plate overnight. M13mp18 was purchased from USB Corporation (Cleveland, OH). All radiochemicals were purchased from MP Biochemicals (Santa Ana, CA) or Perkin Elmer (Waltham, MA). Commercial enzymes were from NEB (Ipswich, MA). All other chemicals were analytical grade or better.

Dpo1 and Dpo4 were purified as described except for a few modifications.(*117, 120*) The exonuclease deficient version of Dpo1 (D231A/D318A) was recloned into pET30a (*NdeI*/*XhoI*) to introduce a stop codon and remove the C-terminal His tag. Both polymerases were expressed using an autoinduction protocol using Rosetta 2 cells (Stratagene).(*137*) Cells were lysed by sonication and heat treated at 70 ^{o}C for 30 minutes followed by centrifugation. The Dpo1 lysate was purified using a HiTrap MonoQ, heparin, and Superdex-200 gel filtration columns. The wild-type untagged Dpo4 lysate was purified using a HiTrap MonoQ, heparin, and hydroxylapatite (Sigma-Aldrich) columns.(*117*)

Crosslinking Studies. Dpo4 was dialyzed in crosslinking buffer [50 mM HEPES (pH 7.0), 150 mM NaCl, 10 mM EDTA] and reduced using 10 mM Tris (2-carboxyethyl) phosphine hydrochloride (TCEP-HCl) (Thermo Scientific, Rockford, IL). Dpo4 (8 μM) was then either incubated alone or with 10 M DNA 37 nucleotide hairpin for 5 minutes at room temperature. Chemical crosslinking experiments were initiated with 0.33 mM 1,11-bis-maleimidotriethyleneglycol [BM(PEG)$_3$] or ethylene glycol bis[succinimidylsuccinate] [EGS] (Pierce, Rockford, IL) targeting free cysteines or free amines, respectively, in close proximity. The reaction was then incubated for 15 minutes at 22 ^{o}C. Products were separated on an 8% SDS-PAGE gel and stained with coomassie dye.

Isothermal Titration Calorimetry (ITC). Prior to analysis, titrants and analytes were dialyzed against Buffer A [20 mM HEPES-NaOH (pH 7), 150 mM NaCl, 5% Glycerol, 10 mM $Mg(OAc)_2$, 0.2 mM DTT], filtered by centrifuge tube filters (0.22 M, SPIN-X, Corning Inc., NY), and degassed. Isothermal titration calorimetry was performed using a VP-ITC (MicroCal Inc., Northampton, MA) as described previously (*120*). Titrations were performed by titrating 400 M 37-nt hairpin (primer template) (5-8 L aliquots) into 25 M Dpo4 at 15 ^{o}C or 60 ^{o}C. The heats of the reaction were corrected for the heat of dilution by subtracting the signal after reaching saturation. All data were fit using Origin 7.0 (MicroCal) according to the following equation:

$$Q = \left(\frac{n[M]_t \Delta H^o V_0}{2}\right)\left\{1 + \frac{[L]_t}{n[M]_t} + \frac{1}{nK_a[M]_t} - \left[\left(1 + \frac{[L]_t}{n[M]_t} + \frac{1}{nK_a[M]_t}\right)^2 - \frac{4[L]_t}{n[M]_t}\right]^{\frac{1}{2}}\right\}$$

(Equation 3-1)

where V_0 is the volume of the cell, H^o is the enthalpy of binding per mole of ligand, $[M]_t$ is the concentration of DNA including both bound and free fractions, K_a is the association constant, $[L]_t$ is the total ligand (Dpo4) concentration, and n is the stoichiometry of the reaction.(*120*, *138*)

Analytical ultracentrifugation (AUC) - Sedimentation velocity experiments. Sedimentation velocity experiments were performed using an Optima XLI analytical ultracentrifuge (Beckman Coulter, Fullerton, CA) equipped with a prototype fluorescence optical system (Aviv Biomedical). Samples of protein alone or with (50 nM) fluorescein labeled 37-nt hairpin (primer-template) DNA in Buffer A were loaded into ultracentrifuge cells at various

concentrations (0, 10, 50, 100, 200, 500, 1000, 2000, 5000, and 10,000 nM) into a double-sector charcoal-Epon centerpiece in either a 4- or 8-hole titanium rotor and subjected to an angular velocity of 45,000 rpm with the temperature at 10, 20, or 30 ℃. Absorbance or fluorescence scans as a function of radial position were collected by scanning at 280 nm (protein alone) or at 488 nm (protein with fluorescein DNA) at 20-μm radial increments, averaging 3 revolutions / scan. Sedimentation velocity boundaries were analyzed in the least squares sedimentation coefficient distribution (*ls-g*(s)*) model using program SEDFIT (version 12.1).(*139*) The sedimentation coefficient, s, is given by Svedberg's equation:

$$s = \frac{M_W D_t (1-\bar{v}\rho)}{RT} \qquad \text{(Equation 3-2)}$$

where M_W is the molecular weight, D_t is the diffusion coefficient, $\bar{v}$ is the partial specific volume, ρ is the solvent density, R is the universal gas constant, and T is temperature. Observed weight average sedimentation coefficients were converted to $s_{20,w}$ (standard conditions of 20 ℃ in water) accounting for partial specific volumes, buffer densities, and viscosities, calculated using SEDNTERP.(*140, 141*)

Fluorescence anisotropy, equilibrium binding, and thermodynamic parameters. A 5' Cy3-labeled 37-nt hairpin primer template DNA construct, described previously,(*120*) was used in the fluorescence anisotropy experiments. Titrations were performed in Buffer A using a fixed concentration of DNA (4 nM) and varying concentrations of protein (0-20 μM). Anisotropy measurements were performed using a FluoroMax-3 spectrofluorimeter (HORIBA Jobin Yvon) equipped with automated polarizers and regulated with a thermostated cuvette holder. The DNA and protein were allowed to equilibrate at each temperature for at least 30 minutes prior to

measuring the anisotropy. Titrations at higher temperatures (>45 ^{o}C) were performed in a capped cuvette to limit concentration changes due to evaporation. Fluorescence was excited at 550 nm, and the emission with various combinations of polarizers was monitored at 564 nm during a 5 sec integration time. The fluorescence anisotropy, *r*, was calculated automatically by the instrumental software using the equation:

$$r = \frac{I_{VV} - GI_{VH}}{I_{VV} + 2I_{VH}} \qquad \text{(Equation 3-3)}$$

where *I* is the polarized fluorescence intensity with subscripts *V* and *H* identifying either vertical or horizontal polarized light, respectively. The *G*-factor is a correction for the difference in sensitivities of detection for horizontal and vertically polarized light. In all titrations, protein was titrated into DNA. After each addition, the protein was equilibrated until no further change in anisotropy was detected, generally 1 minute. The fluorescence intensity of Cy3 is known to change with temperature.(*142*) Therefore, the slits were adjusted accordingly at each temperature to give a total fluorescence signal of approximately 10^6 counts per second (CPS) for each titration. As a control for specific binding, the absolute fluorescence intensity at 564 nm did not change significantly with addition of a high concentration of either Dpo1 or Dpo4 measured at the beginning and end of the experiment.

Anisotropy data were fit to either a single

$$v = \frac{A \times [P]}{K_d + [P]} \qquad \text{(Equation 3-4)}$$

or sequential binding sites equation

$$v = \frac{A_1 \times [P]}{K_{d_1} + [P]} + \frac{A_2 \times [P]^n}{(K_{d_2})^n + [P]^n} \quad \text{(Equation 3-5)}$$

or identical sites equation

$$v = \frac{A \times [P]^n}{(K_d)^n + [P]^n} \quad \text{(Equation 3-6)}$$

where *A* is the change in anisotropy, *P* is either Dpo1 or Dpo4 concentration, K_d is the dissociation constant for each binding event (subscript *1* or *2*), and n is the stoichiometry. At least three independent titrations were performed at each temperature to obtain average K_{d1} and K_{d2} parameters. K_{d1} *and* K_{d2} were used to directly calculate free energy change (ΔG^o) for monomer:

$$\Delta G^o = -RTlnK_1 \quad \text{(Equation 3-7)}$$

and oligomer (Dpo1 trimer or Dpo4 dimer):

$$\Delta G^o = -RTlnK_1 - nRTlnK_2 \quad \text{(Equation 3-8)}$$

where R is the universal gas constant and T is temperature.

Thermodynamic parameters were extracted from the temperature dependence of the Gibbs-Helmholtz plot from a multiparametric fit according to the following equations

$$\Delta G^o = \Delta H^o - T\Delta S^o = \Delta C_P^o \left[(T - T_H) - Tln\left(\frac{T}{T_S}\right) \right] \quad \text{(Equation 3-9)}$$

$$\Delta H^o = \Delta C_p^o (T - T_H) \qquad \text{(Equation 3-10)}$$

$$\Delta S^o = \Delta C_p^o ln\left(\frac{T}{T_S}\right) \qquad \text{(Equation 3-11)}$$

where ΔG^o is the standard free energy change, ΔH^o is the change in enthalpy, and ΔS^o is the change in entropy, using a constant heat capacity (ΔC_p^o) at each temperature, T. T_H is the temperature in which $\Delta H^o = 0$, T_S is the temperature where $T\Delta S^o = 0$.

The binding data were also fit to a van't Hoff plot of lnK_{app} versus 1000/T according to the following equation:

$$lnK_{app} = \frac{\Delta C_P^o}{R}\left[\left(\frac{T_H}{T}\right) - ln\left(\frac{T_S}{T}\right) - 1\right] \qquad \text{(Equation 3-12)}$$

where K_{app} is the apparent equilibrium constant and R is the universal gas constant.

Buried surface area calculations. Solvent accessible surface areas for Dpo4 bound to DNA (PDB ID: 2RDJ) were calculated for buried nonpolar (ΔA_{np}) and polar (ΔA_p) surface areas using a 1.4 Å probe radius as described.(*143, 144*) The heat capacity change ΔC_p^{SA} associated with binding was calculated from a surface area-based model according to Spolar *et al.*(*145*)

$$\Delta C_p^{SA}(cal\ mol^{-1}\ K^{-1}) = -(0.32)\Delta A_{np} + (0.14)\Delta A_p \qquad \text{(Equation 3-13)}$$

Polymerase/DNA binding simulations. The cumulative binding data for Dpo1 and Dpo4 were fit and modeled according to the minimal kinetic scheme outlined in Figure 3-11A and B using a simulation with Berkeley Madonna (University of California, Berkeley).

DNA polymerase processivity. Processivity experiments for Dpo1 and Dpo4 were performed and analyzed as previously described but at additional temperatures.(*120*) 5'-^{32}P end-labeling of a DNA primer was performed using Optikinase (USB) and ^{32}P -ATP according to manufacturer's directions. Primed M13mp18 DNA template (40 nM) was preincubated with various concentrations of Dpo1 or Dpo4 (as indicated in the Figure legends) at the experimental temperatures in Buffer A, and the reaction was initiated with the addition of dNTPs (0.1 mM each) and/ or 30 g single strand salmon sperm DNA (Invitrogen, Carlsbad, CA). One volume of stop solution [50 mM NaOH, 1 mM EDTA, 3% (w/v) Ficoll (Type 400, Pharmacia), 0.05 % (w/v) bromocresol green, 0.04 % (w/v) xylene cyanol] was added to terminate the processivity reactions after 60 minutes for 40 ^{o}C, 30 minutes for 50 ^{o}C, and 10 minutes for 60 or 70 ^{o}C reactions. Aliquots were run on an alkaline agarose gel (0.8% agarose, 50 mM NaOH, 1 mM EDTA) or denaturing 20% PAGE gel, dried and imaged using a Storm Phosphorimager (GE Healthsciences). Quantification of the mean band lengths was performed using ImageQuant software (v5.0) compared with a ^{32}P end labeled 1kb ladder (Invitrogen).

3.2 RESULTS

3.2.1 Detection of dimeric Dpo4

After purifying Dpo4, we noticed a small amount of protein consistent with a covalent dimer on SDS-PAGE gels, especially under non-reducing conditions. We investigated the validity of a possible Dpo4 dimer using protein cross-linking. Chemical crosslinkers, $BM(PEG)_3$, which targets native reduced cysteines, or EGS, which targets free amines in close proximity (<18 Å), were both used to capture a dimer in solution. Dpo4 contains a single native cysteine residue (C31) which allows for the possibility of inferring information about the structure of a crosslinked species. Using the thiol-thiol crosslinker [$BM(PEG_3)$], we were able to crosslink a dimeric Dpo4 both in the absence and presence of DNA (Figure 3-1A, lanes 2 and 3). There is no significant difference in the amount of crosslinked Dpo4 complex in the presence of DNA. Therefore, a monomer-dimer equilibrium exists both on and off DNA. Unreduced Dpo4 loaded onto the SDS-PAGE gel also shows a small quantity of dimeric product suggesting that a disulfide bond can form between subunits without added crosslinker (Figure 3-1A, lane 4). Reduction of this disulfide bond with TCEP reduces the fraction of dimer in favor of monomer (Figure 3-1, lane 1). We were also able to detect an equivalent reduced dimeric Dpo4 species using an amino-amino crosslinker (EGS) which crosslinks lysine residues in an interface. These crosslinking results suggest that dimeric Dpo4 complexes can exist in solution and that at least one conformation positions the single cysteine residue at the protein-protein interface, similar to that observed in an x-ray structure of Dpo4 bound to DNA (Figure 3-1B).(*146*)

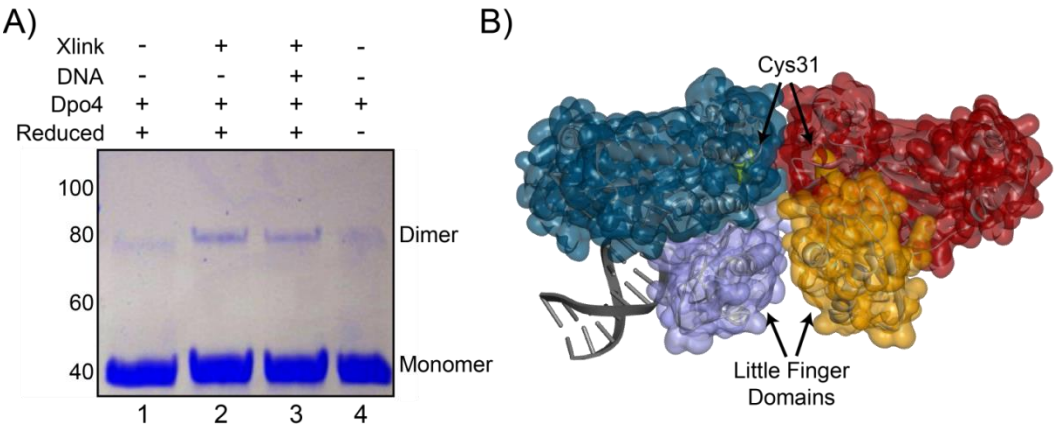

Figure 3-1. Dimeric Dpo4 complex formation. A) Covalent protein crosslinking of Dpo4 in the absence and presence of DNA hairpin or thiol-thiol crosslinker [$BM(PEG)_3$]. Lane 1: reduced Dpo4, Lane 2: reduced Dpo4 with crosslinker, Lane 3: reduced Dpo4-DNA complex (37-nt hairpin) with crosslinker, and Lane 4: unreduced Dpo4. The positions corresponding to monomer (40 kDa) and dimer (80 kDa) form of Dpo4 are shown in the right margin. B) X-ray structure of one possible dimeric Dpo4 conformation found in the crystal unit (PDB ID: 2W9B) consistent with crosslinking at the C31 interface between molecules. Highlighted in purple and orange surfaces are the little finger domains from each Dpo4 molecule.

3.2.2 Stoichiometry of Dpo4 binding to DNA by isothermal titration calorimetry

In order to verify that a dimeric Dpo4 complex can exist on DNA over a broad temperature range, we used ITC to quantify the thermodynamics and stoichiometry of binding at 15 °C and 60 °C (Figure 3-2). At 15 °C, binding is primarily entropically driven, and a fit of the binding isotherm to Equation 3-1 gave the following values: K_{app} = 6.5 ± 0.6 x 10^5 M^{-1}, ΔH^o_{ITC} = 8.1 ± 0.2 kcal mol^{-1}, and n = 0.64 ± 0.01. The resulting ΔG^o_{ITC} is –7.7 kcal mol^{-1} and the calculated entropic contribution ($T\Delta S_{ITC}$) is 15.7 kcal mol^{-1}. At 60 °C the binding is primarily enthalpically driven, and a fit of the binding isotherm to Equation 3-1 gave K_{app} = 2.2 ± 0.5 x 10^6 M^{-1}, ΔH^o_{ITC} = -8.0 ± 0.5 kcal mol^{-1}, and n = 0.66 ± 0.01. The resulting ΔG^o_{ITC} is -9.7 kcal mol^{-1} and the calculated $T\Delta S_{ITC}$ is 1.7 kcal mol^{-1}. Importantly, the stoichiometries at 15 °C and 60 °C are similar and are consistent with more than one molecule of Dpo4 bound to DNA. A dimer was

also seen using chemical crosslinking. Although the titrations appear to go to completion, the stoichiometries do not saturate to n = 0.5 (two Dpo4 molecules per DNA) indicating that the dimeric Dpo4 complex is in equilibrium with monomer-DNA complex under these conditions.

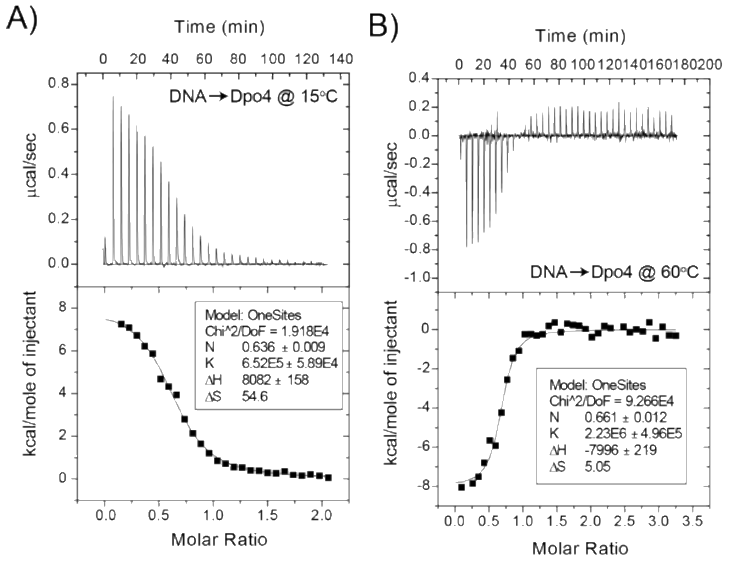

Figure 3-2. Stoichiometry and thermodynamics of Dpo4 binding to DNA. ITC titration of 400 µM DNA hairpin into 25 µM *Sso*Dpo4 at A) 15 ^{o}C and B) 60 ^{o}C as described in Materials and Methods. Data were fit using Equation 3-1 to yield stoichiometries (n) 0.64 ± 0.01 or 0.66 ± 0.01 (DNA:Dpo4), apparent equilibrium association constants (K_{app}) 6.52 ± 0.59 x 10^5 or 2.23 ± 0.50 x 10^6 M, enthalpy changes (ΔH^o_{ITC}) 8.08 ± 0.16 or 8.00 ± 0.22 kcal mol^{-1}, and entropy changes (ΔS^o_{ITC}) 54.6 or 5.1 cal mol^{-1} K^{-1} at 15 ^{o}C and 60 ^{o}C, respectively.

3.2.3 Analytical velocity sedimentation detects the formation of oligomeric Dpo1 and Dpo4 complexes with DNA

Analytical ultracentrifugation (AUC) sedimentation velocity experiments were performed with either protein alone (Dpo1 or Dpo4) at 10, 20 or 30 ^{o}C to monitor the concentration and any temperature dependent equilibria. For either Dpo1 or Dpo4 alone, there was an increase in the peak position of the sedimentation reaction boundary, *ls-g*(s)*, with concentration (1 or 10 µM),

as expected at each temperature based on 280 nm detection. The sedimentation reaction boundaries were corrected for changes in the diffusion coefficient with temperature to give the sedimentation coefficient, $s_{20,w}$, and represent solution equilibrium distribution values for each experimental condition. Increasing the concentration of Dpo4 from 1 to 10 μM did not change the $s_{20,w}$ values significantly. At constant concentrations of Dpo1 or Dpo4, the weight average $s_{20,w}$ value shifts slightly larger with increasing temperature (Figure 3-3). Analysis of the reaction boundaries for 10 M Dpo1 resulted in weight average $s_{20,w}$ distribution values of 4.19 ± 0.01, 4.29 ± 0.01, and 4.32 ± 0.01 for 10, 20, and 30 °C, respectively. Similarly, analysis of the reaction boundaries for 10 μM Dpo4 resulted in weight average $s_{20,w}$ distribution values of 2.52 ± 0.01, 2.55 ± 0.01, and 2.59 ± 0.01 for 10, 20, and 30 °C, respectively. Increasing $s_{20,w}$ values are consistent with a shift in the equilibrium towards formation of larger species. For protein alone (Dpo1 or Dpo4), these changes in $s_{20,w}$ are only slightly significant over this limited temperature range.

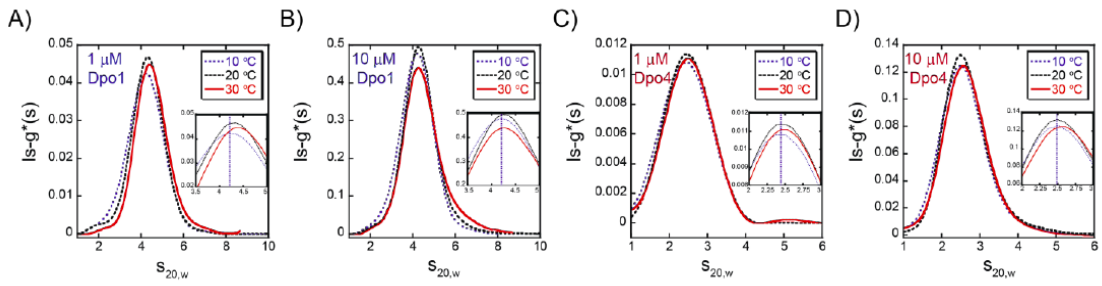

Figure 3-3. Analytical ultracentrifugation (AUC) velocity absorbance experiments of Dpo1 and Dpo4 alone. Shown are the *ls-g*(s)* distribution profiles for A) 1 μM or B) 10 μM Dpo1 or C) 1 μM or D) 10 μM Dpo4 alone at 10 (blue), 20 (black), or 30 °C (red). The inset highlights the region of the weigh average $s_{20,w}$ values, and the vertical blue line indicates the weight average $s_{20,w}$ value at 10 °C.

More specific information on complex assembly can be obtained by examining the reaction boundaries for titration of each polymerase with a constant concentration (50 nM) of fluorescent hairpin primer-template DNA using analytical ultracentrifugation fluorescence-detected sedimentation (AU-FDS) (*147*). By monitoring the reaction boundaries of fluorescent DNA in the AUC velocity experiments, we are able to examine a much greater dynamic range of protein concentrations (50 - 5000 nM) than with absorbance alone. Titration of Dpo1 at 10, 20, and 30 ^{o}C shows a clear increase in the $s_{20,w}$ distributions and boundaries with concentration, consistent with the detection of multiple protein bound DNA complexes (Figure 3-4A-C). Here, discrete $s_{20,w}$ populations for monomeric and trimeric Dpo1 can be identified. Interestingly, the $s_{20,w}$ reaction boundaries at identical concentrations of Dpo1 bound to DNA shift towards larger species with increasing temperature more significantly than for the free protein alone. For example, specifically examining 100 nM Dpo1 across the three temperatures, the weight average $s_{20,w}$ values increase with increasing temperature: 4.66 ± 0.03, 4.77 ± 0.01, to 4.86 ± 0.01 at 10, 20, and 30 ^{o}C, respectively (Figure 3-5A). At 1 μM Dpo1, the weight average $s_{20,w}$ values increase from 5.71 ± 0.01, 5.89 ± 0.01, to 6.04 ± 0.01 at the same temperatures, respectively (Figure 3-5B).

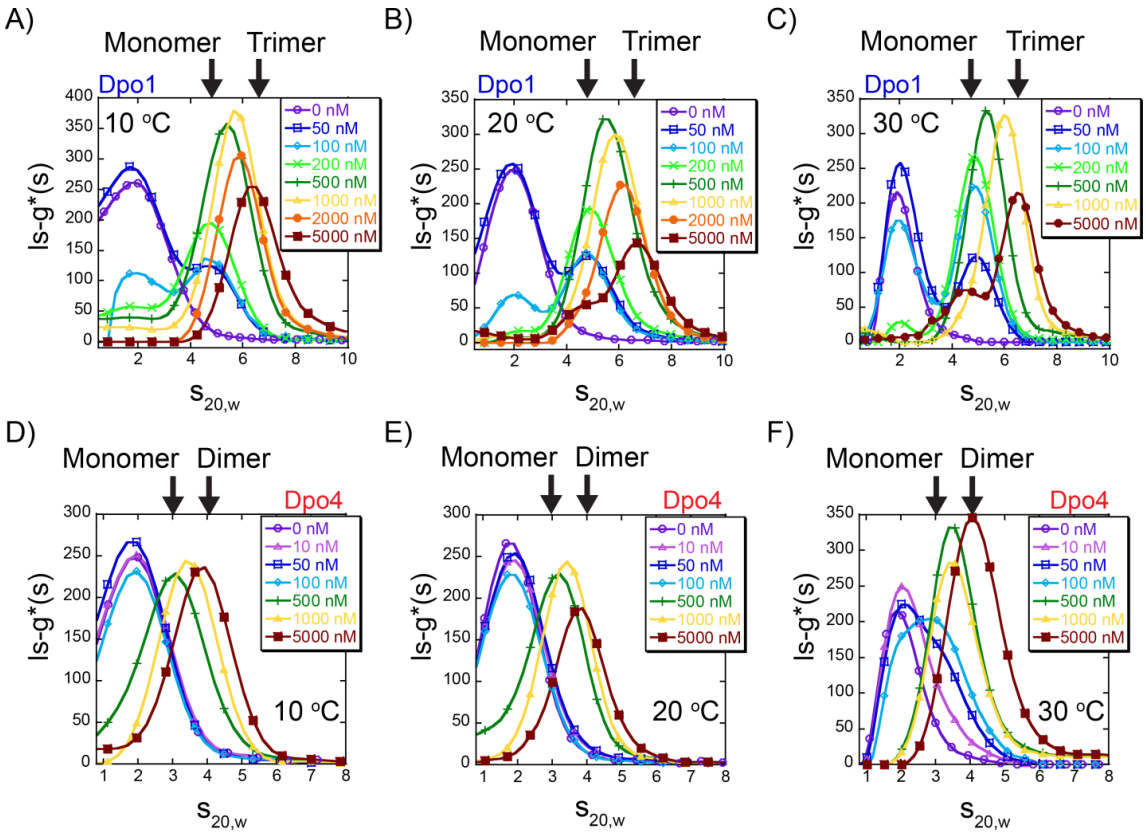

Figure 3-4. Solution assembly of oligomeric polymerases on DNA. Analytical ultracentrifugation velocity fluorescence detected sedimentation (AU-FDS) experiments showing the *ls-g*(s)* distribution profiles as a function of Dpo1 or Dpo4 concentrations: 0 (-○-, purple) , 10 (-Δ-, pink), 50 (-□-, blue), 100 (-◊-, cyan), 200 (-x-, light green), 500 (-+-, dark green), 1000 (-▲-, yellow), 2000 (-●-, orange) and 5000 nM (-■-, brown) at A) and D) 10 ^{o}C , B) and E) 20 ^{o}C , or C) and F) 30 ^{o}C, respectively. Every fifth data point is indicated for simplicity and all data were fit as described in Materials and Methods. $s_{20,w}$ positions representing monomer or trimer Dpo1 and monomer or dimer Dpo4 are indicated by arrows.

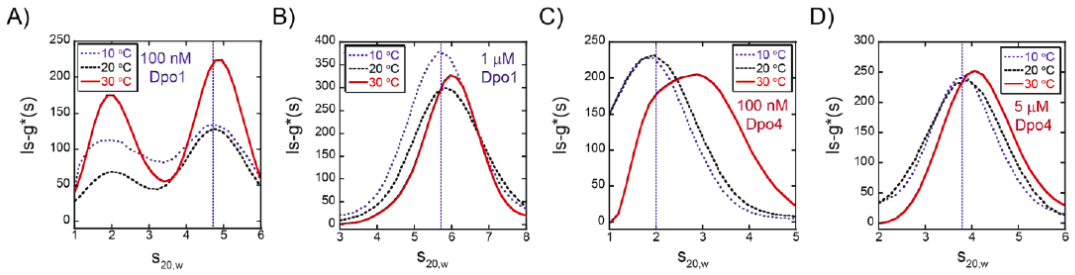

Figure 3-5. Analytical ultracentrifugation velocity fluorescent experiments (AU-FDS) of Dpo1 and Dpo4 bound to DNA. Shown are the *ls-g*(s)* distribution profiles for 50 nM fluorescent DNA hairpin primer-template and Dpo1 at A) 100 nM and B) 1 µM or Dpo4 at C) 100 nM and D) 5 µM as a function of temperature [10 (blue dotted) , 20 (black dotted), and 30 °C (red solid)]. Data was analyzed as described in Materials and Methods. The vertical dotted blue line indicates the position of the weight average *s20,w* value at 10 °C.

Titration of Dpo4 on fluorescent hairpin primer-template DNA using AU-FDS also shows an increase in the $s_{20,w}$ boundaries at each temperature (Figure 3-4D-F) consistent with populations consisting of both monomeric and dimeric Dpo4-DNA complexes. Binding of Dpo4 to DNA does not appear to occur until the Dpo4 concentration exceeds 100 nM at 10, 20, or 30 °C. Moreover, the reaction boundary continually shifts to larger species between 500 - 5000 nM. Similar to the behavior of Dpo1, the reaction boundaries at constant concentrations of Dpo4 measured at 10, 20, and 30 °C also increase or shift to slightly larger weight-average complexes more significantly than protein alone. Examination of 5 µM Dpo4 across the three temperature ranges (10, 20, and 30 °C) shows that the weight average $s_{20,w}$ values increase from 3.79 ± 0.02, 3.84 ± 0.01, to 4.12 ± 0.01, respectively (Figure 3-5D). The equilibrium shift in the sedimentation coefficients with temperature can be most clearly seen at 100 nM Dpo4 (Figure 3-5C) where initial binding is only observed at 30 °C. This observation agrees well with the fluorescence anisotropy data below which measures a K_{d1} value of 0.130 ± 0.004 µM at 33 °C but has larger K_{d1} values at lower temperatures (Table 3-1).

3.2.4 Temperature dependent separation of polymerase binding events using fluorescence anisotropy

In order to investigate further the individual binding events of Dpo1 or Dpo4 on DNA, we used fluorescence anisotropy to evaluate the constants for the monomeric (K_{d1}) and subsequent oligomeric (K_{d2}) binding steps over a range of temperatures. The melting temperature (T_M) of the DNA primer template hairpin was measured from a shift in the UV absorbance and found to be 88 ^oC, which is well above our experimental temperature range. Dpo1 and Dpo4 were titrated into low concentrations of a Cy3 labeled DNA primer template hairpin and the increase in fluorescence anisotropy due to binding was monitored (Figure 3-6). The increase in anisotropy as a function of Dpo1 concentration was fit to each of a single (Equation 3-4), a sequential (Equation 3-5), or an identical-sites mode (Equation 3-6). The sequential mode fit best to the fluorescence anisotropy data of both Dpo1 and Dpo4. While single binding mode gave a significant larger chi-square factor, the identical-sites mode had only slightly larger chi-square value than the sequential mode. However, in Chapter 2 and Chapter 4, EMSA experiments demonstrate that the binding is comprised of an initial high-affinity binding site followed by a second sequential lower-affinity binding. The second and third individual binding events for Dpo1 cannot be separated from our EMSA or ITC data (Chapter 4) suggesting that simultaneous or cooperative binding is probable.(*120*) Therefore, the sequential binding mode better represents the binding scenario. The fits to these individual equations to the data are consistent with stoichiometric values and processes measured by ITC, chemical crosslinking, AUC, EMSA, and gel filtration.(*120*) The differences in the individual K_d values (1 and 2) for each DNA polymerase are greater than 10-fold (Table 3-1) and generally decrease concurrently with temperature up to 50 ^oC. K_{d2}, fit from the anisotropy experiments, is the intrinsic constant for

binding of one of the two monomers in the second step, while K_{d2}^2 represents the constant for simultaneous binding of both Dpo1 monomers in the second "step" to form the trimeric Dpo1-DNA complex.

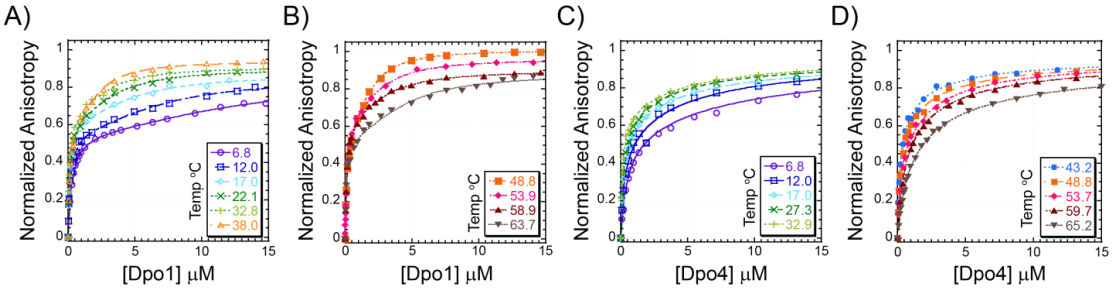

Figure 3-6. Quantification of individual binding steps leading to oligomeric polymerase-DNA complexes. Representative normalized individual equilibrium fluorescence anisotropy titrations for A) - B) Dpo1 and C) - D) Dpo4 binding to DNA at low or high temperatures, respectively. Data are included for both lower 6.8 (-○-, purple), 12.0 (-□-, blue), 17.0 (-◊-, cyan), 22.1 or 27.3 (-x-, dark green), 32.8 or 32.9 (-+-, light green), 38.0 (-Δ-, light orange) and upper temperatures 43.3 (-●-, blue), 48.8 (-■-, dark orange), 53.7 or 53.9 (-♦-, pink), 58.9 or 59.7 (-▲-, brown), and 63.7 or 65.7 ^{o}C (-▼-, grey). The individual data points were fit to Equation 3-5 to determine K_{d1} and K_{d2} values for Dpo4 or Dpo1, respectively. At least three independent titrations were performed and fit at each temperature and the resulting values are reported in Table 3-1.

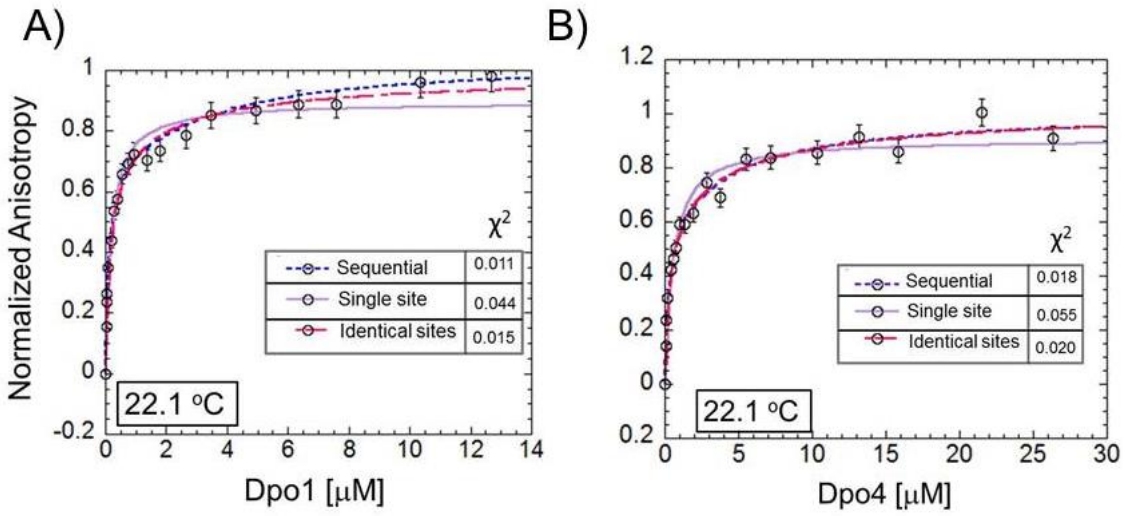

Figure 3-7. Representative equilibrium fluorescence anisotropy titrations. A) Dpo1 at 22.1 °C binding to a 5' Cy3 labeled DNA hairpin. The purple solid line (χ^2 = 0.044) show the fit for single binding (Dpo1 $K_{d,app}$ = 0.185 ± 0.021) (Equation 3-4). The blue dashed line (χ^2 = 0.011) shows the fits for a sequential binding mode (Dpo1 K_{d1} = 0.110 ± 0.021 μM and K_{d2} = 3.82 ± 1.67 μM) (Equation 3-5). The red dashed line (χ^2 = 0.015) shows the fits for an identical-sites mode (Dpo1 $K_{d,app}$ = 0.270 ± 0.038) (Equation 3-6) B) Dpo4 at 22.1 °C binding to a 5' Cy3 labeled DNA hairpin. The purple solid line (χ^2 = 0.055) shows the fit for single binding (Dpo4 $K_{d,app}$ = 0.540 ± 0.070) (Equation 3-4). The blue dashed line (χ^2 = 0.0018) shows the fits for a sequential binding mode (Dpo4 K_{d1} = 0.178 ± 0.102 μM and K_{d2} = 4.23 ± **2.73 μM) (Equation 3-5). The red dashed line (χ^2 = 0.020) shows the fits for an identical-sites mode (Dpo1 $K_{d,app}$ = 0.860 ± 0.186) (Equation 3-6)**

Table 3-1Equilibrium fluorescence anisotropy binding parameters for polymerase binding to DNA

Dpo1			Dpo4		
Temp (°C)	K_{d1} (μM)[a]	K_{d2} (μM)[a]	Temp (°C)	K_{d1} (μM)[a]	K_{d2} (μM)[a]
6.8	0.322 ± 0.023	17.2 ± 0.3	6.8	0.435 ± 0.116	9.32 ± 0.88
12.0	0.208 ± 0.057	8.01 ± 1.21	12.0	0.329 ± 0.107	5.16 ± 0.05
17.0	0.170 ± 0.023	5.78 ± 0.13	17.0	0.214 ± 0.003	4.70 ± 1.01
22.2	0.109 ± 0.016	4.70 ± 0.78	22.1	0.176 ± 0.010	3.22 ± 0.72
27.4	0.105 ± 0.003	3.70 ± 0.32	27.3	0.164 ± 0.009	2.82 ± 0.35
32.8	0.094 ± 0.001	2.68 ± 0.11	32.9	0.130 ± 0.004	3.01 ± 0.92
38.0	0.097 ± 0.003	2.48 ± 0.06	37.8	0.140 ± 0.066	2.33 ± 0.40
43.3	0.144 ± 0.003	2.60 ± 0.22	43.2	0.133 ± 0.026	1.72 ± 0.46
48.8	0.144 ± 0.015	1.82 ± 0.36	48.8	0.125 ± 0.051	2.32 ± 0.95
53.9	0.113 ± 0.032	2.41 ± 0.79	53.8	0.155 ± 0.065	2.71 ± 0.99
58.9	0.208 ± 0.022	3.21 ± 0.21	58.9	0.444 ± 0.115	3.81 ± 0.28
63.7	0.198 ± 0.026	4.52 ± 0.40	65.2	0.674 ± 0.080	7.18 ± 0.93

[a]K_{d1} and K_{d2} are the equilibrium dissociation constants for the first and second binding events, respectively. Values are means and standard errors from parameters fit to Equation 3-5 from at least three independent titration experiments at each temperature.

The temperature dependences of the monomeric and trimeric binding equilibria for Dpo1 to DNA are plotted in a Gibbs-Helmholtz plot (ΔG^o vs. T) (Figure 3-8A) or a van't Hoff plot (*lnK* vs. 1000/T) (Figure 3-8B), and reported in Table 3-2 and 3-3. Analysis by these two methods allows for easy visualization of any nonlinearity in the temperature dependence of binding for each molecular event. The overall free energy for trimeric Dpo1 binding to DNA is the sum of the free energies for the first and second binding steps, where the second "step" represents the simultaneous or cooperative binding of two additional monomers to the monomeric Dpo1-DNA complex (described in Table 3-4). The free energy minima for monomeric and trimeric Dpo1 binding both occur at ~61 ^{o}C. The predicted critical temperatures for T_H (where $\Delta H = 0$) and T_S (where $T\Delta S = 0$) are 36 ℃ and 60 ^{o}C for monomeric and 41 ℃ and 60 ℃ for trimeric Dpo1, respectively. T_H represents the temperature where K_a is at a maximum, and T_S represents the temperature where ΔG is most favorable. This binding behavior is indicative of a temperature dependent binding enthalpy (ΔH^o) with fitted heat capacity changes (ΔC^o_p) (Equation 3-9) for monomer and trimeric Dpo1 binding equal to –0.43 ± 0.07 cal mol^{-1} K^{-1} and -1.02 ± 0.12 cal mol^{-1} K^{-1}, respectively (Table 3-2). The parallel large decreases in ΔH^o and $T\Delta S^o$ with temperature are compensatory, resulting in smaller changes in ΔG^o, and are generally characteristic of sequence specific DNA binding proteins (Figure 3-9A and B).(*128, 129, 148*) It seems possible that Dpo1 and the DNA at the primer-template junction achieve a degree of structural complementarity comparable to that in sequence-specific protein-DNA interfaces, thus making a significant contribution to the large negative C^o_p. Subsequent structural specific binding of two additional molecules of Dpo1 at that site completes the trimeric Dpo1-DNA complex as identified previously by DNA footprinting.(*120*)

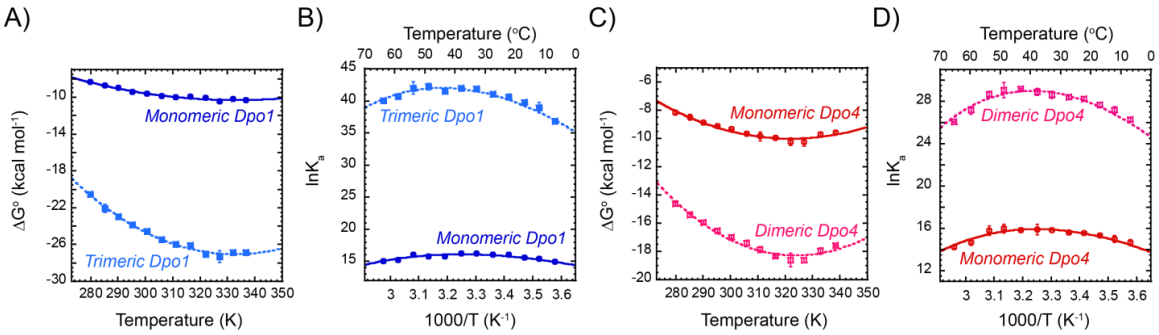

Figure 3-8. Thermodynamic differences of monomeric and oligomeric Dpo1 and Dpo4 binding to DNA. Gibbs-Helmholtz plots of free energy of binding (DG^o) for A) monomeric (solid -●-, blue) or trimeric (dashed -■-, light blue) Dpo1 and C) monomeric (solid -○-, red) or dimeric (dashed -□-, pink) Dpo4 as a function of temperature. Error bars represent the standard error from multiple experiments at each point. Lines show the fits of the data to Equation 3-9 giving C^o_p (cal mol^{-1} K^{-1}) values of for monomeric (-0.43 ± 0.07) and trimeric (-1.45 ± 0.14) Dpo1 and monomeric (-0.68 ± 0.10) and dimeric (-1.22 ± 0.15) Dpo4. van't Hoff plots highlighting the individual binding states for B) Dpo1 or D) Dpo4. Lines show the fits to Equation 3-12.

Table 3-2 Thermodynamic parameters for DNA binding by Dpo1.

	Monomeric Dpo1			**Trimeric Dpo1**		
Temp (^oC)	G^o (kcal mol^{-1})[a]	H^o (kcal/mol)[c]	$T\Delta S^o$ (kcal mol^{-1})[c]	ΔG^o (kcal mol^{-1})[b]	ΔH^o (kcal/mol)[c]	$T\Delta S^o$ (kcal mol^{-1})[c]
6.8	-8.3 ± 0.1	12.3	20.7	-20.5 ± 0.1	49.1	69.8
12.0	-8.7 ± 0.2	10.1	18.9	-22.1 ± 0.4	41.6	63.5
17.0	-9.0 ± 0.1	8.0	17.0	-23.0 ± 0.1	34.4	57.3
22.2	-9.4 ± 0.1	5.8	15.1	-23.9 ± 0.3	26.8	50.7
27.4	-9.6 ± 0.1	3.6	13.2	-24.6 ± 0.1	19.3	44.0
32.8	-9.8 ± 0.1	1.3	11.1	-25.5 ± 0.1	11.5	36.9
38.0	-10.0 ± 0.2	-0.9	9.0	-26.0 ± 0.2	4.0	30.0
43.3	-9.9 ± 0.1	-3.2	6.9	-26.1 ± 0.1	-3.7	22.7
48.8	-10.1 ± 0.1	-5.5	4.7	-27.0 ± 0.3	-11.7	15.1
53.9	-10.4 ± 0.2	-7.7	2.6	-27.3 ± 0.6	-19.1	7.9
58.9	-10.2 ± 0.1	-9.8	0.5	-26.9 ± 0.2	-26.3	0.7
63.7	-10.4 ± 0.1	-11.8	-1.6	-26.9 ± 0.1	-33.2	-6.3

[a]Calculated from the Gibbs free energy Equation 3-7, $\Delta G^o = -RTlnK_1$ for monomeric Dpo1 binding. [b]Calculated from the Gibbs free energy Equation 3-8, $\Delta G^o = -RTlnK_1 - 2RTlnK_2$ for formation of the trimeric Dpo1-DNA complex. [c]The predicted enthalpy (ΔH^o) and entropy ($T\Delta S^o$) components are calculated from the fit to the Gibbs-Helmholtz Equations 3-9~11.

Table 3-3 Thermodynamic parameters for DNA binding by Dpo4.

	Monomeric Dpo4			Dimeric Dpo4		
Temp (^{o}C)	ΔG^o (kcal mol^{-1})[a]	ΔH^o (kcal/mol)[c]	$T\Delta S^o$ (kcal mol^{-1})[c]	ΔG^o (kcal mol^{-1})[b]	ΔH^o (kcal/mol)[c]	$T\Delta S^o$ (kcal mol^{-1})[c]
6.8	-8.2 ± 0.2	18.6	26.6	-14.6 ± 0.1	35.4	49.9
12.0	-8.5 ± 0.2	15.0	23.5	-15.4 ± 0.2	29.0	44.4
17.0	-8.9 ± 0.1	11.6	20.5	-16.0 ± 0.1	22.9	39.0
22.1	-9.1 ± 0.1	8.2	17.4	-16.5 ± 0.1	16.7	33.4
27.3	-9.3 ± 0.1	4.6	14.1	-17.0 ± 0.1	10.3	27.5
32.9	-9.7 ± 0.1	0.8	10.5	-17.4 ± 0.1	3.5	21.1
37.8	-9.8 ± 0.3	-2.5	7.3	-17.9 ± 0.2	-2.5	15.4
43.2	-10.0 ± 0.1	-6.2	3.8	-18.3 ± 0.1	-9.1	9.0
48.8	-10.2 ± 0.3	-10.0	-0.02	-18.6 ± 0.5	-16.0	2.3
53.8	-10.3 ± 0.3	-13.4	-3.4	-18.6 ± 0.2	-22.1	-3.8
58.9	-9.7 ± 0.2	-17.4	-7.6	-18.0 ± 0.2	-29.3	-11.2
65.2	-9.6 ± 0.1	-21.2	-11.5	-17.6 ± 0.1	-36.2	-18.3

[a]Calculated from the Gibbs free energy Equation 3-7, $\Delta G^o = -RT\ln K_1$ for monomeric Dpo4 binding. [b]Calculated from the Gibbs free energy Equation 3-8, $\Delta G^o = -RT\ln K_1 - RT\ln K_2$ for formation of the dimeric Dpo4-DNA complex. [c]The predicted enthalpy (ΔH^o) and entropy ($T\Delta S^o$) components are calculated from the fit to the Gibbs-Helmholtz Equations 3-9~11.

Table 3-4 Definition of Equilibrium Steps and Polymerase States.

	Dpo1		Dpo4	
Step[a]	K_{app}	$\Delta C°_{P\ (app)}$	K_{app}	$\Delta C°_{P\ (app)}$
First	K1	–0.43	K_1	–0.68
Second	$K2^2$	–1.02	K_2	–0.51
Overall [b]	$K_1K_2^2$	-1.45	K_1K_2	-1.22
a As measured from fluorescence anisotropy. [b] Product of equilibrium constants leading to trimetric Dpo1 and dimeric Dpo4				

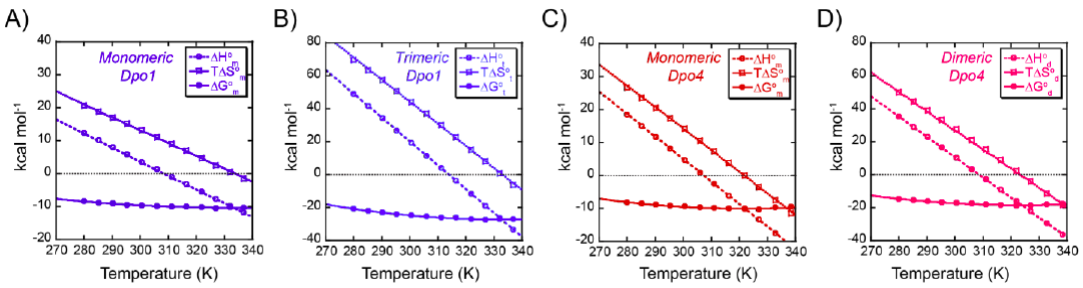

Figure 3-9. Fitted thermodyanamic parameters ΔH^o (dashed -○-) , $T\Delta S^o$ (dotted -□-), and ΔG^o (solid -●-), for A) monomeric Dpo1 (dark blue) B) trimeric Dpo1 (light blue), C) monomeric Dpo4 (red), or D) dimeric Dpo4 (pink) assemblies on DNA primer template plotted from values in Tables 3-2 and 3-3

Dpo4 also shows a nonlinear temperature dependence of binding for both the monomer and dimer, as visualized in a Gibbs-Helmholtz plot (Figure 3-8C) or van't Hoff plot (Figure 3-8D), and reported in Table 3-4. The free energy minima for monomeric and dimeric Dpo4 assemblies occur at ~49 ^{o}C, and 51 ^{o}C, respectively. The predicted critical temperatures for T_H and T_S are 34 ^{o}C and 49 ^{o}C for monomeric and 39 ^{o}C and 55 ^{o}C for dimeric Dpo4, respectively. The temperature at which Dpo4 binding shifts from primarily entropically driven to enthalpically driven occurs in the range of 35 ^{o}C to 40 ^{o}C and is consistent with the ITC results from Figure 3-2. This binding behavior is also indicative of a temperature dependent ΔH^o with fitted ΔC^o_p values (Equation 3-9) for monomer and dimeric Dpo4 binding of -0.68 ± 0.09 cal mol^{-1} K^{-1} and -1.22 ± 0.15 cal mol^{-1} K^{-1}, respectively. Again, parallel changes in ΔH and $T\Delta S$ with temperature are indicative of temperature dependent enthalpy/entropy compensation (Figure 3-9 C and D).

3.2.5 Calculated ΔC_p values from burial of nonpolar and polar surfaces upon Dpo4-DNA complex formation

The burial of polar and nonpolar surface areas upon binding has been used as a predictive measure relating structural details to thermodynamic parameters. Heat capacity data for the transfer of small molecule model hydrocarbons and amides from the liquid state to the aqueous solution were used to obtain an empirical relationship for the calculation of ΔC_p^{ASA} (see Equation 3-13) from computed values of changes in nonpolar and polar surfaces upon protein folding or protein-ligand interaction.(*145, 149*) For the folding of many proteins and the interaction of proteins with small ligands, there has been adequate agreement between the experimentally observed ΔC_p values and those predicted from burial of surface area. However, for association of macromolecules and some protein-folding reactions, there are many additional solution factors that contribute to the strongly negative observed ΔC_p values. A significant source of the discrepancy between ΔC^o_p and ΔC_p^{ASA} values is the restriction of configurational (conformational-vibrational) degrees of freedom upon association.(*134, 150-154*)

Although the buried surface area for Dpo1 binding to DNA cannot be determined directly due to the lack of an appropriate crystal structure, 3437 $Å^2$ of surface area are buried when a Dpo4 monomer binds to primer template DNA.(*143*) The changes in polar (ΔA_p) and nonpolar (ΔA_{np}) solvent accessible surface area upon Dpo4 binding to DNA are -1753 $Å^2$ and -1683 $Å^2$, respectively. From these values, we calculate a ΔC_p^{ASA} value of -0.29 cal mol^{-1} K^{-1} at 25 ^oC for monomeric Dpo4 binding to DNA from surface area contributions alone. As noted above,

although the burial of nonpolar (ΔA_{np}) or polar (ΔA_p) surface areas is often considered the most important factor contributing to ΔC^o_p, other factors such as electrostatics, solvation, protonation, conformational strain, thermal or vibrational fluctuations, and linked equilibria can often have much larger contributions to ΔC^o_p accounting for deviation from the experimental value.(*155*)

3.2.6 Modeling temperature dependent binding populations of Dpo1 and Dpo4

Using a sequential assembly scheme with a cooperativity parameter for Dpo1 or with no cooperativity parameter for Dpo4, and the parameters from the anisotropy experiments, we are able to model the relative populations of monomer or oligomer for Dpo1 or Dpo4 bound to DNA as a function of temperature (Figure 3-10). Using this analysis, there is both a concentration and temperature dependent effect on the formation of monomeric or oligomeric Dpo1 or Dpo4. Below 400 nM, there is preferential binding of a monomeric Dpo1 and Dpo4 to DNA. In the range between 400 – 2000 nM, there is a mixed population of monomer and oligomeric Dpo1 or Dpo4 complexes with DNA. At concentrations greater than 2 μM, there is preferential binding of trimeric Dpo1 and dimeric Dpo4. In this analysis, it is also clear that the assemblies and populations are influenced by temperature. For Dpo1, there is an increase in affinity for both the first and second binding events up to 50 ^{o}C. Above 50 ^{o}C, there is a slight decrease in the second binding step in favor of the first. A similar trend occurs for Dpo4 with the cutoff being around 45 ^{o}C. More than 50% of the Dpo1 population exists in a trimeric state at concentrations greater than 1.5 μM while a Dpo4 concentration of 3 μM is required for 50% dimer.

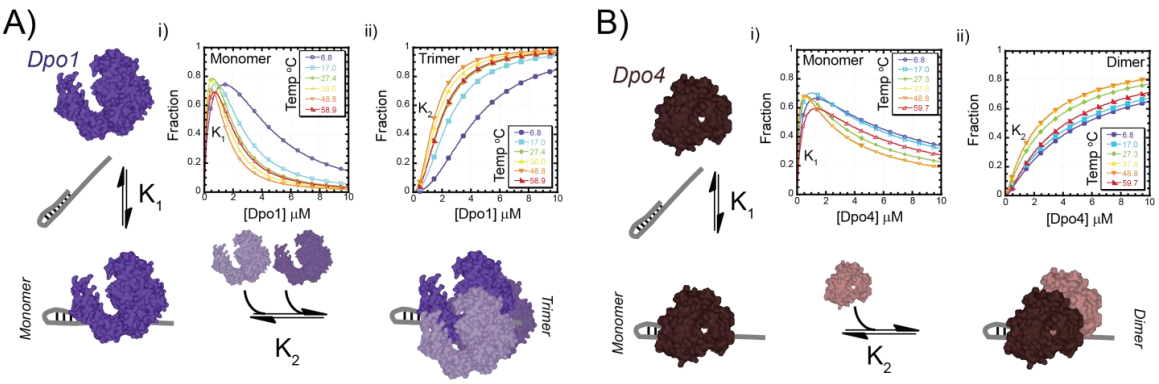

Figure 3-10. Concentration dependent assembly of oligomeric polymerase-DNA complexes. A) Trimeric Dpo1 assembly on DNA follows initial higher affinity binding of one molecule (K_1) followed by a second step of cooperative assembly of two additional molecules (K_2). B) Dimeric Dpo4 assembly on DNA that includes two sequential binding events with differing affinities (K_1 and K_2). Simulations of the relative populations for monomeric i) Dpo1 or Dpo4 (open symbols, representing K_1) or ii) trimeric Dpo1 or dimeric Dpo4 (closed symbols, representing K_2) as a function of temperature and concentrations as described in the Supporting Information. Simulations are shown for 6.8 (purple ○ or ●), 17.0 (cyan □ or ■), 27.4 (green ◊ or ♦), 38.0 (yellow Δ or ▲), 48.8 (orange ▽ or ▼), and 58.9 or 59.7 (red ◺ or ◣) ^{o}C temperatures.

3.2.7 Dpo1 and Dpo4 Processivities Increase with Temperature and Concentration

To provide a biochemical explanation for the different binding specificities for DNA polymerases across a variety of temperatures, we assayed the temperature dependent polymerization processivity for Dpo1 and Dpo4. Processivity is a measure of the stability of an enzyme substrate complex during successive catalytic steps. Processive DNA polymerases have a higher rate constant for the catalytic step of DNA synthesis (k_{pol}) than for dissociation from the template (k_{dis}).(*156*) The ratio between these kinetic parameters determines the processivity value. The processivity for Dpo4 has been measured previously over a limited concentration range of 0.5 – 200 nM representing primarily monomer, and although there is a slight increase in processivity with concentration, it was concluded that Dpo4 is essentially a distributive enzyme with processivity value of 1 to 2 nucleotides.(*117*) Interestingly, in processivity reactions where the concentration of Dpo4 was in 20-fold excess to DNA, products of over a hundred nucleotides

in length were synthesized, suggesting that polymerase interactions may modestly increase processivity. Another report of processivity when DNA template was in excess to Dpo4 (35 nM) gave a value of 16 at 37 ^{o}C.(*123*) More strikingly, we have previously measured a large increase in processivity for Dpo1 when it is in the trimeric conformation over that of the monomeric form.(*120*)

We have performed additional DNA polymerization experiments at various temperatures (40, 50, 60 and 70 ^{o}C) to determine if higher temperatures promote greater rates or processivities for Dpo1 due to increased binding specificity. Both kinetic and processivity experiments were performed at either 200 nM or 2.0 μM Dpo1 to represent contributions from primarily monomeric or trimeric species, respectively (Figure 3-11A). We chose 40 ^{o}C over room temperature experiments due to slower rates of synthesis that would limit detection. The DNA synthesis rate for trimeric Dpo1 at 40, 50, 60, and 70 ^{o}C was measured to be 36 ± 3, 209 ± 4, 447 ± 30, and 529 ± 35 bp/min, respectively, and always greater than monomeric Dpo1 rate at 36 ± 12, 76 ± 14, 366 ± 45, and 400 ± 55 bp/min, respectively (Figure 3-12). Processivity experiments were initiated with the simultaneous addition of dNTPs and a high concentration of unlabeled DNA trap. Polymerase molecules that dissociate from the prebound radioactive primer-M13 template will be captured by binding to a cold DNA substrate and no longer contribute to the signal for the experiment. The concentration of trap required to be effective at all polymerase concentrations was determined empirically by titrating trap until no further increase in processivity was noted. Reactions were incubated for different times at each temperature depending on the rate of synthesis. Dpo1 processivity at 200 nM (representing monomer) increased slightly with increasing temperature from 41 ± 12, 62 ± 14, 187 ± 45, and 220 ± 56 nucleotides at 40, 50, 60, and 70 ^{o}C, respectively, (Figure 3-11B). The processivity at 2 M

(representing trimer) increased more dramatically from 98 ± 2, 493 ± 5, 933 ± 39, to 1191 ± 52 nucleotides at 40, 50, 60, and 70 °C, respectively (Figure 3-11B). At temperatures greater than or equal to 50 °C, the processivity of the trimeric state of Dpo1 is much greater than that of the monomeric complex and reflects a change in the specificity of binding DNA consistent with the fluorescence anisotropy data presented above.

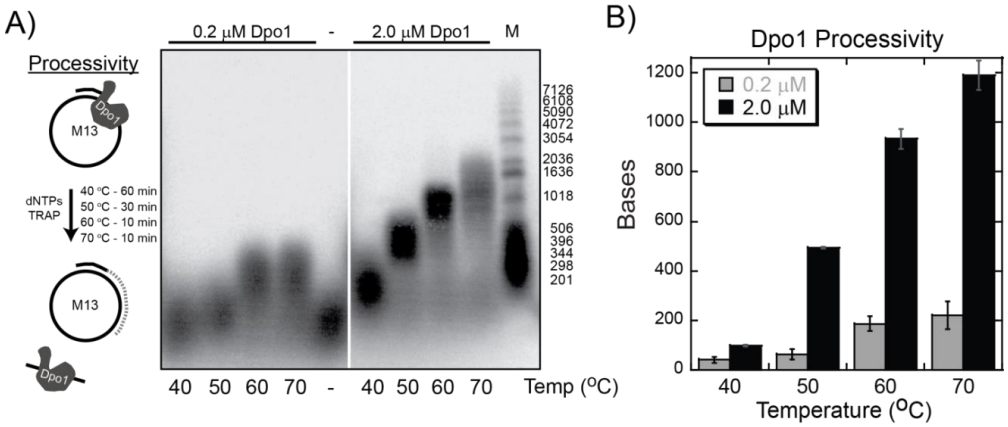

Figure 3-11. Processivity of Dpo1 increases with temperature and concentration. A) Dpo1 processivity assays were performed at 40, 50, 60, and 70 °C representing monomer (0.2 μM) (left panel) or trimer (2.0 μM) (right panel) concentrations and separated on a denaturing alkaline agarose gel as described in the Materials and Methods. The inset cartoon describes the experimental protocol for processivity experiments. Longer reaction times were used for lower temperatures to compensate for slower polymerase rates. Processivity values were calculated from DNA size markers and calculated using ImageQuant software. Quantification of the processivity values (bp) comparing monomeric (0.2 μM, grey) or trimeric (2.0 μM, black) Dpo1 at 40, 50, 60, and 70 °C.

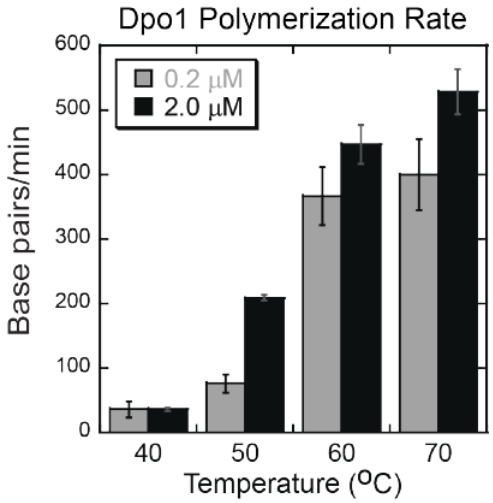

Figure 3-12. Quantification of the average rate (bp/min) for 0.2 μM (grey) and 2.0 μM (black) Dpo1 at 40, 50, 60, and 70 °C from alkaline agarose gels. DNA length values were obtained compared to DNA size markers and calculated using ImageQuant software. Error bars represent the standard error from at least three independent kinetic experiments. Kinetic experiments were quenched after 4 minutes for all temperatures.

For Dpo4, processivities also increase with increasing enzyme concentration at a variety of temperatures (Figure 3-13) but to a lesser extent than for Dpo1. As for Dpo1, the Dpo4 processivity

increases slightly at 200 nM (representing monomer) and more dramatically at 5 μM (representing dimer) with increasing temperature (Figure 3-14). This is not only visualized by longer products separated on the gel, but also more radioactivity seen in the wells at the higher concentrations or temperatures. Interestingly at both monomeric and dimeric Dpo4 concentrations, there is an apparent decrease in processivity when going from 60 to 70 ^{o}C consistent with decreased specificity of binding measured for Dpo4 at those temperatures using fluorescence anisotropy (Figure 3-8C). Similar to Dpo1, the processivity values increase when dimeric Dpo4 concentrations are used compared with monomeric Dpo4 concentrations at all temperatures.

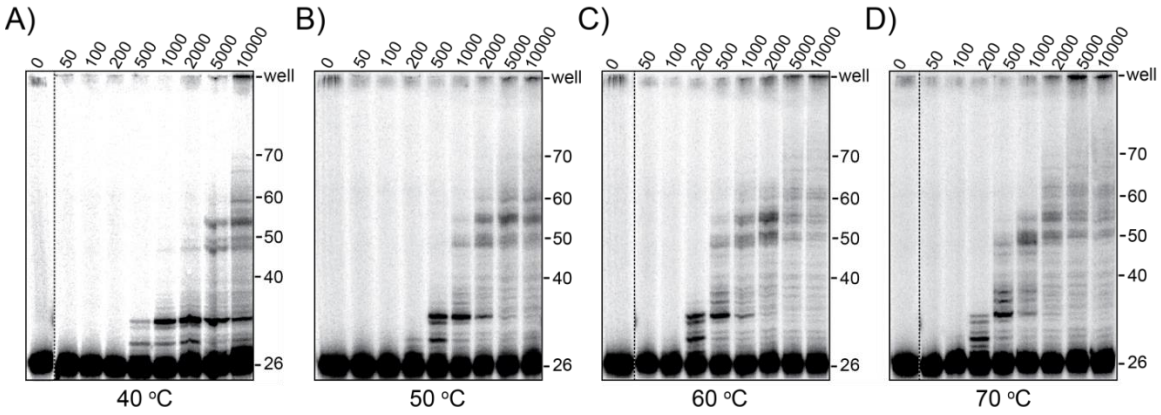

Figure 3-13.. Processivity of Dpo4 increases with temperature and concentration. Dpo4 processivity assays were performed at A) 40, B) 50, C) 60, and D) 70 ^{o}C for concentrations ranging from 0.05 – 10 μM and separated on a denaturing acrylamide gel. Reactions were initiated with dNTPs and excess ssDNA trap as described in the Materials and Methods.

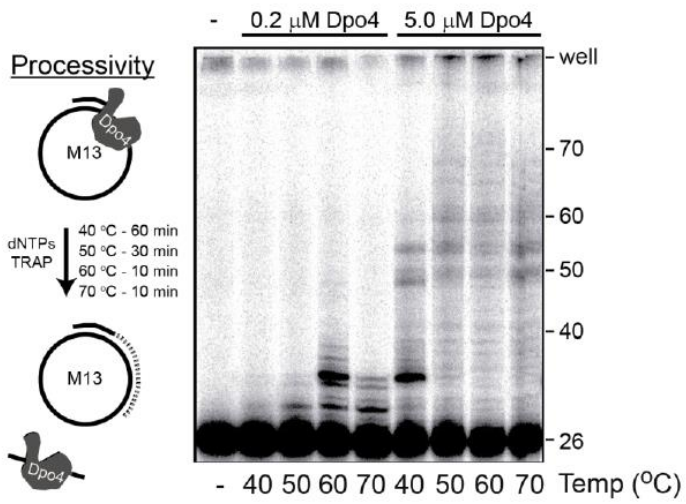

Figure 3-14..Dpo4 processivity assays were performed at 40, 50, 60, and 70 oC representing monomer (0.2 μM) (left panel) or dimer (5.0 μM) (right panel) concentrations and separated on a denaturing acrylamide gel as described in the Materials and Methods. The inset cartoon describes the experimental protocol for processivity experiments. Longer reaction times were used for lower temperatures to compensate for slower polymerase rates.

3.3 DISCUSSION

Using chemical crosslinking, isothermal titration calorimetry, analytical ultracentrifugation, and fluorescence anisotropy, we have been able to identify, separate, and quantify multiple binding events for DNA replication (Dpo1) and repair polymerases (Dpo4) to DNA that lead to different specificities and activities with temperature. Consistent with our previous report,(*120*) Dpo1 forms a concentration dependent trimer at all temperatures. Unexpectedly, Dpo4 behaves similarly, forming a dimeric complex that becomes more favored at higher temperatures. For both Dpo1 and Dpo4, the affinities of monomeric and subsequent oligomeric binding generally increase as the temperature approaches the physiological range. The changes in polymerase equilibria with concentration and temperature can be clearly visualized using analytical ultracentrifugation even over a limited temperature range (10 - 30 ^{o}C).

Comparison of monomeric polymerase binding to DNA shows that the differentially stronger affinity of Dpo1 than Dpo4 becomes even more exaggerated as physiological temperatures (75 ^{o}C) are approached, providing for thermodynamic selection of a DNA replication polymerase on undamaged templates. These thermodynamic results are reflected in the enzymatic behaviors, in that we measured a greater processivity for nucleotide incorporation at higher temperatures and oligomeric states for both DNA polymerases. The equilibrium microenvironment in the cell or more importantly at the replication fork will direct binding and association of a variety of DNA polymerase complexes to promote efficient DNA replication in the presence of any damage.

3.3.1 Evidence for Oligomeric Dpo1 and Dpo4 Complexes Bound to DNA

Identification, isolation, and assembly of the trimeric Dpo1 complex at the primer template junction have been discussed previously (*120*) but is now verified and quantified across a large temperature range. Similarly, crosslinking and ITC suggest that assembly of a dimeric Dpo4 is also possible. Using AU-FDS experiments, we were able to directly monitor the size distribution of polymerase DNA complexes in solution at multiple temperatures. Interestingly, for both Dpo1 and Dpo4 bound to DNA, there is a modest but reproducible shift in the sedimentation boundaries to larger coefficients with increasing temperature. Unfortunately, analytical ultracentrifugation can only be performed over a limited temperature range, 10 ^{o}C to 30 ^{o}C; as these effects may have been greater if higher temperatures could have been probed. A shift to a larger $s_{20,w}$ value in sedimentation velocity experiments is consistent with a change in the population of complexes towards a larger average size. The shifts in reaction boundaries occur at lower concentrations for Dpo1 than for Dpo4, consistent with the anisotropy result that Dpo1 has a higher affinity for DNA than Dpo4 at identical temperatures. Distinct $s_{20,w}$

populations are more easily seen for Dpo1, due to large differences in the molecular weight between the complexes of monomer and trimer with DNA. For Dpo4, the size difference between monomeric and dimeric bound states is much less, causing a general broadening of the $s_{20,w}$ distribution and discrete $s_{20,w}$ weight average values for each state are not observed. The most obvious temperature dependent reaction boundary shifts occur at concentrations equal to the dissociation constant for polymerase binding to DNA (i.e. 100 nM Dpo4 at 30 ^{o}C in Figure 3-5C). Shifts in the reaction boundaries of Dpo1 bound to DNA with increasing temperature are more subtle, but reproducible, in this experimental range; these shifts are characterized by better resolution between monomeric and trimeric Dpo1 at 30 ^{o}C (Figure 3-4C). Although only qualitatively, the individual sedimentation boundaries correlate well with the K_{d1} and K_{d2} binding affinities (K_1 and K_2 in Figure 3-10) for Dpo1 and Dpo4 to DNA measured by fluorescence anisotropy. Sedimentation equilibrium experiments would be useful in quantifying the actual populations for either Dpo1 or Dpo4 alone or bound to DNA, but unfortunately resulted in uninterpretable spectra, probably due to some precipitation or aggregation during the long times required to attain sedimentation equilibrium. No loss in spectral signal was detected in the analytical velocity experiments suggesting that aggregation and precipitation is not an issue for shorter time scales.

Although there are a number of biochemical, kinetic and structural papers involving the mechanism of action for Dpo4,(*117, 118, 123, 124, 143, 157-161*) none of them suggest that a dimeric DNA polymerase complex is the active species. However, we have confirmed Dpo4 binding to DNA as a dimer using chemical crosslinking, the stoichiometry values from ITC, and analytical ultracentrifugation. The apparent dissociation constants measured by ITC at 15 ^{o}C (K_d^{ITC} = 1.5 M) or 60 ^{o}C (K_d^{ITC} = 0.45 M) are much larger than expected based on AUC,

fluorescence anisotropy and EMSA results previously published and most likely represent contributions of equilibria from monomer and dimer Dpo4 binding to DNA.(*104, 162, 163*) The analytical ultracentrifugation results show that binding begins at a concentration of 100 nM and then proceeds in a concentration dependent manner towards dimer above 500 nM. According to the fits of the fluorescence anisotropy experiments, dimer assembly persists across a range of temperatures. From a variety of Dpo4:DNA X-ray structures, the site size of Dpo4 on DNA consists of roughly 10 bases of dsDNA and 4 bases of ssDNA straddling the primer template junction.(*118*) The DNA hairpin primer-template used in these studies has a 12 base pair duplex and a 10 base single strand region, thus restricting binding site size to a single DNA polymerase. The location of the protein crosslink can be pinpointed because there is only a single native cysteine residue (C31) in Dpo4 but does not exclude other dimeric Dpo4 structures. Unlike what we observed for Dpo1,(*120*) the presence of DNA did not significantly affect the degree of crosslinking, suggesting that at the concentrations used for this experiment, Dpo4 can form a dimer in the absence of DNA.

Within the RCSB Protein Data Bank (www.rcsb.org), there exist roughly 100 structures of Dpo4 both without DNA and bound to various types of DNA templates (damaged and undamaged). Roughly, one-third of these structures have multiple Dpo4 molecules interacting in the crystal unit in various conformations. Many of these multimeric structures show Dpo4 in a conformation that would allow the cysteine residues in the interface to be in close enough proximity for crosslinking to occur.(*164-166*) The rest of the oligomeric Dpo4 structures are in a variety of alternative dimeric or tetrameric complexes. Additionally, a number of structures for the analogous Dbh polymerase from *Sulfolobus acidocaldarius* also show oligomeric complexes in the crystal unit with the homologous cysteine residue in close enough proximity for

crosslinking.(*167, 168*) Although we cannot be certain of the exact conformation, we are able to detect and verify a previously unrecognized dimeric Dpo4 complex across all temperature ranges that is consistent with our thermodynamic binding data. Moreover, the variety of dimeric and tetrameric states of Dpo4 seen by X-ray crystallography may suggest that the binding equilibria are even more complex than we include in our model (Figure 3-10B).

3.3.2 Thermodynamic differences in binding oligomeric replication and repair polymerases to primer-template DNA

In fluorescence anisotropy experiments, optimum fits to binding isotherms for the titration of Dpo1 or Dpo4 with DNA are obtained using a model for a sequential assembly path involving two binding events. Information from crosslinking, EMSA, gel filtration, AUC, and ITC experiments about the initial (monomeric) and final (trimeric for Dpo1 and dimeric for Dpo4) forms of polymerase-DNA complexes was essential for differentiating between single and multiple binding events in the anisotropy experiments.(*120*) For Dpo1 and Dpo4, there is an initial higher affinity binding of one polymerase molecule to DNA. The binding of the second and third molecule of Dpo1 to complete the trimer is proposed to occur cooperatively;(*120*) however since a dimeric Dpo1-DNA complex cannot be resolved, our data are insufficient to separate these secondary binding events. Formation of a Dpo4 dimer proceeds through two sequential binding events. For both Dpo1 and Dpo4, binding of additional polymerase molecule(s) to the first is inferred primarily from the limited DNA template size and the direct contacts found using chemical crosslinking.(*120*) Previous reports on binding affinity for Dpo1 and Dpo4 are consistent with our values for monomeric assembly at room temperature but those studies did not test higher concentrations required for multimeric assemblies.(*163, 169*)

A comparison of the DNA binding affinities of monomeric Dpo1 and Dpo4 shows that binding affinity is only slightly more favorable for monomeric Dpo1 across all temperature ranges but becomes more selective at physiological temperatures (Figure 3-15 and Figure 3-16). The free energy change for binding the first molecule of Dpo1 decreases steadily with temperature up to at least ~65 ^{o}C, where binding is preferred by about -0.8 kcal mol^{-1} over Dpo4. Dpo4, on the other hand, has a free energy binding minimum around 50 ^{o}C, disfavoring binding to undamaged DNA in the presence of Dpo1. Dpo4 is smaller, known to have a more open active site than typical B-family polymerases, exists in two distinct conformations, and has subtle repositioning of active site residues upon binding.(*118, 143, 170, 171*) The little finger domain and associated linker in particular seem to be most important for stable binding to DNA. On the other hand, the binding affinity of Dpo1 to DNA is more favorable at higher temperatures, consistent with formation of a tight closed conformation on DNA, resulting in greater DNA stabilizing ability/annealing noted previously.(*172*)

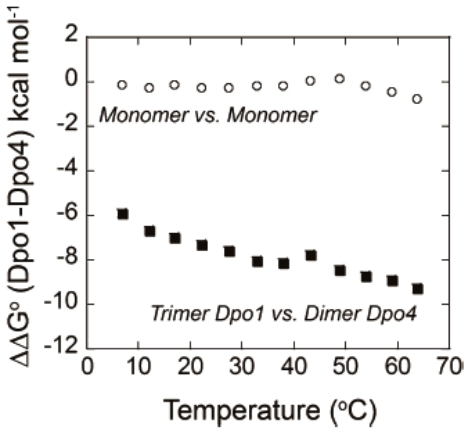

Figure 3-15. Gibbs free energy differences ($\Delta\Delta G^{o}$) for DNA binding, comparing Dpo1 to Dpo4 monomers (○) or comparing trimeric Dpo1to dimeric Dpo4 (■), plotted as a function of temperature.

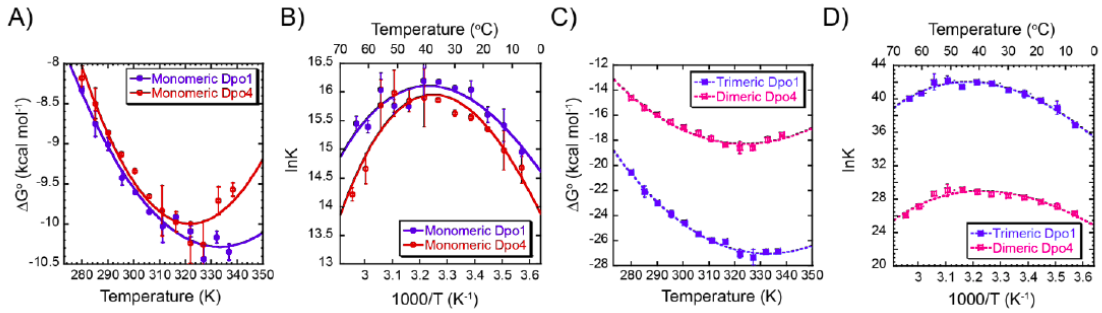

Figure 3-16. Thermodynamic differences between Dpo1 and Dpo4 binding to DNA. A) Gibbs-Helmholtz or B) van't Hoff plot comparison of the free energy of binding (ΔGo) for monomeric Dpo1 (solid -●-, blue) or Dpo4 (solid -○-, red) as a function of temperature. C) Gibbs-Helmholtz or D) van't Hoff plot comparison of the free energy (ΔGo) for formation of trimeric Dpo1 (dashed -■-, light blue) or dimeric Dpo4 (dashed -□-, pink) as a function of temperature. Error bars represent the standard error from multiple experiments at each point. Lines in the Gibbs-Helmholtz plots show the fits of the data to Equations 3-9~11. Lines in the van't Hoff plots show the fits to Equation 3-12.

There is a larger differential in the free energies of binding of the oligomeric forms of the polymerases (trimeric Dpo1 or dimeric Dpo4) (Figure 3-14 and Figure 3-16) than for the monomeric forms. The ΔG° for formation of a trimeric Dpo1 complex is much more favorable than that for formation of a dimeric Dpo4 complex. The difference in binding energies becomes even more exaggerated at higher temperatures, thus increasingly favoring the trimeric Dpo1 complex at physiological temperatures. At 64 °C, binding of trimeric Dpo1 is enormously favored (by about -9.3 kcal/mol) over dimeric Dpo4. The slight preference for binding primer-templates by the Dpo1 monomer (over that of the Dpo4 monomer) will lead to trimeric Dpo1 complex formation, thus selecting against Dpo4 binding.

3.3.3 Formation of both monomeric and oligomeric polymerase-DNA complexes produces large negative ΔC^{o}_{p} values

Amongst the thermodynamic parameters (ΔG, ΔH, ΔS, ΔC_P, and volume) ΔC_p is one of the least well known, but potentially the most informative with respect to extracting molecular

information about specificity. Because ΔC_p was first analyzed for protein folding, the working hypothesis was that the net negative ΔC_p reflected primarily the burial of nonpolar surface area.(*145, 149*) However, a number of studies on site-specific protein-DNA complexes have shown large deficits between the ΔC_p^{ASA} values predicted from surface burial and experimental ΔC^o_p values.(*128, 129, 134, 148, 151-153, 155*) In addition to desolvation of nonpolar surface upon binding, other factors such as restriction of conformational-vibrational motions of the macromolecules, interfacial waters, and linkage of other binding equilibria (protonation, cation and anion binding, and conformational changes) contribute to the protein-DNA binding reaction and can potentially account for the deficit between ΔC_p^{ASA} and ΔC^o_p.(*128, 129, 173-180*)

Although a strongly negative ΔC^o_P value has generally been considered a key signature of sequence-specific DNA-protein interactions,(*128*) large negative values of ΔC^o_P have also been observed for the formation of interfaces with high structural complementarity between DNA polymerases and their primer-template substrates.(*130, 131, 181, 182*)

In the absence of appropriate monomeric or oligomeric polymerase-DNA structures, contributions of surface area burial cannot be directly assessed. The only appropriate data set is for a monomeric Dpo4-DNA structure, which underestimates the contributions of buried surface area (ΔC_p^{ASA} = -0.29 cal mol^{-1} K^{-1}) to the experimental value. The ΔC^o_P values are similar for monomeric Dpo1 (-0.43 cal mol^{-1} K^{-1}) and Dpo4 (-0.68 cal mol^{-1} K^{-1}) but significantly more negative than the ΔC_p^{ASA} value suggesting that other factors in addition to surface area burial contribute to the experimental ΔC^o_p values.

Because we have been able to monitor the sequential steps in polymerase binding, we have also found that the ΔC^{o}_{p} values for assembly of trimeric Dpo1 and dimeric Dpo4 complexes are strongly negative, suggesting that structure-specific binding is occurring during formation of these oligomeric DNA complexes as well. The sign and magnitude of the ΔC^{o}_{p} values for formation of Dpo1 and Dpo4 oligomers are consistent with other specific dimerization or binary protein binding events.(*183-186*) No structural information is available for an oligomeric Dpo1 complex, nor can we be certain of the molecular arrangement of a dimeric Dpo4 complex, which makes calculation of buried surface area difficult. Nevertheless, exclusion of water molecules, favorable surface interactions between the polymerase molecules, and restriction of configurational freedom within the oligomeric complex are consistent with the magnitudes for the oligomeric polymerase-DNA ΔC^{o}_{p} values. Therefore, many of the factors discussed above may contribute to the strongly negative ΔC^{o}_{P} values observed for the formation of trimeric Dpo1 and dimeric Dpo4 complexes with primer-template DNA substrates.

3.3.4 Oligomeric DNA Polymerases Have Increased Activities and Processivities

Generally, processivity is thought to be a temperature independent parameter although slight decreases in processivity with increasing temperature have been noted for the telomerase enzyme.(*187*) DNA polymerases alone are fairly distributive enzymes unless accompanied by their respective circular clamp proteins which can increase processivity from less than 20 to greater than 10,000 bases.(*188*) Previously, we found that the processivity of Dpo1 was dependent on concentration, such that that trimeric complex had much greater processivity (~1000 bases) than the monomer at 60 ^{o}C.(*120*) We have now shown that the processivity for both Dpo1 and Dpo4 increases with temperature. An increase in processivity with temperature

was noted for both monomeric and oligomeric complexes of Dpo1 and Dpo4 although the effect was more dramatic for the oligomeric states. Trimeric Dpo1 was 4-5 fold more processive than monomeric Dpo1; dimeric Dpo4 was significantly more processive than monomeric Dpo4; but the processivity of trimeric Dpo1 was more than 15-fold greater than that of dimeric Dpo4 at higher temperatures. Even though Dpo4 is generally considered to be a distributive enzyme, the increased affinities for binding DNA noted with increasing temperatures and concentrations also increase the processivity. We reason that for Dpo1 and Dpo4, a more tightly bound monomeric or oligomeric complex promotes greater processivities at higher temperatures. For Dpo1, the affinity for DNA generally increases with temperature, and formation of a trimeric Dpo1 reduces the off-rate of the complex from DNA over monomeric Dpo1 explaining the larger processivity values. The combination of higher intrinsic processivity for monomeric Dpo1 compared with Dpo4, as well as increased binding affinity at higher temperatures of the Dpo1 trimer, contribute to the enzymatic activity resulting in high trimeric Dpo1 processivity.(*120*) In fact, phi29 is the only other characterized DNA polymerase with a greater processivity value and acts analogously by topologically encircling the DNA template.(*189, 190*)

Increased binding affinity of Dpo4 to DNA also correlates well with increasing processivity up to 60 ^{o}C. At 70 ^{o}C, the processivity decreases slightly, consistent with the measured affinity values. Previously, when high concentrations of Dpo4 were used, an increase in the length of product synthesized was observed suggesting that either faster repeated binding was occurring in the absence of trap or cooperation between molecules at higher concentrations afforded greater processivity.(*171*) The authors implicated the little finger domain of Dpo4 in maintaining moderate processivity by creating a closed more stable enzyme complex on DNA. The conformational change of the little finger domain is considered to be the rate limiting step

and occurs both before and after chemistry.(*123, 191*) Kinetic experiments have shown that of the 7 steps within the catalytic cycle for a single nucleotide incorporation event, the conformational change step that precedes chemistry is most affected by temperature increasing 20-fold from 37 to 56 ^{o}C.(*158*) Moreover, the little finger domains are in close proximity with one another in a variety of dimeric and tetrameric Dpo4 crystal structures including our crosslinking model in Figure 3-1B, suggesting that dimerization may stabilize a closed complex, decrease the off-rate, and increase the rate limiting conformational change step to positively affect processivity.

Clearly, a tightly bound trimeric Dpo1 complex will increase the speed and processivity of polymerization and may be utilized in various genomic maintenance applications. At 75 ^{o}C, binding of Dpo4 will be disfavored on undamaged primer-templates where Dpo1 is directing synthesis. Selection and increased processivity will also be provided through interactions with the processivity clamp, *Sso*PCNA123, but the affinities of Dpo1 for PCNA2 and Dpo4 for PCNA1 are very similar.(*192, 193*) Switching from Dpo1 to Dpo4 will depend on a change in the thermodynamics of binding either due to polymerase stalling, repeated shuttling between polymerase and exonuclease sites, detection of DNA damage, or a change in the local concentrations. In those cases, binding of Dpo4 would become preferred. It has been recently estimated that the concentration of Dpo1 is at least an order of magnitude greater than that of Dpo4 in the cell suggesting that Dpo1 will be preferentially bound and will have a significant population of trimer at the replication fork.(*104*) Interestingly, mRNA levels of Dpo1 decrease when cells are exposed to DNA damage in favor of Dpo4 and another B-family DNA polymerase (Dpo2),(*194, 195*) suggesting that equilibrium changes will direct appropriate binding of the required DNA polymerase.

Although the oligomeric state of Dpo1 modulates both the speed and processivity of replication, the biological role of a dimeric Dpo4 remains elusive. Due to only slight increases in biochemical activity, we would predict that a dimeric Dpo4 would not be essential for cellular catalysis, but rather in either increasing the concentration of DNA polymerases at sites of DNA damage or stabilizing the closed conformational state promoting catalysis. Accurate and efficient DNA replication at high temperatures requires minimal differences in the thermodynamics of DNA polymerase binding to DNA for easy exchange of enzymes for uninterrupted synthesis. This thermodynamic compensation will be affected by small changes in the cellular equilibria that direct formation of higher order protein complexes that promote a variety of genomic maintenance activities. The detection of multimeric polymerase complexes for both Dpo1 and Dpo4 suggests a possible mechanism for exchange, whereby direct interactions between polymerases maintain high local concentrations at the replication fork that can thermodynamically switch binding modes when required.

3.4 CONCLUSION

In Chapter 2, we observed that Dpo1 can form a trimeric complex on DNA using a variety of experimental techniques. Here, we have also detected the oligomerization of Dpo4 by cross-linking (Figure 3-1). While Dpo1's trimer complex is stimulated by the association with DNA, the dimerization of Dpo4 at a native cysteine can occur off DNA. The physiological environment of Dpo4 in *Sso* cell is around 150 nM, which lies squarely in the concentration range of the monomeric DNA complex. On the other hand, the calculated cellular concentration of Dpo1 (2.2 μM) would suggest that it will have significant enzymatic contributions of trimer to

DNA replication (Chapter 2).(*54*) Therefore, Dpo4's role will be secondary to assist in DNA replication by bypassing site specific lesions. In some instances, Dpo4 may still use the oligomerization to increase the local availability of enzyme at the replication fork.

We have found that each polymerase binds to DNA in a stepwise manner with an initial higher-affinity binding and a sequential lower-affinity binding by EMSA (Chapter 2 and Chapter 4) and fluorescence anisotropy (this chapter). For the initial binding to DNA, the affinities of Dpo1 and Dpo4 are very similar over the temperature range between 6.8 and 65.7 ^{o}C. However, trimeric Dpo1 is more stable and with a lower free energy than dimeric Dpo4 with increasing temperature, especially at the physiological temperature of *Sso* (~75 ^{o}C). The temperature-dependent preference in the oligomeric affinities demonstrates a strategy for how *Sso* chooses Dpo1 as a primary player in DNA replication.

A recent study shows that the T_H (the temperature where the heat enthalpy equals to zero) reveals the temperature where DNA polymerases begin to have enzymatic activity).(*1*) Here, in Figure 3-9, we further support this idea with the fact that at 40 ^{o}C (T_H for both oligomeric form of Dpo1 and Dpo4 complex), both Dpo1 and Dpo4 have significant higher activities than that at room temperature. Our results also suggest that at T_s (at the temperature the binding entropy equals to zero), Dpo1 (65 ^{o}C) and Dpo4 (55 ^{o}C) are close to their maximum activities. We would have to test this hypothesis directly to understand the thermodynamic rationale behind this observation in the future.

4.0 TEMPERATURE DEPENDENT COUPLED EQUILIBRIA INFLUENCES BINDING THERMODYNAMICS FOR OLIGOMERIC DNA POLYMERASES COMPLEXES

DNA polymerases are responsible for faithfully incorporating nucleotides opposite a DNA template during DNA replication or repair to maintain the genomic integrity of all organisms. B-family DNA replication polymerases have high intrinsic DNA synthesis accuracy that is augmented further by an exonuclease proofreading domain. Y-family DNA polymerases act specially to replicate across damaged templates in a potentially error prone manner. Therefore, B-family polymerases are proposed to stall at sites of DNA damage awaiting the temporary recruitment of a Y-family polymerase to bypass the lesion.(*196*) Core structural and mechanistic aspects between these polymerase families are shared highlighting conserved binding modes, although plasticity in the active site of Y-family polymerases allows for incorporation opposite DNA damage in the template strand.(*197*) Similar binding affinities and specificities for replication and lesion bypass polymerases to primer/template DNA will abrogate high fidelity DNA synthesis in the absence of other molecular factors that direct binding. Undoubtedly, multiequilibria processes including self-associations, specific interactions with other accessory proteins, and individual kinetic steps will control access to DNA and ensure high fidelity synthesis even in the presence of DNA damage.

The molecular signal responsible for the exchange of polymerases at sites of damage has not been identified, although in yeast and bacteria, it is proposed to occur through coupled interactions with the processivity clamp, which destabilize binding of one polymerase in favor of the other.(*198-202*) Alternatively, the repeated shuttling between polymerization and exonuclease modes of the B-family polymerase at sites of damage(*107*) may locally destabilize binding allowing a Y-family polymerase to bind more specifically to bypass the lesion. There has also been some evidence suggesting that multiple DNA polymerases are concentrated at the replication fork and dynamically exchange during replication and repair processes.(*34, 112, 113, 120*)

In Chapter 3, DNA binding by various DNA polymerases has been examined using fluorescence anisotropy and analytical ultracentrifugation, suggesting the specificities of Dpo1 and Dpo4 to DNA can be regulated by oligomerization, which is directly affected by the concentration and temperature. In this chapter, the detailed coupled equilibrium between different oligomeric states has been described thermodynamically by isothermal titration calorimetry (ITC). ITC provides the most complete thermodynamic profile. The change in enthalpy (ΔH_{obs}) can be directly measured and fit to a binding isotherm to give the stoichiometry (n) and the equilibrium binding constant (K_a). From ΔH_{obs} and the K_a, the change in the binding free energy (ΔG_{obs}) and the change in entropy (ΔS_{obs}) can be calculated. Determination of the temperature dependences of ΔH^o and ΔS^o gives the heat capacity change (ΔC_p^o), which can provide insight in to the specificity of the binding process.(*128, 129*) Determination of ΔC_p^o is

especially important for differentiating binding processes for multiple enzymes within a cell that have similar substrate preferences.

Although a strongly negative ΔC_p^o has been shown to be the thermodynamic signature of sequence-specific binding,(*129*) the non-sequence specific binding to primer template DNA by the A-family DNA polymerases from *T. aquaticus* (Taq) and *E. coli* (Klenow) is also associated with large and negative ΔC_p^o values.(*128, 130-134*) Even though there is no sequence specificity, the negative ΔC_p^o is consistent with high structural complementarity of the DNA polymerase binding to the primer template junction visualized in a variety of crystal structures.(*118, 120, 128, 135, 136*) Importantly, an accurate interpretation of ΔC_p^o relies on the ability to understand all the molecular contributions to the bound conformations to define the energetics.(*203, 204*) The inherent thermostability of proteins from *Sso* (where the growth temperature is ~75 ^oC) allows us to fully investigate the energetic constraints of DNA polymerase binding to DNA. Access to this broad temperature range results in a more complete thermodynamic characterization of the differences in binding B and Y-family polymerases to an undamaged DNA primer-template. These thermodynamic differences can be evaluated directed by determining the ΔC_p^o, K_as, and stoichiometries for binding each polymerase.

We have analyzed the temperature dependence of the thermodynamic parameters for DNA binding by B-family (Dpo1) and Y-family (Dpo4) polymerases from *Sso*. Electrophoretic mobility shift assays (EMSAs) at low and high temperatures were used to define the polymerase stoichiometries and equilibria for binding DNA. The assembly of Dpo1 proceeds though a

monomeric/DNA complex followed by the cooperative assembly of two additional molecules to form a trimeric Dpo1/DNA complex. Binding of Dpo4 to DNA is similar but proceeds through assembly of monomer, dimer, and tetramer complexes. As has been shown for many sequence-specific DNA-binding proteins and also for the non-sequence-specific *Taq* and Klenow DNA polymerases,(*131*, *205-207*) Dpo1 and Dpo4 binding to DNA measured by ITC shifts from being entropy-driven to enthalpy-driven as the temperature is increased. This entropy-enthalpy compensation has the consequence that ΔG^{o} changes only slightly over a broad range of temperatures. Surprisingly for both Dpo1 and Dpo4, the heat capacity values (ΔC_p^o) are strongly temperature dependent and in some cases actually switch from a positive to a negative value over the experimental range. Interestingly, the presence of DNA thermodynamically stabilizes Dpo1 predicting high structural complementarity for a Dpo1/DNA complex that corresponds to a large negative ΔC_p^o at high temperatures. Neither buried solvent exposed surface areas, associated structural changes, protonation, nor electrostatics can account for the large temperature dependent heat capacity change ($\Delta\Delta C_p^o$). Instead, coupled equilibria associated with oligomeric polymerase binding are highly temperature dependent directly affecting ΔC_p^o. Therefore, we conclude that the observed ΔC_{obs}^o is the summation of a constant intrinsic $\Delta C_{intrinsic}^o$ for binding DNA and coupled equilibria $\Delta C_{coupled}^o$ that changes with temperature. Taken together, these results suggest that complex thermodynamics and solution equilibria direct non-sequence

specific binding and assembly of these oligomeric DNA polymerases to DNA resulting in greater structural complementarity and free energy selection at higher temperatures.

4.1 MATERIALS AND METHODS

Materials. Oligonucleotide substrates were purchase from Integrated DNA Technologies (IDT (Coralville, IA). The sequence of the 37 base DNA hairpin was 5'-TTTTTTTTTTCCCGGGCCGGCGTTTCGCCGGCCCGGG, which included a 12 base pair duplex region, a three residue loop, and a ten base single strand template. DNA was dissolved in annealing buffer [20 mM HEPES (pH 7.0) and 200 mM NaCl], heated to 95 ^{o}C for 15 minutes, and then cooled to room temperature by turning off the hot plate overnight. Untagged exonuclease deficient Dpo1 (D231A/D318A) and wild-type Dpo4 were purified as described previously.(*208*) All other chemicals were analytical grade or better.

DNA Hairpin Denaturation Studies. 600 nM DNA hairpin was dissolved in [20 mM] Sodium cacodylate buffer (J.T.Baker) with 150 mM NaCl. The UV adsorption profile was measured using a Cary 100 UV-Vis Spectrophotometer (Varian, CA) over temperature ranges (4 to 95 ^{o}C). The melting point was determined from the peak of derivative of adsorption profile as described previously.(*172*)

Electrophoretic Mobility Shift Assays (EMSA). Native gel-electrophoretic mobility shift assays were performed in a 10 μl reaction mixture containing reaction buffer [10 mM BisTris, 40 mM Tricine (pH 7.0), 10 mM $Mg(OAc)_2$, and 1.25 v/v % Glycerol], 4 nM DNA hairpin labeled at the 5'-end using a standard polynucleotide kinase reaction and ^{32}P-γ-ATP using Optikinase (USB), and the indicated amount of polymerase and the DNA hairpin. Binding reactions were

allowed to equilibrate for 10 min at the indicated temperature followed by directly loading onto a temperature equilibrated 6% polyacrylamide gel [10mM BisTris, 40mM Tricine (pH 7.0)]. Gels were run for 20 minutes at 20 volts cm^{-1} in the running buffer [10mM BisTris, 40mM Tricine (pH 7.0)] and then imagined using a Storm phosphorimager (GE Healthscience). Quantification of the fraction of band shift was performed using the ImageQuant software (v5.0). Afterwards, EMSA gels were stained with coomasie dye to visualize protein species. The EMSA data for Dpo1 or Dpo4 was fit and modelled according to the Schemes 4-1 & 4-2 using Berkeley Madonna (University of California, Berkeley, CA) as described previously.(*208*)

Isothermal Titration Calorimetry (ITC). Prior to analysis, titrants and analytes were dialyzed against Buffer A [20mM HEPES-NaOH (pH 7.0), 150 mM NaCl, 5% Glycerol, 10 mM $Mg(OAc)_2$, 0.2 mM DTT], filtered by centrifuge tube filters (0.22 μm, SPIN-X, Corning Inc., NY), and degassed. Buffer A is different than the ITC buffer used in Chapter 2 to better mimic physiological conditions. Isothermal titration calorimetry was performed using a VP-ITC (MicroCal Inc., Northampton, MA) as described previously.(*120, 208*) Titrations were performed both in the forward (DNA into protein) and reverse directions (protein into DNA) at various temperatures and concentrations. Typical forward titration experiments included 500 μM DNA titrated into 25 μM protein in at least 30 injections of 5-6 μL. Reverse titrations included ~190 μM protein titrated into 1-3 μM DNA in at least 30 injections of 5 μL. The heats of the reaction were corrected for the heat of dilution by subtracting the signal after reaching saturation. All data were fit using non-linear least squares analysis in Origin 7.0 (MicroCal) according to the following identical single sites equation:

$$Q = \left(\frac{n[P]_t \Delta H^0 V_0}{2}\right)\left\{1 + \frac{[D]_t}{n[P]_t} + \frac{1}{nK_{obs}[P]_t} - \left[\left(1 + \frac{[D]_t}{n[P]_t} + \frac{1}{nK_{obs}[P]_t}\right)^2 - \frac{4[D]_t}{n[P]_t}\right]^{1/2}\right\}$$

(Equation 4-1)

where V_0 is the volume of the cell, ΔH^o is the enthalpy of binding per mole of ligand, $[P]_t$ is the total concentration of protein including both bound and free fractions, K_{obs} is the apparent association constant, $[D]_t$ is the total DNA concentration, and n is the stoichiometry of the reaction, or to a sequential binding sites equation with two separate apparent binding constants ($K_{1,obs}$ and $K_{2,obs}$) and enthalpies ($\Delta H_{1,obs}$ and $\Delta H_{2,obs}$):

$$Q = [P]_t V_0 \left\{\frac{K_{1,obs}[D](\Delta H_{1,obs}) + K_{1,obs}K_{2,obs}[D]^2(\Delta H_{1,obs} + \Delta H_{2,obs})}{1 + K_{1,obs}[D] + K_{1,obs}K_{2,obs}[D]^2}\right\} \quad \text{(Equation 4-2)}$$

where the concentration of free DNA (D) was obtained from the following equation:

$$[D]_t = [D] + [D]_{bound} = [X] + \left[\frac{K_{1,obs}[D] + K_{1,obs}K_{2,obs}[D]^2}{1 + K_{1,obs}[D] + K_{1,obs}K_{2,obs}[D]^2}\right][P]_t \quad \text{(Equation 4-3)}$$

according to the Scheme 4-1 for Dpo1 binding equilibria:

$$K_{1,obs} = K_1 \quad \text{(Equation 4-4)}$$

$$K_{2,obs} = (K_2)^2 \quad \text{(Equation 4-5)}$$

while in Scheme 4-2 for Dpo4 binding equilibria

$$K_{1,obs} = K_1 \quad \text{(Equation 4-6)}$$

$$K_{2,obs} = K_2 \times (K_3)^2 \quad \text{(Equation 4-7)}$$

The Gibbs free energy of binding (G^o) was calculated as

$$\Delta G^o = -RT \times lnK_{app} \quad \text{(Equation 4-8)}$$

where R is the universal gas constant and T is the temperature. Thermodynamic parameters were extracted from a fit of the temperature dependence of the Gibbs-Helmholtz plot according to the following equation:

$$\Delta G^o = \Delta H^o - T\Delta S^o = \Delta C_p^o \left[(T - T_H) - Tln\left(\frac{T}{T_S}\right)\right] \quad \text{(Equation 4-9)}$$

where ΔG^o is the standard free energy change, ΔH^o is the change in enthalpy, and ΔS^o is the change in entropy, using a constant heat capacity (ΔC_p^o) at each temperature, T. T_H is the temperature in which $\Delta H^o = 0$, T_S is the temperature where $T\Delta S^o = 0$.

The temperature dependent heat capacity $(\Delta\Delta C_p^o)$ was determined from a fit of the ITC data of H as a function of temperature (T) using the following equation.

$$\Delta H(T) = \Delta H_r + \Delta C_{p_r}(T - T_r) + \Delta\Delta C_p^o \left[\left(\frac{T^2 - T_r^2}{2}\right) - T_r(T - T_r)\right] \quad \text{(Equation 4-10)}$$

where $\Delta H(T)$ is the binding enthalpy measured at different temperatures, ΔC_{p_r} is the fitted heat capacity and ΔH_r is the fitted enthalpy values at any chosen reference temperature T_r. All fitting was performed using KaleidaGraph (ver 3.52, Synergy Software) or Origin (ver 9, OriginLab).

Electrophoretic mobility measurements. The electrophoretic mobility of Dpo1 or Dpo4 alone or bound to the 31base hairpin was measured using a Beckman Coulter ProteomeLab PA800 instrument and a 60 cm, 50 μm ID, eCap amine capillary. An electrosmotic flow marker (EFO), 0.02% v/v DMSO, was injected with each sample with detection at 214 nm. A voltage of 6 kV was applied and the protein electrophoretic mobility (μ_p) was calculated from the sample velocity (ν_x), the EOF velocity (ν_{EOF}), and the electric filed (E) according to the following equation.(*209, 210*)

$$\mu_p = \frac{\nu_X - \nu_{EOF}}{E} \qquad \text{(Equation 4-11)}$$

The apparent charge (z*) was calculated using $_p$ and the diffusion coefficient (D) from the sedimentation velocity data according to the following equation:

$$z^* = \frac{\mu_p k_B T}{De} \qquad \text{(Equation 4-12)}$$

where k_B is the Boltzmann's constant (1.3807 x 10^{-16} erg/K), T is temperature (K), and e is the elementary charge (1.60 x 10^{-19} C) using ZUtilities (v 1.1).(*211*)

Circular Dichroism (CD) Structural Measurements. Circular dichroism (CD) experiments were performed using a DSM 17 (Olis Inc., Bogart, GA) and a 1 or 5 mm path length cell. Thermostability experiments were assembled either in the presence or absence of the

31 base DNA hairpin (2 μM) and either Dpo1 (4 μM) or Dpo4 (4 μM). The molar ellipticity (Θ) at 222 nm was monitored over a temperature range from 20 to 95 ^{o}C in 5 ^{o}C intervals controlled by a peltier. The spectra from at least three separate scans at were averaged and analyzed as described.(*212*) Structural assays were performed at 20 and 60 ^{o}C using DNA hairpin 10 μM DNA hairpin or 10 μM Dpo1 or Dpo4. The individual spectra were averaged and compared with the spectrum of their mixture (1:1 vol. %).

Scheme 4-1

Scheme 4-2

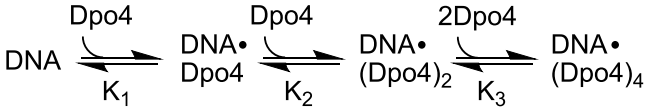

4.2 RESULTS

4.2.1 Detection of Discrete Polymerase/DNA Complexes by EMSA

Previously, we have shown the stepwise assembly of Dpo1 onto primer template DNA included a single higher affinity binding site followed by the cooperative assembly of two additional molecules of Dpo1 with lower affinity.(*120, 208*) In order to directly verify and visualize the stoichiometry and affinity of multiple states of Dpo1-DNA complexes at higher temperatures, we performed electrophoretic mobility shift assays (EMSA) at 22 ^{o}C (Figure 4-1) and 50 ^{o}C (Figure 4-2) binding to a 37 base hairpin DNA substrate. The size of the hairpin (12 base duplex, 10 base duplex, and 3 base hairpin loop) was chosen to restrict binding of

polymerase at a single primer-template junction site, limit nonspecific binding, and be highly thermostable. The melting temperature (T_m) of the DNA hairpin was measured from a shift in the UV absorbance and found to be 88 ± 1 ^oC, which is well above our experimental temperature range. Titration of Dpo1 at low concentrations of DNA (5 nM) clearly showed the presence of multiple gel shifted species (monomer or trimer) with different apparent affinities (Figure 4-1A and 4-2A). For Dpo1, the dissociation constant ($K_{d1,Dpo1}$) for the monomeric species is estimated to be 200 nM, while the trimeric species forms at concentrations greater than 500 nM (Figure 4-1B and 4-2B). Note that the formation of the trimeric Dpo1 species is dependent on prior formation of the monomeric Dpo1 species. Also, no significant dimer species can be resolved using these conditions. Therefore, the binding equilibria can be explained by higher affinity monomeric Dpo1 binding ($K_{1,Dpo1}$) followed by the cooperative assembly of two additional molecules at higher concentrations ($K_{2,Dpo1}$) to form the trimeric species (Scheme 4-1).

Dpo4 has a slightly different binding equilibrium to DNA, where a monomer, dimer, and oligomeric species are individually isolated on EMSAs at 22 ^oC (Figure 4-1C) and 50 ^oC (Figure 4-2C). Based on a number of crystal structures, the oligomeric species most likely represents a tetrameric Dpo4 bound with one molecule of DNA.(*208*) Monomeric Dpo4 binding to DNA has a slightly greater apparent affinity ($K_{d1,Dpo4}$ <100 nM) than monomeric Dpo1 (Figure 4-1B). The dimeric Dpo4 species begins to form at concentrations greater than 300 nM before converting to the oligomeric species at concentrations greater than 1 μM. The binding equilibrium for Dpo4 proceeds through higher affinity monomeric binding ($K_{1,Dpo4}$) followed by subsequent formation

of a dimeric Dpo4 ($K_{2,Dpo4}$) before conversion to the tetrameric species ($K_{3,Dpo4}$) (Scheme 4-2) and are consistent with experiments at 50 °C (Figure 4-2) and those performed previously.(*120*) The EMSAs were very similar at 22 °C and 50 °C.

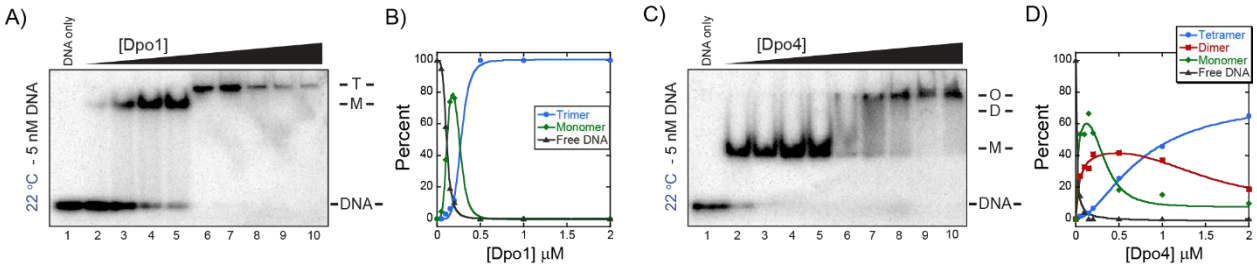

Figure 4-1. EMSA titrations of A) Dpo1 and C) Dpo4 on 4 nM ^{32}P-labelled DNA hairpin at 22 °C. Positions of monomer (M) and trimer (T) for Dpo1, monomer (M), dimer (D), and oligomer (O) for Dpo4 and free DNA are indicated. Quantifications of B) Dpo1 or D) Dpo4 titrations and complexes for free DNA (-▲-), monomer (-♦-), dimer (-■-), or oligomer (-●-) were simulated and fit as described in Experimental Procedures.

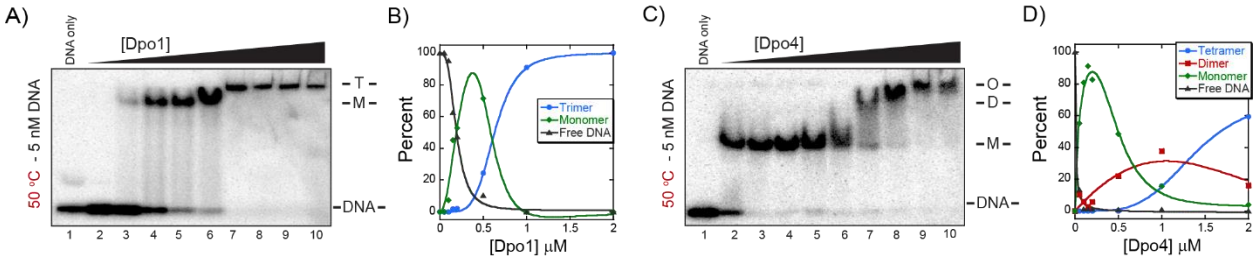

Figure 4-2. EMSA titrations of A) Dpo1 and C) Dpo4 on 4 nM ^{32}P-labelled DNA hairpin at 50 °C. Positions of monomer (M) and trimer (T) for Dpo1, monomer (M), dimer (D), and oligomer (O) for Dpo4 and free DNA are indicated. Quantifications of B) Dpo1 or D) Dpo4 complexes for free DNA (-▲-), monomer (-♦-), dimer (-■-), trimer or oligomer (-●-) were simulated and fit as described in Experimental Procedures.

4.2.2 EMSA that mimic the forward ITC (DNA into protein) at low and high temperature

Before performing forward ITC experiments, we decided to mimic these titrations by performing EMSA experiments at 22 °C (Figure 4-3) and 50 °C (Figure 4-4) to visualize individual protein/DNA complexes during the course of the titration and inform our fitting

parameters. At low concentrations of DNA, a trimeric Dpo1 species is clearly seen (Figure 4-3A-C and 4-4A-C). After titrating increasing concentrations of DNA, there is a concerted conversion to a monomeric Dpo1/DNA species converting to at 1:1 species at the appropriate stoichiometry. Similar results are apparent for Dpo4 where an oligomeric complex is converted stepwise through dimeric Dpo4/DNA and monomeric Dpo4/DNA species also with appropriately quantified stoichiometries (Figure 4-3D-F and 4-4D-F).

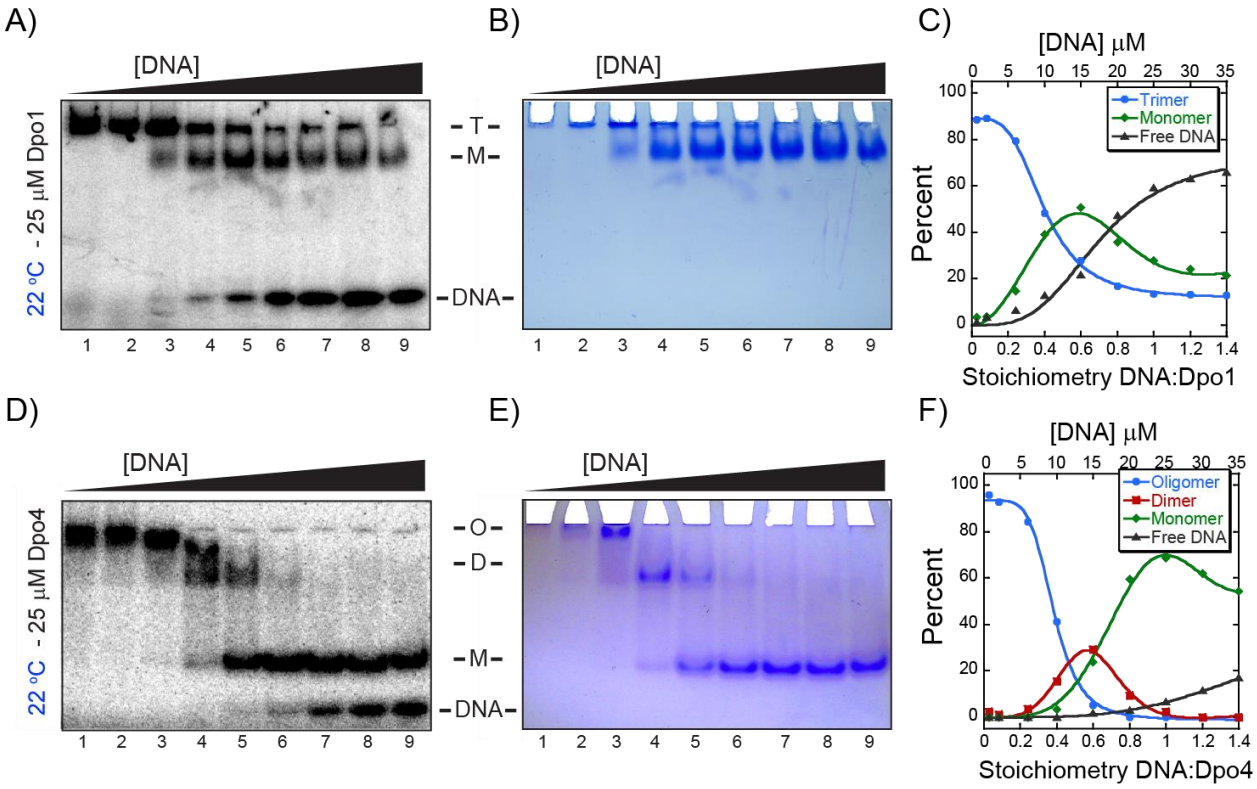

Figure 4-3. Stoichiometric EMSA titrations of DNA hairpin into 25 μM A) Dpo1 and D) Dpo4 at 22 °C. Constant trace amounts of ^{32}P-labelled DNA are present in each lane. Corresponding Coomassie-stained gels of B) Dpo1 and E) Dpo4. Positions of monomer (M) and trimer (T) for Dpo1 and monomer (M), dimer (D), and oligomer (O) for Dpo4 and free DNA are indicated. Quantifications of C) Dpo1 or F) Dpo4 titrations and complexes for free DNA (-▲-), monomer (-♦-), dimer (-■-), or oligomer (-●-) were simulated and fit as described in Experimental Procedures.

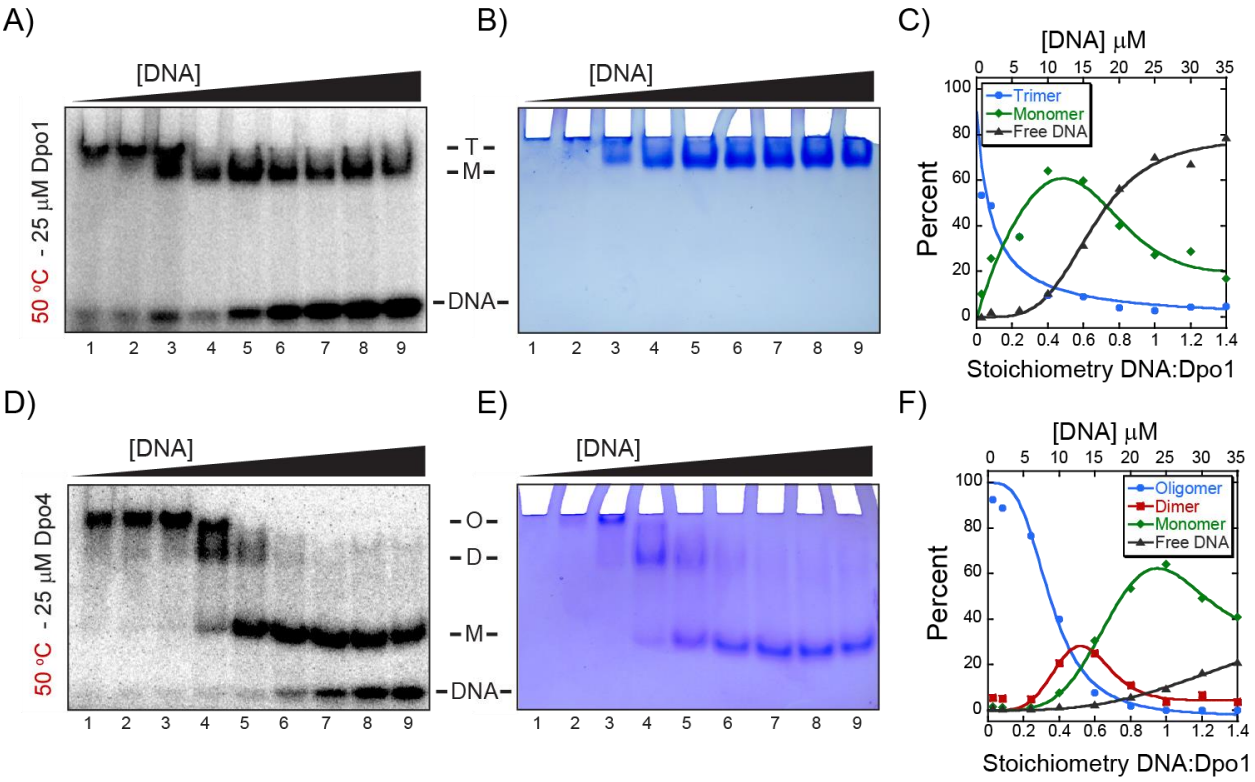

Figure 4-4. Stoichiometric EMSA titrations of DNA hairpin into 25 μM A) Dpo1 and D) Dpo4 at 50 °C. Constant trace amounts of ^{32}P-labelled DNA are present in each lane. Corresponding Coomassie-stained gels of B) Dpo1 and E) Dpo4. Positions of monomer (M) and trimer (T) for Dpo1 and monomer (M), dimer (D), and oligomer (O) for Dpo4 are indicated. Quantifications of C) Dpo1 or F) Dpo4 titrations and complexes for free DNA (-▲-), monomer (-♦-), dimer (-■-), or oligomer (-●-) were simulated and fit as described in Experimental Procedures.

4.2.3 Temperature dependence of binding Dpo1 and Dpo4 to primed DNA as determined by forward isothermal titration calorimetry (ITC) experiments (DNA titrated into protein)

In the forward ITC titrations (DNA into protein) experiments, DNA is titrated into a constant amount (~25 μM) of protein and the observed enthalpies are measured. Titrations were performed from 5 - 60 °C and the change in enthapies (ΔH_{obs}), stoichiometries (n), and association constants (K_a) for Dpo1-DNA and Dpo4-DNA complex formation were measured as a function of temperature. These parameters and the calculated binding free energy (ΔG^o) and change in entropy ($T\Delta S_{obs}$) are calculated from a fit to a single-site equation (Equation 4-1) and listed in Tables 4-1 & 4-2 for Dpo1 and Dpo4, respectively. With these experimental conditions,

DNA will be titrated into an equilibrium solution that quickly favors oligomeric complex formation for both Dpo1 (trimer) and Dpo4 (dimer/tetramer) on DNA as a result of excess protein over DNA. As the titration proceeds, the equilibrium will shift towards more monomeric polymerase binding to DNA. Figure 4-5 shows representative titrations and fits (Equation 4-1) for forward titrations of Dpo1 and Dpo4 at 20 and 60 ^{o}C, respectively. Binding of either thermophilic polymerase to DNA is again primarily entropically driven at lower temperatures and enthalpically driven at higher temperatures.

Table 4-1.Thermodynamic parameters for ITC forward titrations of DNA into Dpo1[1]

Temp (^{o}C)	ΔH^{o} (kcal/mol)	$T\Delta S^{o}$ (kcal/mol)	*Ka* (10^{6})	ΔG^{o} (kcal/mol)	*n* (Dpo1:DNA)	ΔC^{o}_{p} (kcal/mol K)[2]
5	13.6	20.8	0.53	-7.3	2.5	0.99
10	15.0	22.3	0.42	-7.3	2.3	0.69
15	20.0	27.4	0.41	-7.4	2.3	0.39
20	19.3 ± 2.0	27.1 ± 3.4	0.65	-7.8 ± 0.2	2.5	0.10
25	20.9 ± 2.7	28.4 ± 2.6	0.33	-7.5 ± 0.1	2.2	-0.20
30	16.2 ± 2.0	23.5 ± 1.7	0.19	-7.3 ± 0.3	2.0	-0.49
32	18.9	26.5	0.24	-7.5	2.3	-0.61
35	16.4	24.1	0.30	-7.7	2.5	-0.79
37	16.1	23.5	0.15	-7.4	1.8	-0.90
40	10.2	18.3	0.45	-8.1	2.9	-1.08
44	5.1	13.0	0.26	-7.9	2.6	-1.32
45	4.7	12.9	0.39	-8.1	2.1	-1.38
49	-2.7	6.5	1.7	-9.2	5.0	-1.61
50	-2.4	8.0	11.3	-10.4	5.6	-1.67
52	-6.2	2.3	0.49	-8.5	6.3	-1.79
55	-13.3	-4.2	1.22	-9.2	2.6	-1.97
60	-21.8 ± 2.0	-12.7 ± 3.6	0.96	-9.1 ± 0.1	2.6	-2.26

[1]Standard error calculated from multiple ITC experiments. Calculated form a single site mode (Equation 4-1). [2]Calculated from the tangent to the fit in Figure 4-6A.

Table 4-2.Thermodynamic parameters for ITC titrations of DNA into Dpo4[1]

Temp (^oC)	ΔH^o (kcal/mol)	$T\Delta S^o$ (kcal/mol)	*Ka* (10^6)	ΔG^o (kcal/mol)	*n* (Dpo4:DNA)	ΔC^o_p (kcal/mol K)[2]
2.2	6.9	14.6	1.3	-7.7	1.4	0.03
5	7.4	14.9	0.89	-7.6	1.6	-0.01
7	7.9	15.5	0.87	-7.6	1.6	-0.04
10	7.4 ± 0.5	15.1 ± 0.6	0.78	-7.6 ± 0.1	1.4	-0.08
15	7.9	15.7	0.74	-7.7	1.5	-0.14
20	8.5	16.4	0.78	-7.9	1.5	-0.21
25	8.9 ± 0.9	16.6 ± 0.7	0.44	-7.7 ± 0.1	1.7	-0.27
27	4.6	12.8	0.82	-8.1	1.3	-0.30
30	4.9	12.9	0.67	-8.1	1.4	-0.34
35	-1.7	7.0	1.4	-8.7	2.8	-0.27
40	-2.0	7.0	2.2	-9.1	2.9	-0.47
45	-3.0 ± 0.3	7.3 ± 0.9	13.5	-10.4	2.0	-0.53
50	-7.7 ± 0.3	1.4 ± 0.4	1.5	-9.1 ± 0.1	2.3	-0.60
55	-7.6	7.8	2.9	-9.2	1.8	-0.66
60	-9.7 ± 1.0	6.5 ± 0.3	1.5	-9.1 ± 0.3	1.7	-0.73

[1]Standard error calculated from multiple ITC experiments. Calculated form a single site mode (Equation 4-1). [2]Calculated from the tangent to the fit in Figure 4-6B.

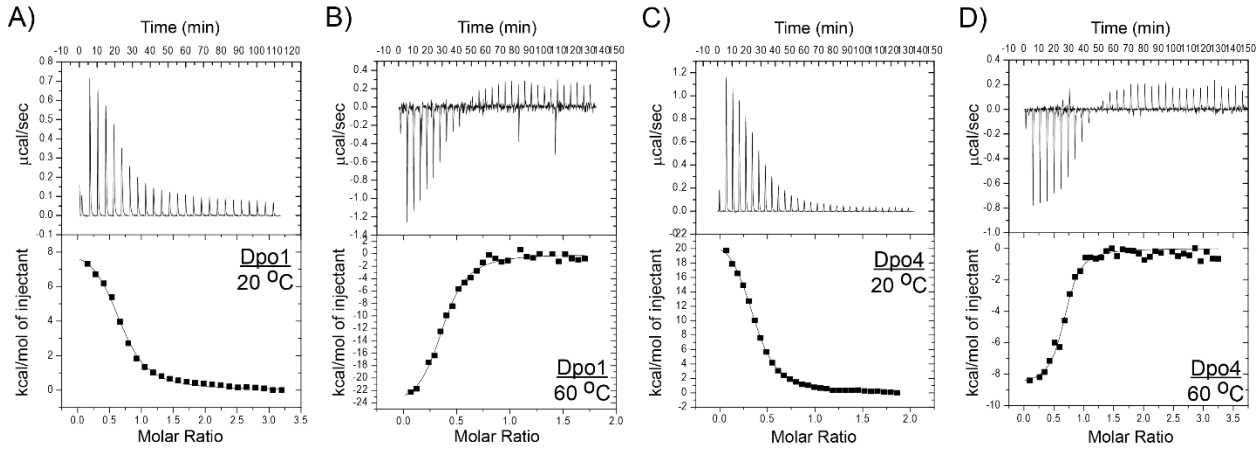

Figure 4-5. Representative ITC forward titrations of primer template DNA into Dpo1 at A) 20 ^oC and B) 60 ^oC; and Dpo4 at C) 20 ^oC and D) 60 ^oC. Top panels are raw isotherms and bottom panels are integrated heats and their fitting. Binding is endothermic at 20 ^oC and exothermic at 60 ^oC for both DNA polymerases. The thermodynamic parameters for all experiments are reported in Table 4-1 and 4-2.

The individual enthalpies obtained from the forward ITC fits to Equation 4-1 were plotted as a function of temperature to measure the calorimetric heat capacity change for the binding equilibria of Dpo1 or Dpo4 to DNA (Figure 4-6). The resulting thermodynamic parameters ΔH^o and $T\Delta S^o$ are again found to be parallel and temperature dependent leading to

small changes in ΔG^o. Interestingly a plot of ΔH^o as a function of temperature for Dpo1 binding show that the change in heat capacities ($\Delta C^o_{p,Dpo1}$) are not independent of temperature. In fact in both cases, ΔC^o_p is strongly temperature dependent and changes from an unusual positive to a more conventional negative value as the temperature is increased indicative of more specific complementarity of binding without any change in solution conditions (Figure 4-6C). A fit of the ΔH^o for Dpo1 to Equation 4-10 extracted large temperature dependent heat capacity values ($\Delta\Delta C^o_{p,Dpo1}$) of -59 ± 3 cal mol^{-1} K^{-2}, respectively (Figure 4-6). Note that, this large negative $\Delta\Delta C^o_{p,Dpo1}$ causes a change in values of $\Delta C^o_{p,Dpo1}$ from 1.10 kcal mol^{-1} K^{-1} at 3 ^oC to -2.26 kcal mol^{-1} K^{-1} at 60 ^oC.

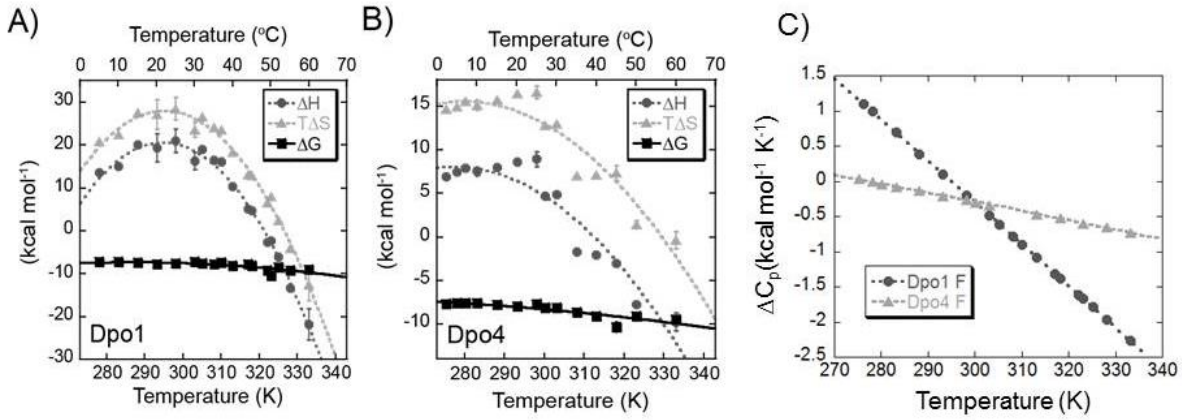

Figure 4-6. Temperature dependencies of the enthalpies (ΔH^o, -●-), entropies ($T\Delta S^o$, -▲-), or free energies (ΔG^o, -■-) for the forward ITC titrations (DNA into protein) fitted to single-site mode for A) Dpo1 or B) Dpo4. Error bars represent the standard error from multiple experiments. C) The enthalpies for ΔH_{Dpo1} were fit to Equation 4-10 for $\delta H^{cal}/\delta T$. $\Delta\Delta C^o_{p,Dpo1}$ was found to be -59 ± 3 cal mol^{-1} K^{-2}. $\Delta C^o_{p,Dpo1}$ values ranged from 1.10 kcal mol^{-1} K^{-1} at 3 ^oC to -2.26 kcal mol^{-1} K^{-1} at 60 ^oC. The enthalpies for ΔH^o_{Dpo4} were also fit to Equation 4-10 for $\delta H^{cal}/\delta T$. $\Delta C^o_{p,Dpo4}$ was found to be -13 ± 4 cal mol^{-1} K^{-2}. $\Delta C^o_{p,Dpo4}$ values for ΔH^o_{Dpo4} ranged from 0.02 kcal mol^{-1} K^{-1} at 3 ^oC to -0.73 kcal mol^{-1} K^{-1} at 60 ^oC. The individual thermodynamic parameters are reported in Table 4-2.

Forward ITC titrations with Dpo4 (Figure 4-6B) shows a similar character as with Dpo1 (Figure 4-6A). Note that at 40 ^oC, the enthalpy of binding approaches the T_H (where $\Delta H = 0$) and could not be measured accurately. The $\Delta\Delta C^o_p$ value for Dpo4 in the forward titration was found

to be -13 ± 4 cal mol^{-1} K^{-2} causing ΔC^{o}_{p} to range from 0.02 kcal mol^{-1} K^{-1} at 3 ^{o}C to -0.73 kcal mol^{-1} K^{-1} at 60 ^{o}C. Both measured enthalpic values and associated equilibria for Dpo4 binding to DNA are also strongly affected by temperature. Based on the stoichiometries described below, K_3 in Scheme 2 has little influence in these forward titrations. (Figure 4-7)

The stoichiometry for Dpo1 binding to DNA (protein:DNA) are consistent with a trimeric Dpo1/DNA complex at almost all temperatures (Table 4-1). In these forward ITC titrations, the concentration of protein is high in the cell (~20 μM) and small amounts of DNA are titrated into the cell promoting an initial equilibrium shift towards trimer formation. Equilibrium exchange of Dpo1 subunits from a trimeric Dpo1/DNA complex towards a monomeric Dpo1/DNA complex during the course of the titration would result in a slightly greater stoichiometry value from theoretical (i.e. < 3). This along with a change in solution equilibria with temperature will make the stoichiometry measured by ITC a lower limit of the binding. Interestingly, the stoichiometry values seem decrease slightly with increasing temperature (Figure 4-7) suggesting that a trimeric Dpo1/DNA complex is thermodynamically favored at higher temperatures.

Similarly, a multimeric stoichiometry, (protein:DNA), is also measured for Dpo4 that also decreases slightly with temperature (Table 4-2 & Figure 4-7). This slight temperature dependence in the stoichiometry values suggests that multiequilibria processes also vary across the temperature range for this enzyme. Instead of converging on a tetrameric Dpo4/DNA stoichiometry (i.e. n = 4), the values are more consistent with a dimer under these ITC titration conditions and concentrations. Although the increase in stoichiometry values with temperature for the forward ITC experiments are not statistically significant for both Dpo1 and Dpo4 according to the statistical T-test, the temperature-dependence trend is consistent with other

techniques such as EMSA, analytical ultracentrifugation (Chapter 3) and fluorescence anisotropy (Chapter 3).

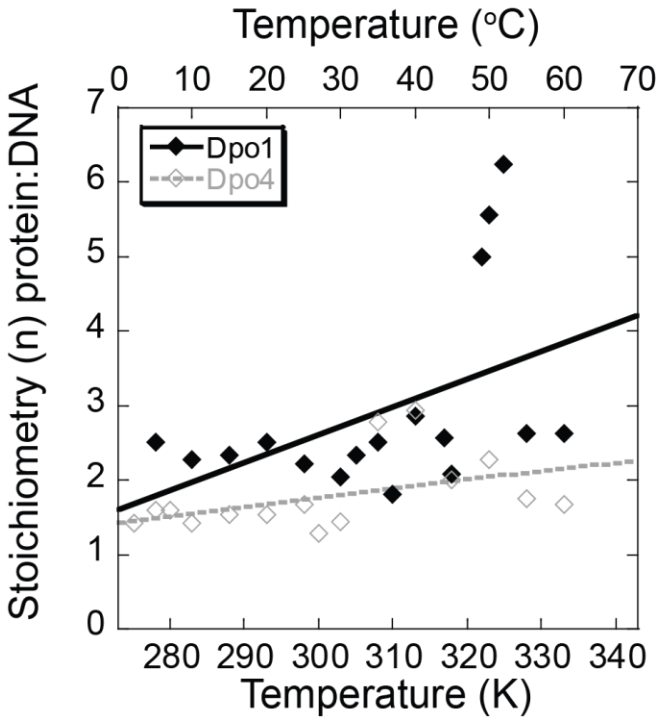

Figure 4-7. Plot of the reciprocal stoichiometry (n) of binding (protein:DNA) for Dpo1 (-♦-) and Dpo4 (-◊-) as a function of temperature in the forward ITC titrations. Individual data is included in Tables 4-1 and 4-2. Included are lines indicating the stoichiometry position of dimer, trimer, and tetramer bound to DNA.

4.2.4 EMSA that mimic the reverse ITC (Protein into DNA) at low and high temperature

Again, we used EMSAs that mimic the titration course of reverse ITC to understand the relative population of oligomeric and monomeric polymerase-DNA complexes at 22 and 50 ^{o}C. Similar to the EMSA that mimicked the forward ITC, monomeric and trimeric Dpo1 species are also clearly seen in the reverse titration (Figure 4-8A-B). Quantification of the ^{32}P shifted DNA bands, show an intermediate stoichiometry (Dpo1:DNA) peak around 1.5 followed by a conversion to a stoichiometry of three, consistent with trimer Dpo1 (Figure 4-8C). Monomeric, dimeric, and tetrameric species for Dpo4 are also verified on phophorimaged (Figure 4-8D) and commasie stained (Figure 4-8E) EMSA gels and quantified appropriately (Figure 4-8F).

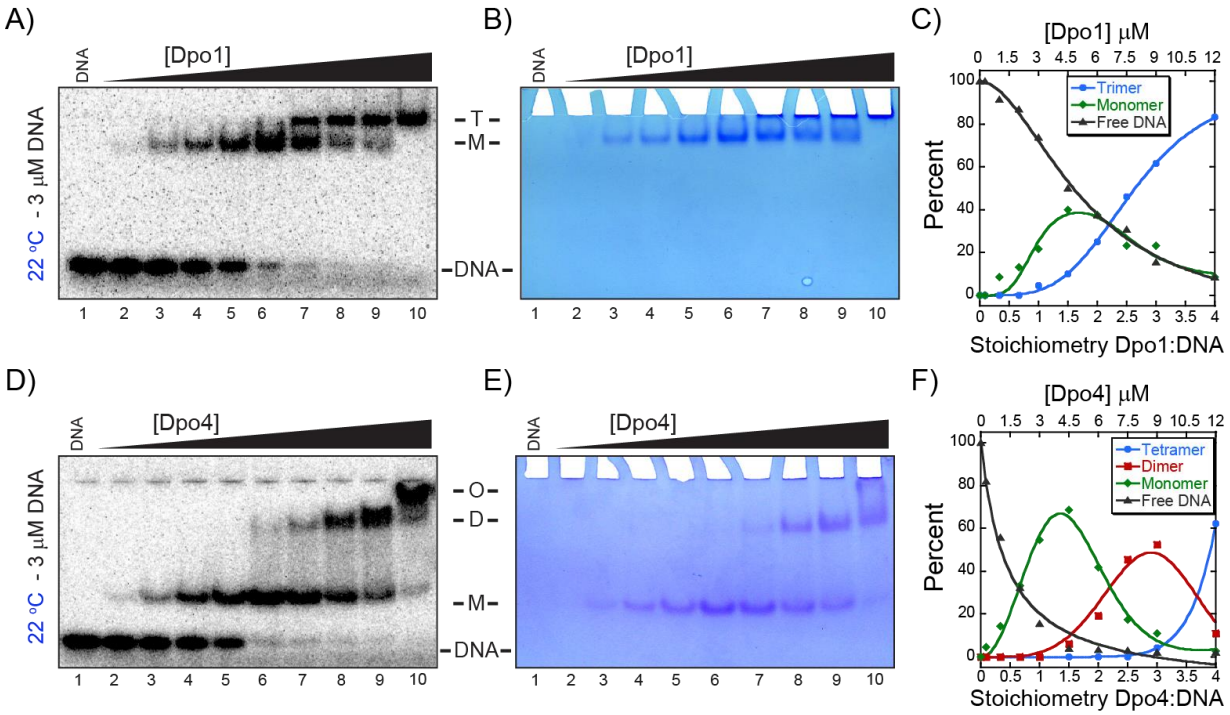

Figure 4-8. Stoichiometric EMSA titrations of A) Dpo1 and D) Dpo4 on 3 M DNA hairpin at 22 °C. Constant trace amounts of ^{32}P-labelled DNA are present in each lane. Corresponding Coomassie-stained gels of B) Dpo1 and E) Dpo4. Positions of monomer (M) and trimer (T) for Dpo1 and monomer (M), dimer (D), and oligomer (O) for Dpo4 are indicated. Quantifications of C) Dpo1 or F) Dpo4 titrations and complexes for free DNA (-▲-), monomer (-♦-), dimer (-■-), or oligomer (-●-) were simulated and fit as described in Experimental Procedures.

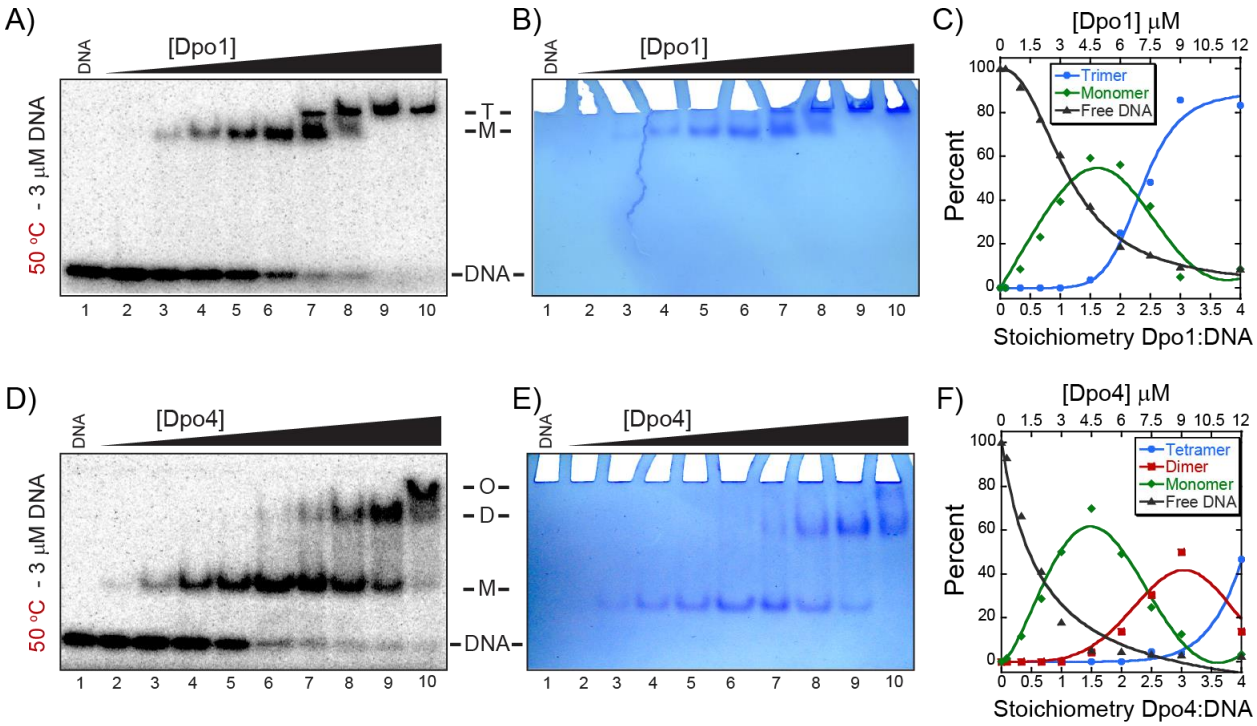

Figure 4-9. Stoichiometric EMSA titrations of A) Dpo1 and D) Dpo4 on 3 M DNA hairpin at 50 °C. Corresponding Coomassie-stained gels of B) Dpo1 and E) Dpo4. Constant trace amounts of ^{32}P-labelled DNA are present in each lane. Positions of monomer (M) and trimer (T) for Dpo1, monomer (M), dimer (D), and oligomer (O) for Dpo4 and free DNA are indicated. Quantifications of C) Dpo1 or F) Dpo4 titrations and complexes for free DNA (-▲-), monomer (-♦-), dimer (-■-), trimer or oligomer (-●-) were simulated and fit as described in Experimental Procedures.

4.2.5 Temperature dependence of binding Dpo1 and Dpo4 to primed DNA determined by reverse isothermal titration calorimetry experiments (protein titrated into DNA) fitting to single-site mode (Equation 4-1)

In order to more completely understand the thermodynamic parameters of polymerase assembly onto DNA, we measured the change in enthalpy (ΔH_{obs}) and association constants (K_a) for Dpo1-DNA and Dpo4-DNA complex formation as a function of temperature using ITC in a reverse experiment (protein into DNA). Data were fitted to a single-site mode (Equation 4-1) resulting in thermodynamic parameters and the calculated binding free energy ΔG^o and change in entropy ($T\Delta S_{obs}$), which are listed in Tables 4-3 and 4-4 for Dpo1 and Dpo4, respectively. Reverse titrations of each polymerase titrated into DNA were performed from 5 - 60 ^oC. With these experimental conditions, protein will be titrated into a multiequilibria solution that initially favors monomeric polymerase/DNA complex formation similar to the EMSA in Figure 4-8A-C. As the titration proceeds, an equilibrium between monomer and oligomer binding will dominate. ITC experiments were performed across a range of temperatures to investigate both the enthalpic and entropic contributions to binding. Figure 4-10 shows representative titrations and fits for titrations of Dpo1 or Dpo4 into DNA at low and high temperatures, respectively. Binding of either thermophilic polymerase to DNA is primarily entropically driven at lower temperatures and enthalpically driven at higher temperatures. Although other equations including two sites sequential (Equation 4-2) and two independent sites were used to fit the raw isotherm data, a single site mode (Equation 4-1) has been used to report $\Delta\Delta C^o_p$ values that more close to the average of $\Delta\Delta C^o_p$ for 26 different systems.(*38*) A three-step sequential binding equation (n=3) was not able to fit most of the data accurately or consistently.

Table 4-3.Thermodynamic parameters for ITC titrations of Dpo1 into DNA[1]

Temp (^oC)	ΔH^o (kcal/mol)	$T\Delta S^o$ (kcal/mol)	*Ka* (10^6)	ΔG^o (kcal/mol)	*n* (Dpo1:DNA)	ΔC^o_p (kcal/mol K)[2]
3	8.0 ± 0.1	15.0 ± 0.1	0.3	-7.0 ± 0.1	1.4	0.51
5	7.9 ± 1.8	15.1 ± 1.6	0.4	-7.2 ± 0.2	1.4	0.48
7.5	5.5 ± 1.9	13.0 ± 1.8	0.7	-7.5 ± 0.2	1.8	0.44
10	5.8 ± 0.8	13.5 ± 0.6	0.8	-7.7 ± 0.2	1.4	0.40
15	5.8 ± 0.4	13.6 ± 0.3	0.8	-7.8 ± 0.1	1.5	0.33
20	5.5 ± 0.7	13.8 ± 0.7	1.5	-8.3 ± 0.2	1.3	0.26
25	8.1 ± 1.1	16.0 ± 1.0	0.7	-8.0 ± 0.2	1.2	0.19
30	6.8 ± 0.8	15.3 ± 0.7	1.2	-8.5 ± 0.1	1.5	0.11
35	9.3 ± 2.1	17.2 ± 2.1	0.4	-7.9 ± 0.1	1.1	0.04
40	2.3 ± 1.7	11.5 ± 1.7	2.4	-9.1 ± 0.3	1.4	-0.03
45	2.8 ± 2.1	11.9 ± 2.2	1.8	-9.1 ± 0.3	1.1	-0.10
50	1.8 ± 1.6	10.9 ± 1.6	1.4	-9.1 ± 0.1	1.2	-0.18
55	-2.3 ± 1.4	7.8 ± 1.6	5.8	-10.1 ± 0.3	1.9	-0.25
60	-7.2 ± 1.3	2.1 ± 1.4	1.2	-9.3 ± 0.2	1.3	-0.32

[1]Standard error calculated from multiple ITC experiments. Fit to a single site mode (Equation 4-1). [2]Calculated from the tangent to the fit in Figure 4-11A.

Table 4-4. Thermodynamic parameters for ITC titrations of Dpo4 into DNA[1]

Temp (^oC)	ΔH^o (kcal/mol)	$T\Delta S^o$ (kcal/mol)	*Ka* (10^6)	ΔG^o (kcal/mol)	*n* (Dpo4:DNA)	ΔC^o_p (kcal/mol K)[2]
3	3.8 ± 0.2	12.1 ± 0.5	3.3	-8.2 ± 0.3	1.6	-0.02
5	4.4 ± 0.5	12.6 ± 0.6	2.6	-8.2 ± 0.2	1.5	-0.03
10	3.7 ± 1.1	12.5 ± 0.9	7.2	-8.9 ± 0.2	1.5	-0.07
15	4.5 ± 0.4	13.2 ± 0.6	4.5	-8.8 ± 0.2	1.5	-0.10
20	2.3 ± 0.2	11.6 ± 0.2	7.9	-9.2 ± 0.1	1.5	-0.13
25	2.6 ± 0.2	11.6 ± 0.1	4.2	-9.0 ± 0.1	1.6	-0.17
30	2.3 ± 0.2	11.2 ± 0.1	3.0	-9.0 ± 0.2	1.3	-0.20
35	0.2 ± 1.2	10.0 ± 1.4	9.8	-9.9 ± 0.3	1.3	-0.24
40	-2.4 ± 1.3	6.3 ± 1.1	1.1	-8.7 ± 0.2	1.6	-0.27
45	-5.1 ± 2.1	3.9 ± 2.5	1.4	-8.9 ± 0.4	1.8	-0.30
50	-3.0 ± 1.0	6.3 ± 1.6	1.8	-9.3 ± 0.7	1.6	-0.34
55	-4.3 ± 0.5	5.5 ± 0.5	3.4	-9.8 ± 0.2	2.1	-0.37
60	-8.6 ± 0.3	1.2 ± 0.2	2.7	-9.8 ± 0.2	1.2	-0.41

[1]Standard error calculated from multiple ITC experiments. Fit to a single site mode (Equation 4-1). [2]Calculated from the tangent to the fit in Figure 4-11B.

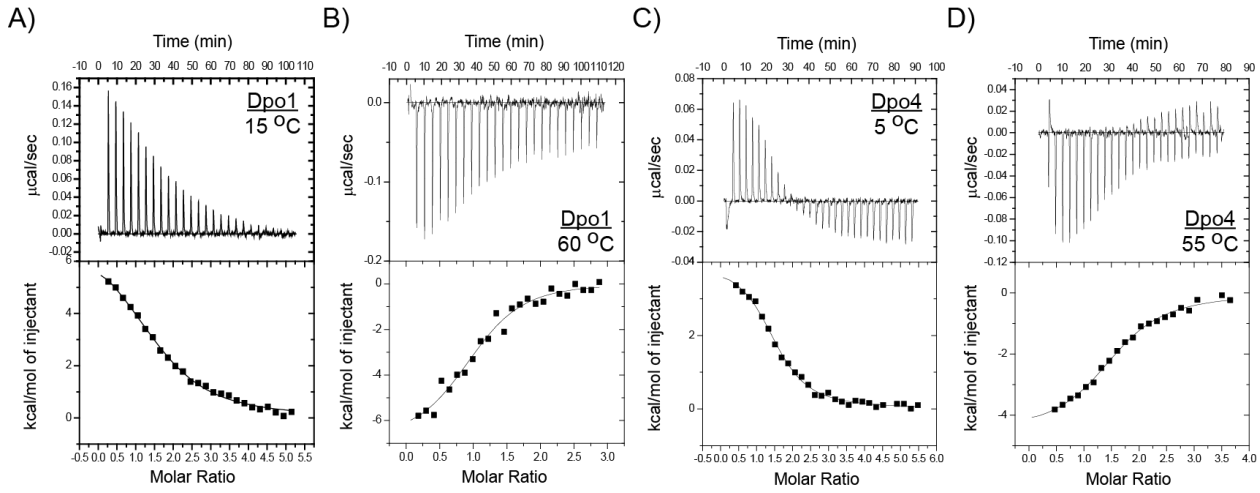

Figure 4-10. Representative ITC titrations of Dpo1 at A) 15 °C and B) 60 °C; and Dpo4 at C) 5 °C and D) 55 °C into hairpin DNA. Top panels are raw isotherms and bottom panels are integrated heats and their fitting. Binding is endothermic at low temperatures and exothermic at higher temperatures for both DNA polymerases. The thermodynamic parameters for all temperatures are reported in Tables 4-3 and 4-4.

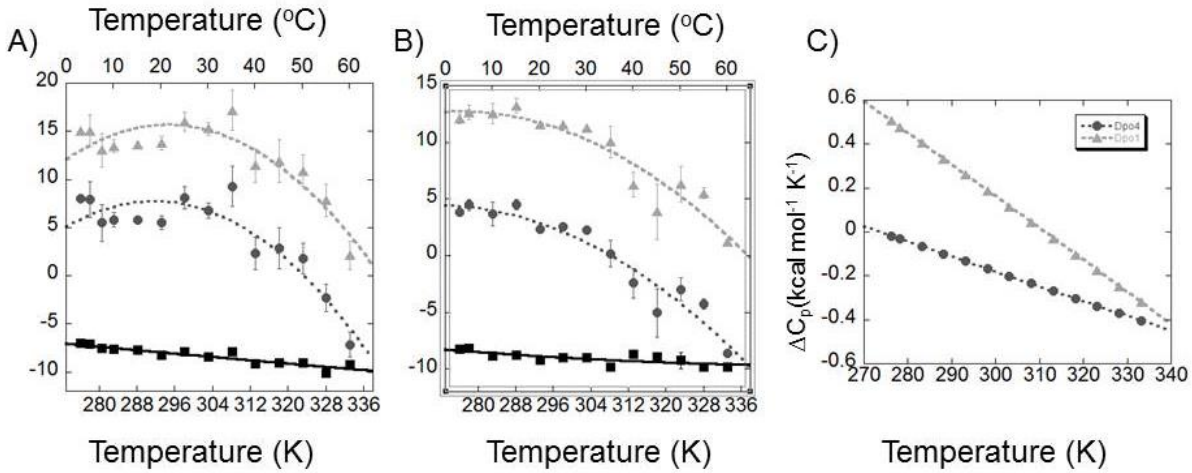

Figure 4-11. Temperature dependencies of the enthalpies (ΔH^o, -●-), entropies ($T\Delta S^o$, -▲-), or free energies (ΔG^o, -■-) for the reverse ITC titrations (protein into DNA) for A) Dpo1 or B) Dpo4. Error bars represent the standard error from multiple experiments. C) The enthalpies for ΔH^o_{Dpo1} were fit to Equation 4-10 for $\delta H^{cal}/\delta T$. $\Delta\Delta C^o_{p,Dpo1}$ was found to be -16 ± 4 cal mol^{-1} K^{-2}. $\Delta C^o_{p,Dpo1}$ values ranged from 0.25 kcal mol^{-1} K^{-1} at 3 °C to -0.66 kcal mol^{-1} K^{-1} at 60 °C. The enthalpies for ΔH^o_{Dpo4} were also fit to Equation 4-10 for $\delta H^{cal}/\delta T$. $\Delta\Delta C^o_{p,Dpo4}$ was found to be -6 ± 2 cal mol^{-1} K^{-2}. $\Delta C^o_{p,Dpo4}$ values for ΔH^o_{Dpo4} ranged from -0.03 kcal mol^{-1} K^{-1} at 3 °C to -0.37 kcal mol^{-1} K^{-1} at 60 °C. The individual thermodynamic parameters are reported in Table 4-3 and 4-4.

The individual enthalpies obtained from the reverse ITC fits were plotted as a function of temperature to measure the calorimetric heat capacity change for the binding equilibria of Dpo1

to DNA (Figure 4-11). Similar to the forward ITC, the change in enthalpy of monomeric Dpo1 binding to DNA as a function of temperature shows a curvature in the data indicating that the change in heat capacity is temperature dependent, but this curvature is shallow than the curvature of the forward titration. A fit of the data to Equation 4-10 gives a temperature dependent heat capacity value ($\Delta\Delta C^{o}_{p,Dpo1}$) of -16 ± 4 cal mol^{-1} K^{-2} (Figure 4-11). A derivative of the fit to Equation 4-10 and resulting tangent show that the heat capacity values ($\Delta C^{o}_{p,Dpo1}$) change from 0.25 kcal mol^{-1} K^{-1} at 3 ^{o}C to -0.66 kcal mol^{-1} K^{-1} at 60 ^{o}C and including both positive and negative values. This apparent sign reversal in ΔC^{o}_{p} as well as the detection of multiple DNA bound species of Dpo1 suggests that the coupled equilibria changes (K_1 through K_2 in Scheme 4-1) as a function of temperature to where more structural complementary exists at higher temperatures associated with larger negative ΔC^{o}_{p} values.

For Dpo4 binding to DNA, the change in enthalpies as a function of temperature also shows slightly curvature. Fitting to Equation 4-10 gave $\Delta\Delta C^{o}_{p,Dpo4}$ values of -6 ± 2 cal mol^{-1} K^{-2}. A derivative of the fit for ΔH^{o}_{Dpo4} and resulting tangent show that the heat capacity values ($\Delta C^{o}_{p,Dpo4}$) change from -0.03 kcal mol^{-1} K^{-1} at 3 ^{o}C to -0.37 kcal mol^{-1} K^{-1} at 60 ^{o}C.

4.2.6 Temperature dependence of binding Dpo1 and Dpo4 to primed DNA determined by reverse isothermal titration calorimetry experiments (protein titrated into DNA) fitting to the two-site sequential binding mode (Equation 4-2)

In order to separate the thermodynamic parameters of polymerase for the stepwise assembly onto DNA, we also fitted the reverse ITC (protein into DNA) with the two-site sequential mode (Equation 4-2&3) for both Dpo1 and Dpo4. The resulting parameters and the

calculated binding free energy (ΔG^o) and change in entropy ($T\Delta S_{obs}$) are listed in Tables 4-5 and 4-6 for Dpo1 and Dpo4, respectively, and plotted into Figure 4-12. For both the first and second association step, binding of polymerase to DNA is primarily entropically driven at lower temperatures and enthalpically driven at higher temperatures consistent with the single site models above.

The individual enthalpies (ΔH^o_1 &ΔH^o_2) obtained from the reverse ITC fits were plotted as a function of temperature to measure the calorimetric heat capacity change for the binding equilibria ($\frac{\partial \Delta H^o_{cal}}{\partial T} = \Delta C^o_{p,cal}$) of Dpo1 to DNA (Figure 4-12C). The individual values for ΔH^o_1 and ΔH^o_2 at each temperature are dependent on the quality of the fit to the raw isotherm and the ability to accurately separate these parameters using Equation 4-2.

Similar to the fittings with the single-site mode, a plot of the change in enthalpy ($\Delta H^o_{1,Dpo1}$) of monomeric Dpo1 binding to DNA as a function of temperature shows a curvature in the data indicating that the change in heat capacity ($\Delta C^o_{p,Dpo1}$) is temperature dependent. A fit of the data to Equation 4-10 gives a temperature dependent heat capacity value ($\Delta\Delta C^o_{p,Dpo1}$) of -15 ± 3 cal mol^{-1} K^{-2} (Figure 4-12C). A derivative of the fit to Equation 4-10 and resulting tangent show that the heat capacity values ($\Delta C^o_{p,1,Dpo1}$) change from 0.27 kcal mol^{-1} K^{-1} at 3 ^{o}C to -0.58 kcal mol^{-1} K^{-1} at 60 ^{o}C and including both positive and negative values. This apparent sign reversal in ΔC^o_p as well as the detection of multiple DNA bound species of Dpo1 again suggest that the coupled equilibria changes (K_1 through K_2 in Scheme 4-1) as a function of temperature to where more structural complementary exists at higher temperatures associated with larger negative ΔC^o_p values. A plot of the change in enthalpy ($\Delta H^o_{2,Dpo1}$) resulting from formation of the

trimeric Dpo1 complex on DNA is more linear and giving a more traditional temperature independent change in heat capacity ($\Delta C^o_{p,2,Dpo1}$) of -0.15 kcal mol^{-1} K^{-1}, which is very different from K_2 detected in fluorescence assays (Chapter 3) (-1.0 kcal mol^{-1} K^{-1}). The difference may result from the failure of the fitting by sequential binding mode to the complicated reverse ITC binding scenario or the assumptions made when deriving the ΔC_p values from only equilibrium binding using anisotropy.

For Dpo4 binding to DNA, the change in enthalpies for both $\Delta H^o_{1,Dpo4}$ and$\Delta H^o_{2,Dpo4}$ as a function of temperature also show extreme curvature (Figure 4-13). Fitting of $\frac{\partial \Delta H_1^o}{\partial T}$ or $\frac{\partial \Delta H_2^o}{\partial T}$ to

Equation 4-10 gave $\Delta\Delta C^o_{p,Dpo4}$ values of -6 ± 1 and -3 ± 1 cal mol^{-1} K^{-2}, respectively. A derivative of the fit for $\Delta H^o_{1,Dpo4}$ and resulting tangent show that the heat capacity values ($\Delta C^o_{p,1,Dpo4}$) change from -0.06 kcal mol^{-1} K^{-1} at 3 ^{o}C to -0.31 kcal mol^{-1} K^{-1} at 60 ^{o}C. $\Delta H^o_{1,Dpo4}$ primarily represents the enthalpy associated with monomeric binding (K_1) with smaller contributions from K_2. A similar change is noted for $\Delta H^o_{2,Dpo4}$ where $\Delta C^o_{p,2,Dpo4}$ changes from 0.00 kcal mol^{-1} K^{-1} at 3 ^{o}C to -0.29 kcal mol^{-1} K^{-1} at 60 ^{o}C. Although an absolute sign reversal (positive to negative) in ΔC_p^o for Dpo4 binding to DNA is not directly measured over the

experimental temperature range, positive ΔC^o_p values can be inferred from the fit at temperatures below 0 ^{o}C. Again, larger negative ΔC^o_p values at higher temperatures would imply more structural complementarity of binding. $\Delta H^o_{2,Dpo4}$ in these reverse ITC experiments primarily represents Dpo4 dimer formation (K_2 in Scheme 4-2) with less contribution from the weaker tetrameric association constant, K_3. (Figure 4-7) Therefore, K_1 – K_3 for Dpo4 also have strong dependencies on temperature highlighting changes in couple equilibria processes identified in Figure 4-8 D-F and 4-9 D-F according to the Scheme 4-2.

Interestingly, the free energy (ΔG^o) minima for Dpo1 binding to DNA occurs at a higher temperature than for Dpo4 binding to DNA. $\Delta G^o_{1,Dpo1}$ and $\Delta G^o_{2,Dpo1}$ seem to decrease steadily across the experimental temperature range suggesting that the minima occur at temperatures greater than 60 ^{o}C. ITC experiments performed at temperatures greater than 60 ^{o}C were difficult to interpret because of severe noise in the spectrum from an inability to completely degas buffers at these high temperatures. For Dpo4, $\Delta G^o_{1,Dpo4}$ and $\Delta G^o_{2,Dpo4}$ minima occur at and 27 and 37 ^{o}C, respectively. The greater overall negative values for ΔG^o as well as the shift of the free energy minima to higher temperatures indicates that there is a thermodynamic preference for monomeric and trimeric Dpo1 binding to DNA over Dpo4 at physiological temperatures (~75 ^{o}C) for *Sso*, which was also suggested by fluorescence anisotropy assays (Chapter 3). However, the detected affinities of Dpo4 at temperature less than 40-45 ^{o}C where there is the greatest curvature in $\frac{\partial \Delta H_1^o}{\partial T}$ and $\frac{\partial \Delta H_2^o}{\partial T}$ (Figure 4-11) are roughly ten-times greater in the reverse ITC compared with the fluorescence anisotropy assays (Chapter 3). Interestingly at higher temperatures where $\frac{\partial \Delta H_1^o}{\partial T}$ or $\frac{\partial \Delta H_2^o}{\partial T}$ become more linear and there is less contributions of coupling, the affinities actually agree well between the reverse ITC and fluorescence anisotropy (Chapter 3).

Table 4-5.Thermodynamic parameters for ITC titrations of Dpo1 into DNA[1]

Temp (°C)	ΔH_1° (kcal/mol)	$T\Delta S_1^\circ$ (kcal/mol)	Ka_1 (10^6 M)	ΔG_1° (kcal/mol)	ΔH_2° (kcal/mol)	$T\Delta S_2^\circ$ (kcal/mol)	Ka_2 (10^6)	ΔG_2° (kcal/mol)
3	5.4 ± 0.4	13.1 ± 0.1	2.1	-7.7 ± 1.3	6.1 ± 0.8	11.3 ± 2.1	0.15	-5.2 ± 1.3
5	5.1 ± 0.1	13.0 ± 0.3	2.6	-8.0 ± 0.2	5.9 ± 1.4	12.1 ± 1.5	0.19	-6.2 ± 0.2
7.5	5.1 ± 0.7	13.3 ± 1.2	1.7	-8.2 ± 1.3	5.1 ± 1.0	13.2 ± 2.2	0.29	-8.2 ± 1.3
10	5.0 ± 0.7	13.2 ± 0.7	2.2	-8.2 ± 0.3	4.1 ± 1.5	10.9 ± 1.8	0.19	-6.8 ± 0.3
15	5.2 ± 0.4	13.4 ± 0.4	3.1	-8.2 ± 1.2	3.3 ± 1.2	9.6 ± 1.0	0.42	-6.3 ± 1.2
20	6.5 ± 0.7	14.7 ± 0.5	1.3	-8.2 ± 0.1	1.3 ± 0.6	9.0 ± 0.5	0.52	-7.7 ± 0.1
25	7.7 ± 1.2	16.0 ± 0.9	1.2	-8.3 ± 0.3	1.3 ± 0.6	8.7 ± 0.7	0.25	-7.4 ± 0.3
30	5.5 ± 1.0	15.6 ± 0.5	18.3	-10.0 ± 0.7	3.2 ± 0.9	11.7 ± 0.5	1.39	-8.5 ± 0.4
35	4.9 ± 2.2	13.6 ± 1.9	1.5	-8.7 ± 0.3	0.6 ± 1.4	8.3 ± 1.2	0.30	-7.7 ± 0.3
40	2.4 ± 1.5	12.2 ± 1.2	6.3	-9.7 ± 0.6	-0.1 ± 0.8	8.0 ± 1.0	0.41	-8.0 ± 0.6
45	3.0 ± 1.5	9.8 ± 2.6	1.2	-8.8 ± 0.4	-1.8 ± 1.7	8.6 ± 2.3	0.28	-7.9 ± 0.5
50	0.3 ± 1.5	9.8 ± 1.6	2.3	-9.5 ± 0.7	-1.3 ± 1.1	6.8 ± 0.6	0.15	-8.1 ± 0.7
55	-1.7 ± 1.6	8.8 ± 2.7	7.4	-10.3 ± 0.8	-2.2 ± 1.6	8.8 ± 2.3	0.15	-9.3 ± 0.2
60	-6.1 ± 0.8	4.0 ± 1.1	4.0	-10.1 ± 0.3	-2.6 ± 1.3	6.0 ± 1.4	0.47	-8.6 ± 1.4

[1]Standard error calculated from multiple ITC experiments. Fit to a two-site sequential mode (Equation 4-2&3)

Table 4-6.Thermodynamic parameters for ITC titrations of Dpo4 into DNA[1]

Temp (°C)	ΔH_1° (kcal/mol)	$T\Delta S_1^\circ$ (kcal/mol)	Ka_1 (10^6)	ΔG_1° (kcal/mol)	ΔH_2° (kcal/mol)	$T\Delta S_2^\circ$ (kcal/mol)	Ka_2 (10^6)	ΔG_2° (kcal/mol)
3	3.8 ± 0.6	13.4 ± 0.8	42	-9.6 ± 0.3	2.6 ± 0.5	10.6 ± 0.1	2.2	-8.0 ± 0.3
5	4.0 ± 0.6	13.8 ± 0.9	52	-9.8 ± 0.5	2.2 ± 0.4	10.4 ± 0.2	3.1	-8.3 ± 0.5
10	3.8 ± 0.8	14.3 ± 1.0	130	-10.5 ± 0.1	1.7 ± 0.4	10.6 ± 0.4	8.9	-9.0 ± 0.1
15	4.5 ± 0.5	14.7 ± 0.7	60	-10.2 ± 0.1	1.6 ± 0.3	10.8 ± 0.4	9.0	-9.2 ± 0.1
20	2.3 ± 0.3	13.4 ± 0.7	195	-11.1 ± 0.2	1.5 ± 0.2	10.4 ± 0.4	4.5	-8.9 ± 0.2
25	2.5 ± 0.1	12.9 ± 0.3	45	-10.4 ± 0.2	1.2 ± 0.2	10.3 ± 0.1	5.6	-9.2 ± 0.2
30	2.1 ± 0.1	12.5 ± 0.4	31	-10.4 ± 0.1	0.8 ± 0.2	9.7 ± 0.3	2.7	-8.9 ± 0.1
35	0.1 ± 1.3	10.5 ± 2.1	22	-10.4 ± 0.1	0.1 ± 0.4	9.0 ± 0.3	2.1	-8.9 ± 0.1
40	-2.2 ± 1.2	7.7 ± 0.9	9	-9.9 ± 0.1	-1.5 ± 0.9	7.1 ± 0.8	0.9	-8.5 ± 0.1
45	-3.9 ± 1.2	5.7 ± 1.5	4	-9.5 ± 0.3	-2.9 ± 0.7	5.6 ± 0.5	0.7	-8.5 ± 0.3
50	-2.4 ± 0.5	7.8 ± 1.0	8	-10.2 ± 0.3	-4.1 ± 1.7	4.2 ± 1.4	0.5	-8.4 ± 0.3
55	-3.9 ± 0.2	6.3 ± 0.6	7	-10.3 ± 0.3	-4.0 ± 0.9	5.6 ± 1.1	2.5	-9.6 ± 0.3
60	-8.3 ± 0.5	2.3 ± 1.0	9	-10.6 ± 0.8	-3.9 ± 0.5	4.4 ± 0.5	0.3	-8.3 ± 0.8

Standard error calculated from multiple ITC experiments. Fit to a two-site sequential mode (Equation 4-2&3)

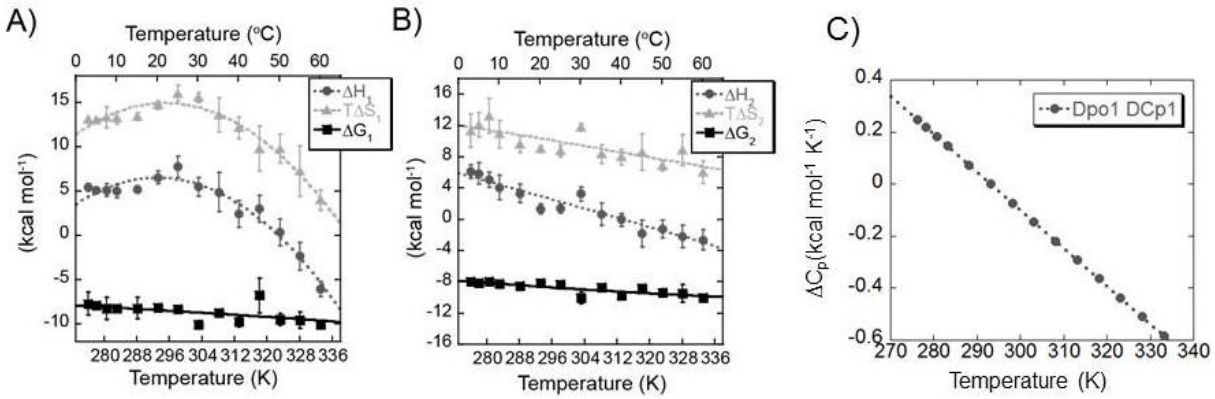

Figure 4-12. Temperature dependencies of the enthalpies (ΔH^o, -●-), entropies ($T\Delta S^o$, -▲-), or free energies (ΔG^o, -■-) for reverse ITC titrations (protein into DNA) for the A) first or B) second binding events for Dpo1. Error bars represent the standard error from multiple experiments. C) The enthalpies for $\Delta H^o_{1,Dpo1}$were fit to Equation 4-10 for $\delta H^{cal}/\delta T$. $\Delta\Delta C^o_{p,1,Dpo1}$ was found to be -15 ± 3 cal mol^{-1} K^{-2} . $\Delta C^o_{p,1,Dpo1}$values ranged from 0.27 kcal mol^{-1} K^{-1} at 3 ^{o}C to -0.58 kcal mol^{-1} K^{-1} at 60 ^{o}C. The enthalpies for $\Delta H^o_{2,Dpo1}$ were fit to Equation 4-10 to yield $\Delta C^o_{p,2,Dpo1}$ = -0.15 ± 0.01 kcal mol^{-1} K^{-1}. The individual thermodynamic parameters are reported in Table 4-7.

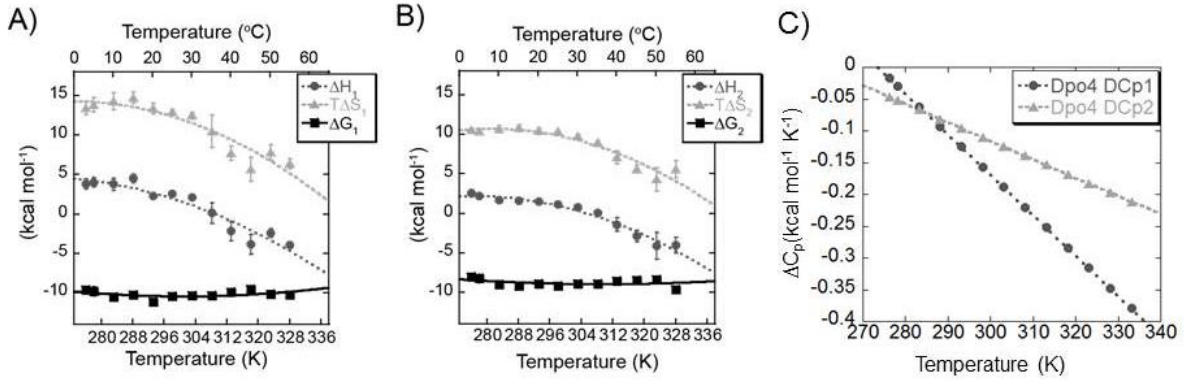

Figure 4-13. Temperature dependencies of the enthalpies (ΔH^o, -●-), entropies ($T\Delta S^o$, -▲-), or free energies (ΔG^o, -■-) for reverse ITC titrations (protein into DNA) for the A) first or B) second binding events for Dpo4. Error bars represent the standard error from multiple experiments. C) The enthalpies for $\Delta H^o_{1,Dpo4}$ were fit to Equation 4-10 for $\delta H^{cal}/\delta T$. $\Delta\Delta C^o_{p,1,Dpo4}$ was found to be -6 ± 1 cal mol^{-1} K^{-2} . $\Delta C^o_{p,1,Dpo}$ 4values ranged from -0.06 kcal mol^{-1} K^{-1} at 3 ^{o}C to -0.31 kcal mol^{-1} K^{-1} at 60 ^{o}C. The enthalpies for $\Delta H^o_{2,Dpo1}$ were also fit to Equation 4-10 for $\delta H^{cal}/\delta T$. $\Delta\Delta C^o_{p,2,Dpo4}$ was found to be -3 ± 1 cal mol^{-1} K^{-2} . $\Delta C^o_{p,2,Dpo4}$values for $\Delta H^o_{1,Dpo4}$ ranged from 0.00 kcal mol^{-1} K^{-1} at 3 ^{o}C to -0.29 kcal mol^{-1} K^{-1} at 60 ^{o}C. The individual thermodynamic parameters are reported in Table 4-8.

4.2.7 ITC Reverse Titration (protein into DNA) shows a floating stoichiometry which depends on initial accessibility to protein for DNA

We have previously measured the stoichiometry of Dpo1 binding to DNA as 3:1 and Dpo4 binding to DNA as 2:1.(*120, 208*) Ideally, the stoichiometry for Dpo1/DNA and Dpo4/DNA in these reverse titrations should be similar, but were experimentally much lower when fit to an independent sites Equation 4-1. To determine if the measured stoichiometry (*n*) is affected by relative concentrations of protein and DNA, we changed the DNA concentration from 2.98 to 1.62 μM in the cell while keeping the concentration of Dpo1 in the syringe constant. Reverse ITC titrations performed at 30 ^{o}C showed an increase in stoichiometry from 1.24 to 1.62 with decreasing concentration of DNA (Figure 4-14). Experiments performed with lower DNA concentrations in the cell shifted the equilibria slightly towards binding additional Dpo1 subunits resulting in an apparent increase in stoichiometry (from 1.24 to 1.62). Therefore, the stoichiometry determined by reverse ITC depends on the initial accessibility to Dpo1 and Dpo4 for DNA. The stoichiometry between polymerase and DNA can therefore be determined more accurately using the forward ITC experiments, in which less DNA is initially titrated into excess polymerase allowing the complete formation of the oligomeric complex earlier in the titration.

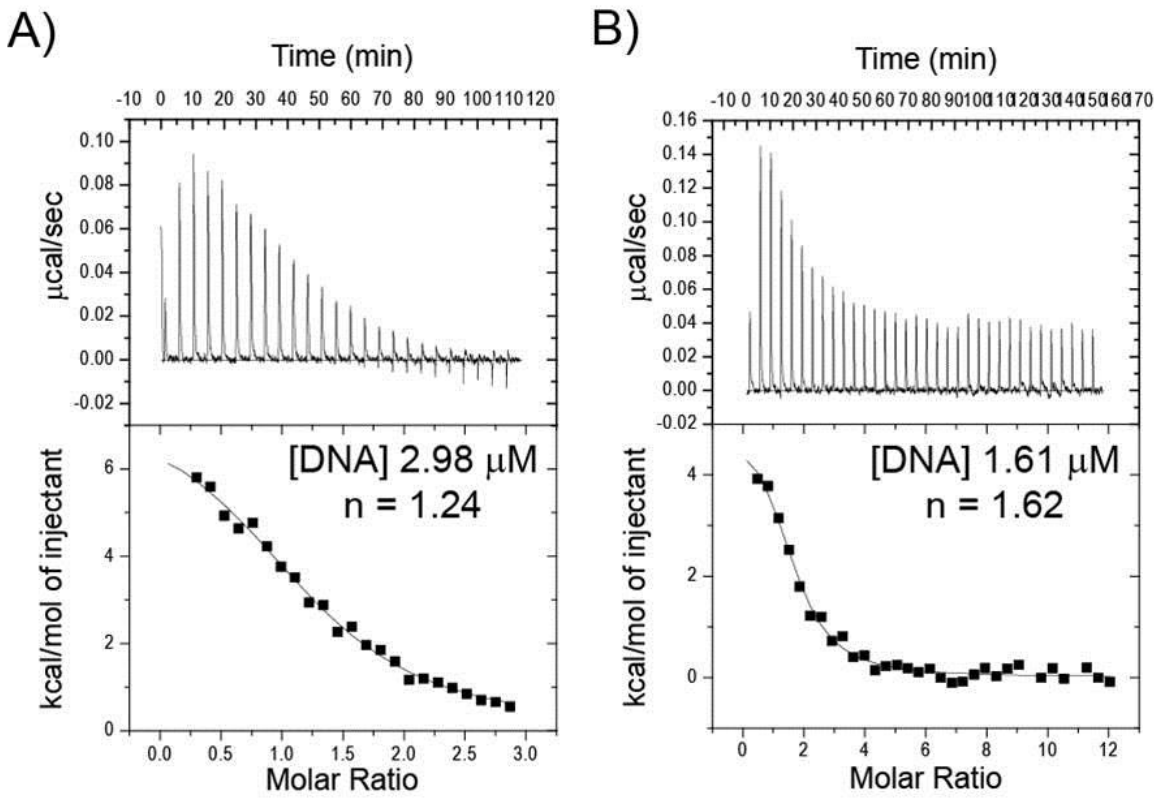

Figure 4-14. Reverse ITC titration of Dpo1 (194.7 µM) into DNA hairpin at 30 ^{o}C at two different concentrations of DNA A) 1.61 µM and B) 2.98 µM were used to examine stoichiometric binding events. Decreasing the concentration of DNA resulted in a greater stoichiometry (n) as indicated suggesting multiple individual binding events. Top panels are raw isotherms and bottom panels are integrated heats and their fitting.

4.2.8 No observed changes in protonation upon polymerase binding to DNA with increasing temperature

The observed enthalpy (ΔH^{o}_{obs}) obtained in the ITC experiments is actually the sum of both the binding enthalpy (ΔH^{o}_{bind}) and the ionization enthalpy of the buffer (ΔH^{b}_{ion}) associated with any change in protonation (ΔN) according to the following equation:(*23*)

$$\Delta H^{o}_{obs} = \Delta H^{o}_{bind} + \Delta N(\Delta H^{b}_{ion} + \Delta H^{b}_{protonation}) \qquad \text{(Equation 4-13)}$$

To assess whether linked protonation occurs along with the binding to explain the temperature dependent heat capacity values ($\Delta\Delta C^{o}_{p}$) measured for Dpo1 and Dpo4 binding to

DNA, we performed forward ITC experiments at different temperatures and with different buffers (phosphate, HEPES, and imidazole) while holding the buffer concentrations and pH (7.0) constant. Each buffer was chosen to represent a broad separation of their ionization enthalpies (ΔH^{b}_{ion}).(*213*) The raw isotherms were fit to Equation 4-1 to determine the total enthalpy (ΔH^{o}_{obs}) associated with binding. A plot of the ΔH^{o}_{obs} as a function of ΔH^{b}_{ion} gives the slope, *ΔN*, as the number of protons being released (positive value) or absorbed (negative value) upon binding.(*214*) The plots in Figure 4-15 and corresponding data in Tables 4-7 and 4-8 show minimal differences in ΔH^{o}_{obs} for Dpo1 or Dpo4 binding to DNA in buffers with different ionizations enthalpies (ΔH^{b}_{ion}). Experiments were performed at three different temperatures resulting in *ΔN* equal to 0.18 ± 0.04, 0.82 ± 0.12, and 0.30 ± 0.10 at 10, 25, and 60 ^{o}C, respectively for Dpo1. *ΔN* was equal to 0.84 ± 0.15, 0.70 ± 0.15, and 0.21 ± 0.10 for 5, 15, and 60 ^{o}C, respectively, for Dpo4. In all cases, the *ΔN* values are also slightly positive but less than one indicating that changes in protonation are not significantly contributing to the binding of either polymerase to DNA, nor to the large changes in ΔC^{o}_{p} with temperature.

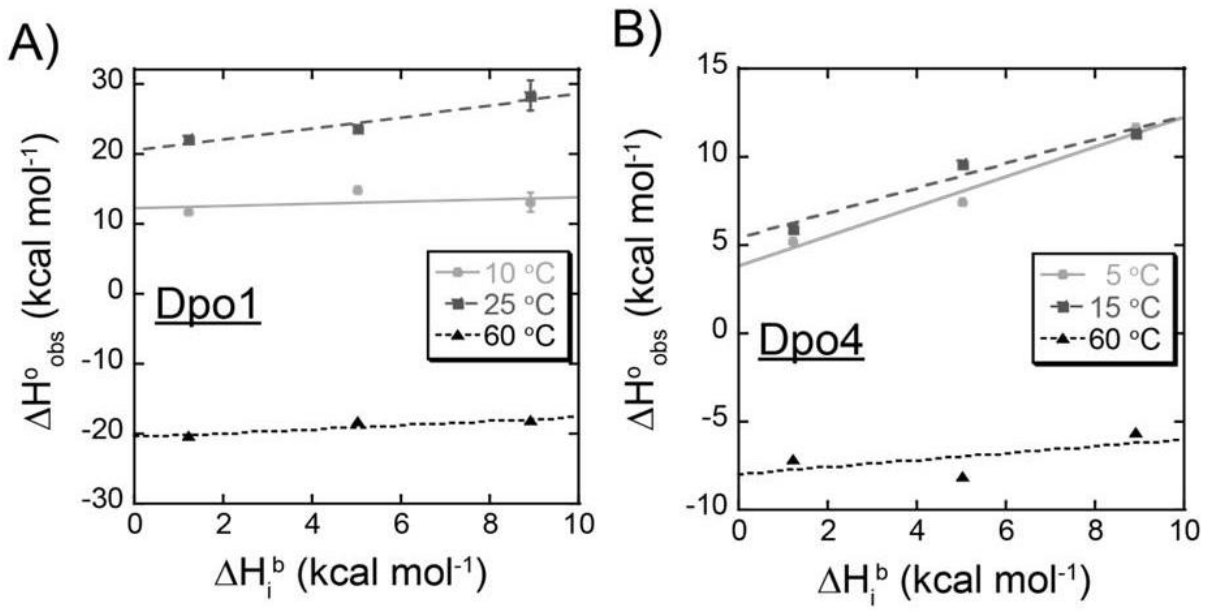

Figure 4-15. Calorimetric ΔH^{o}_{obs}values from individual forward ITC experiments for A) Dpo1 or B) Dpo4 binding to the 37 base hairpin are plotted versus enthalpy associated with proton release from buffer (ΔH^{b}_{ion}) in phosphate (1.22 kcal/mol), HEPES (5.03 kcal/mol), or imidazole (8.92 kcal/mol) buffer at pH = 7.0 and 150 mM NaCl. Thermodynamic values are reported in Tables 4-3 and 4-4. All slopes are less than one indicating less than one proton is being released upon polymerase binding to DNA

Table 4-7. Thermodynamic parameters for forward ITC titrations of DNA into Dpo1 in different buffers

Buffer (pH=7.0)	Temp (^{o}C)	ΔH_{obs} (kcal/mol)	$T\Delta S_{obs}$ (kcal/mol)
NaP	10	11.7 ± 0.1	19.1
	25	22.0 ± 0.5*	29.3 ± 0.5*
	60	-20.4 ± 0.2*	-12.9 ± 0.2*
Imidazole	10	13.0 ± 1.3*	20.2 ± 1.3*
	25	31.3 ± 2.0*	38.3 ± 2.2*
	60	-18.1 ± 3.7	-10.0

* Represents the average and standard error from thee independent experiments.

Table 4-8. Thermodynamic parameters for forward ITC titrations of DNA into Dpo4 in different buffers

Buffer (pH=7.0)	Temp (^{o}C)	ΔH_{obs} (kcal/mol)	$T\Delta S_{obs}$ (kcal/mol)
NaP	5	5.2 ± 0.2	12.5
	15	5.9 ± 0.5	13.3
	60	-7.2 ± 0.9	2.1
Imidazole	5	11.7 ± 0.4	18.6
	15	11.3 ± 0.7	18.4
	60	-7.2 ± 0.4	4.5

4.2.9 No observed changes in electrostatic state upon DNA binding with increasing temperature

Changes in the charge state due to linked protonation or associated ions upon binding can also affect experimental heat capacity values.(*177, 215*) In order to verify that the charge state does not change significantly upon binding and contribute to the temperature dependent heat capacity changes for Dpo1 and Dpo4 measured by ITC, we utilized capillary electrophoresis as a measure of any change in apparent charge (z^*) upon Dpo1 or Dpo4 binding to DNA. z^* was determined (Table 4-9) using experimentally measured electrophoretic mobility values at 30 ^{o}C and the diffusion coefficient values obtained from the sedimentation velocity data above. z^* can be converted to a net charge or valence (z_{calc}) which is the combination of any ionized amino acids and any territorial counter ions associated with the protein/DNA complex surface.(*211*) The net charge is calculated using a classical Debye-Hückel-Henry theory which accounts for the counter ion size, bulk electrostatic screening, and any electrophoretic effects.(*216*) For both Dpo1 and Dpo4 the net charge does not change significantly in the absence or presence of

hairpin DNA (Table 4-9) eliminating the possibility that linked protonation or bound ions are the cause of the temperature dependent ΔC_p^o values.

Table 4-9. Net and Effective Charges or Valences for Dpo1 or Dpo4 Alone or Bound to DNA.

Species	Mobility ($cm^2 V^{-1}s^{-1}$)[a]	Apparent Charge (z*)[b]	Net Charge (z_{calc})[c]
Dpo1	-1.36 x 10^{-5}	0.7	4.1
Dpo1/ DNA[d]	-1.19 x 10^{-5}	0.6	3.9
Dpo4	-1.04 x 10^{-5}	0.4	1.7
Dpo4/ DNA[d]	-8.27 x 10^{-6}	0.3	1.2

[a]Calculated directly from CE experiments. [b]Calculated from the electrophoretic mobility and hydrodynamic radius (R_h) from sedimentation velocity experiments for each. [c]Calculated from the Debye-Hückel-Henry equation. [d]DNA was the 37 base hairpin primer template.

4.2.10 No significant structural changes in protein with increasing temperature.

To measure any conformational/structural changes of either the polymerase or DNA that may occur upon binding and may contribute to the $\Delta\Delta C^o_p$ values, we utilized circular dichroism (CD). CD spectra of the free polymerase and DNA (unbounded) compared to the polymerase-DNA complex (bounded) show only very slight changes in the spectra upon complex formation for both polymerases (Figure 4-16). Protein secondary structure was monitored at 219 nm, while the DNA conformation can be monitored at 250-280 nm. Importantly, the ellipticity values were monitored across a broad wavelength range at both 20 ^oC and 60 ^oC to assess and temperature dependent conformational effects. For both Dpo1 and Dpo4, changes in ellipticity monitoring the protein structure are not significantly different when bound to DNA at either temperature. The DNA structure upon Dpo4 binding has only slight differences in ellipticity, while the ellipticity value for Dpo1 at 260 nm is essentially unchanged. For Dpo4 (Figure 4-16C&D), equivalent but

small protein and DNA conformational changes were observed at both 20 and 60 ^{o}C. This may be consistent with a conformational change in the little finger domain of Dpo4 detected upon binding DNA using x-ray crystallography.(*143*) Most importantly, there are no significant differences in protein or DNA conformations for either Dpo1 or Dpo4 at the different temperatures.

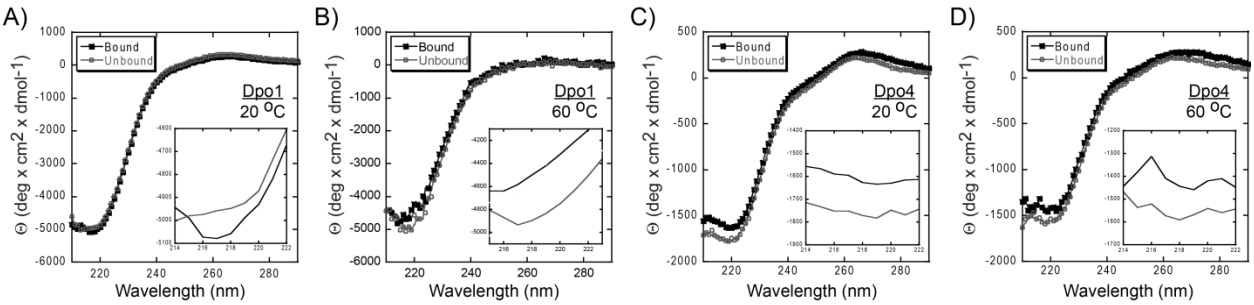

Figure 4-16. Circular dichroism experiments of Dpo1 alone (unbound) or bound to DNA at A) 20 ^{o}C or B) 60 ^{o}C or Dpo4 alone (unbound) or bound to DNA at C) 20 ^{o}C or D) 60 ^{o}C. Wavelengths were monitored from 210-300 nm to cover possible protein or DNA structural changes. The inset highlights the data from 214 to 222 nm of backbone amide structure of either Dpo1 or Dpo4.

4.2.11 Thermostabilization of Dpo1 protein structure when bound to DNA

We also examined the thermostabilities of each polymerase alone and in the presence of the DNA hairpin. We monitored the molar ellipticities at 219 nm as a function of temperature for Dpo1 or Dpo4 bound or unbound to DNA using circular dichroism (Figure 4-17). The protein secondary structures of both Dpo1 and Dpo4 are thermostable at high temperatures with melting temperatures (T_ms) greater than 80 ^{o}C and 90 ^{o}C respectively for the proteins alone. In both cases, protein denaturation does not begin until temperatures greater than 75 ^{o}C are reached. Interestingly in the presence of DNA, the T_m of Dpo1 is stabilized by at least 12 ^{o}C (~92 ^{o}C) (Figure 4-17A), making it more thermodynamically similar to Dpo4. No significant increase in T_m was found for Dpo4 when bound to DNA (Figure 4-17B). The T_m for Dpo1/DNA was

estimated based on the midpoint of the melting curve for Dpo1 alone, as the spectral data doesn't reach a maximum until temperatures greater than 100 ^{o}C are reached. Thermodynamic stabilization of the protein structure of Dpo1 upon binding DNA suggests that this complex exhibits a high degree of structural complementarity.

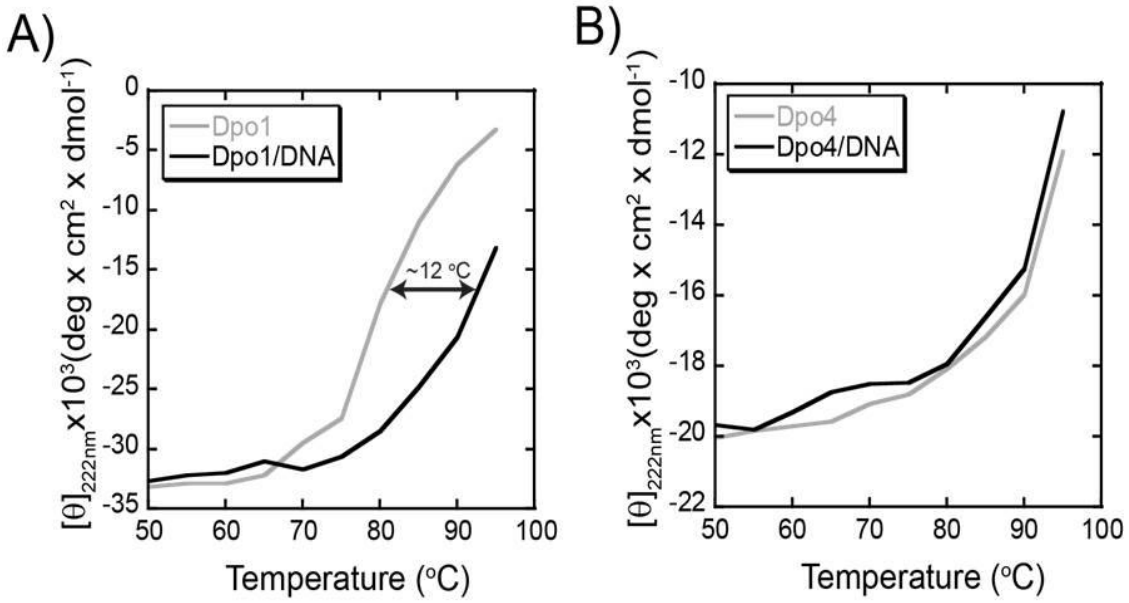

Figure 4-17. Thermal melting of A) Dpo1 alone (unbound, grey) or bound (black) to DNA or B) Dpo4 alone (unbound, grey) or bound (black) to DNA. Circular dichroism experiments were monitored at 222 nm over 5 ^{o}C increments. The temperature shifts for Dpo1 binding DNA measured at the midpoints are indicated by a 12 ^{o}C shift.

4.3 DISCUSSION

We have investigated and compared the binding of DNA replication and repair polymerases to primer-template substrates and found extremely complex thermodynamics, which is caused by the temperature-dependent formation of oligomeric species. We have verified that the DNA replication polymerase from *Sulfolobus solfataricus*, Dpo1, has multimeric stoichiometry that increases slightly with higher temperature due to the changing in equilibria,

indicating a possible biological role for the trimer at physiological temperatures. Similarly, the DNA repair polymerase, Dpo4, primarily forms a dimer but can also oligomerize into a tetramer. Both DNA polymerases display unique and variable changes in heat capacity values that are temperature dependent. The molecular nature for the measured temperature dependent heat capacity has been systematically probed using forward and reverse ITC titrations and found to be most likely a result of a change in the solution coupled equilibria with temperature. We have eliminated the possibility that changes in protonation, associated anions, or the structure of protein or DNA have a large effect on the temperature dependent heat capacity values measured for Dpo1 and Dpo4. Rather, different changes in individual binding affinities of Dpo1 and Dpo4 with temperature described here lead to changes in complex solution multiequilibria processes that affect ΔC^{o}_{p} and lead to high structural complementarity at higher temperatures. In Chapter 3, we measured constant ΔC_p's for Dpo1 and Dpo4 using fluorescence anisotropy assays. The trace amount of DNA in fluorescence anisotropy assay reduces the coupling between the oligomeric and monomeric complex species, and therefore, we assumed that temperature-independent ΔC_p's for both initial and sequential binding (Scheme 4-1 and 4-2) are reasonable. However, in this chapter, our results from ITC are more complicated and with a more significant "mass action" that occurs during the course of the titrations causing equilibria coupling between the monomeric and oligomeric species as a function of temperature. The differences in the coupled equilibria between monomeric and trimeric states of these two oligomeric polymerases to DNA creating fine balance of binding and enzymatic activity required for uninterrupted DNA replication and repair with high fidelity.

4.3.1 Confirmation, Visualization, and Quantification of Oligomeric Polymerase/DNA Complexes

We have previously shown that both trimeric Dpo1 and dimeric/tetrameric Dpo4 complexes exist on DNA.(*120*, *208*) Interestingly, trimeric Dpo1 stimulates both the kinetic and processive synthesis of DNA while oligomeric Dpo4 has little enzymatic enhancement. The hairpin DNA template used in the EMSA and ITC experiments of this chapter is slightly shorter than the primer template (21/31mer) used previously,(*120*) and therefore also precludes multiple binding events associated with longer DNA substrate. EMSA (Figure 4-1&2 A&B) of Dpo1 on DNA clearly show two separately migrating species that are consistent with monomeric and trimeric Dpo1/DNA complexes. Similarly, EMSA of Dpo4 on DNA (Figure 4-1 and 4-2 C&D) shows three separable species that are consistent with monomer, dimer, and tetramer/DNA complexes. Previously, we used TBE gels at basic pH to isolate trimeric Dpo1 complex on DNA (Chapter 2). Here, we use the native Bis/Tris gels at neutral pH were required for both effective separation of polymerase/DNA species and to compare directly with the ITC experiments at pH = 7.0.

The stoichiometry for Dpo1 or Dpo4 binding to DNA determined from the ITC titrations are also consistent with EMSA results, showing monomer-oligomer equilibria with at least two separate binding steps. By performing both forward (DNA into protein) and reverse (protein into DNA) ITC titrations, we can obtain information on the reversibility of the equilibria processes from the fit of ΔH^{o}_{obs} described by Schemes 4-1 & 4-2. In reverse ITC titrations, binding of the higher affinity monomeric polymerases to DNA (K_1) is favored because of the excess of DNA in the cell and will be dominated in enthalpy during the early injections. Smaller contribution from

multimeric binding in the later injections is primarily assigned to the second equilibria process, K_2. We have verified that this coupled equilibria can be affected by reducing the concentration of DNA in the cell and measuring an associated increase in stoichiometry for Dpo1 binding within the same number of injections in reverse ITC titrations (Figure 4-10). Conversely, forward titrations (DNA into protein) allow for binding of multiple polymerase molecules to one DNA molecule in the cell during the initial injections due to the large excess of polymerase and better report the absolute stoichiometry of binding. In the forward ITC titrations, the apparent stoichiometry, the ratio DNA to polymerase decreases with increasing temperature for both Dpo1 and Dpo4, suggesting that oligomeric polymerase complex formation is favored enthalpically.

4.3.2 Temperature dependent changes in heat capacities ($\Delta\Delta C_p^o$) of binding DNA for Dpo1 and Dpo4

Generally, the change in heat capacity of binding is reported as being a temperature independent variable due to most experiments characterizing a single binding event or being performed over a limited temperature range. These ideal results provide a good linear fit for ΔC_p^o from experimentally determined ΔH^o values versus temperature. Large negative ΔC_p^o values are generally indicative of a sequence-specific DNA binding proteins,(*129*, *148*) but similar results have been found for polymerases binding precisely through structural complementarity at primer-template DNA junctions.(*130, 131*) Historically, changes in accessible polar (ΔAp) and nonpolar (ΔA_{np} surface area were proposed to be the main molecular determinate that correlates with the magnitude of ΔC^o_p.(*148*) On the other hand, there is no theoretical requirement that

ΔC^{o}_{p} be linear with temperature(*217*) nor be associated solely with burial of surface area, and as has been reported previously, nonlinearity may actually be a general phenomenon for proteins binding DNA.(*218*)

Temperature dependent changes in ΔC^{o}_{p} can be the result of a combination of changes in protonation, thermal and vibrational fluctuations, electrostatics, water solvation, or multiequilibria coupling as shown in equation 4-14 and have resulted in the derivation of a $\Delta\Delta C^{o}_{p}$ parameter to explain any non-linearity in ΔC^{o}_{p}.(*129, 133, 174, 177, 203, 218, 219*)

$$\Delta C°_{P} = -a\Delta A_{np} + b\Delta A_{p} - c(\Delta ConfVib) + d(Strain) + e(Anions) \pm f(coupled\ equil.)$$

(Equation 4-14).

ΔConfVib and strain are the resulting change of configurationally vibrational freedom and structural strain, respectively. Anions is a general term for an ion effect.

Examples of detected molecular features that alter heat capacity include changes in configurational freedom upon binding,(*220*) temperature effects of ssDNA base stacking,(*221*) as well as the flexibility and conformational changes that occur in proteins.(*174, 222*) The length of the ssDNA in the template strand can also influence the affinity of binding as it makes significant contacts with the polymerase.(*120, 223, 224*) As an example, recognition of uracil in the DNA template strand by the Family-B polymerase from *P. furiosus* was shown to have a moderate ΔC^{o}_{p} primarily due to the limited binding energy associated with polymerase sensing interactions with uracil in this stalled conformation.(*222*)

Although small changes in ΔC^{o}_{p} with temperature have been noted for a number of more complex DNA binding situations,(*203, 218*) sign reversals in ΔC^{o}_{p} (positive to negative) are

more rare. Drastic dependences of ΔC^{o}_{p} with temperature and anion identity and concentration have been reported previously for *E. coli* single stranded binding protein (SSB) binding to DNA where the sign of ΔC^{o}_{p} can actually change with temperature.(*177*) Recently, Lohman and coworkers have attributed this sign reversal in ΔC^{o}_{p} to conformational changes within the SSB tetramer that occur upon binding DNA at a second site to create the fully wrapped complex.(*225*) Another example of a sign reversal in ΔC^{o}_{p} has been found with a mutant of the thermophilic duplex DNA binding protein (Sac7d) from *Sulfolobus acidocaldarius* to DNA.(*226*) In this case, the nonlinear ΔC^{o}_{p} was determined to be the result of conformational distortion in DNA related to unfavorable enthalpy of binding at lower temperatures.

Our results show a dramatic change in ΔC^{o}_{p} for different titrations across a broad temperature range (5 - 65 ^{o}C) for both Dpo1 and Dpo4. More surprising is that the heat capacities are generally positive at lower temperatures and switch to strongly negative values at temperatures greater the 35 ^{o}C. At physiological temperatures for *Sso* (75 - 80 ^{o}C), the binding enthalpy (ΔH^{o}) is strongly exothermic, and the heat capacity (ΔC^{o}_{p}) is strongly negative consistent with high structural complementarity at the interface. At lower temperatures (< 35 ^{o}C), other molecular factors including equilibria changes contribute to unfavorable coupled enthalpies and entropies leading to a looser binding conformation and resulting in a positive ΔC^{o}_{p}. We have eliminated the possibility that changes in protonation, electrostatics, or the structure of either the protein or DNA change significantly with temperature. Rather, we propose that the transition in binding specificity for either polymerase, Dpo1 or Dpo4, is more likely related to a change in the coupled solution multiequilibria with temperature to promote formation of oligomeric polymerase complexes on DNA with high structural complementarity. Changes in the coupled equilibria or coupling of a system with temperature are generally negative(*174*) but can also have

large and unexpected consequences on the ΔC^{o}_{p} value depending on the type of multiequilibria process that occur. In fact, multiequilibria processes can even contribute to a positive ΔC^{o}_{p} if the coupling equilibria constants are more than a log different in their values.(*174*)

Increasing temperature promotes binding of tight oligomeric polymerase conformations on DNA that result in a strong negative change in heat capacity. (Tables 4-1, 2, 5, and 6) Evidence of the structural complementarity comes from both a stabilization in Dpo1 structure (Figure 4-17A) and DNA duplex (Chapter 2) upon binding. The associated $\Delta\Delta C^{o}_{p}$ values measured for Dpo1 and Dpo4 are in line with other DNA polymerases such as Taq or Klentaq binding to DNA (*218*), however, this work provided better quality thermodynamic data over a wider temperature range, and thus the measured $\Delta\Delta C^{o}_{p}$ values have significantly lower associated errors. Changes in thermodynamic coupling with temperature influences the heat capacity change for polymerase binding to DNA

In the forward ITC experiments, we detected significant influences of coupled equilibrium on ΔC_p's for both Dpo1 and Dpo4. Any temperature dependent change in equilibria would result in a conversion from a loose to a tight binding oligomeric conformation resulting in temperature-dependent $\Delta\Delta C^{o}_{p}$. In lower temperature forward ITC titrations, the trimeric Dpo1 or the dimeric Dpo4 will be less favored due to a smaller K_2. At higher temperatures, formation of the oligomeric polymerase-DNA complexes proceeds with high structural complementarity for binding with a larger K_2 resulting in large negative ΔC^{o}_{p}. At high temperatures, the ordered assembly pathway (K_1 and K_2) will have a larger thermodynamic influence for binding. Therefore, flux in the equilibria pathways with temperature and/or restrictions in the oligomeric polymerase-DNA conformations due to direct binding or ordered assembly would account for the temperature dependence on ΔC^{o}_{p} for both Dpo1 and Dpo4. In the forward ITC, the $\Delta\Delta C^{o}_{p}$

are -59 ± 3 and -13 ± 4 cal $mol^{-1}K^{-2}$ for Dpo1 and Dpo4, respectively. However, in the reverse ITC, the $\Delta\Delta C^{o}_{p}$ are -16 ± 4 and -6 ± 2 cal $mol^{-1}K^{-2}$ for Dpo1 and Dpo4, respectively. The smaller values in the reverse titrations most likely result from the difference in the mass environment (equilibria) in the forward ITC. While the forward ITC experience the coexistence of the monomeric and oligomeric state when less amount of DNA initially titrated into excess of polymerases, the reverse ITC (protein in to excess DNA) had the majority of monomeric state during first several titrations.

From our previous fluorescence anisotropy studies (Chapter 3), we detected an interaction between polymerases to DNA that is governed by overall ΔC_p's corresponding to first and second steps of binding, (Scheme 4-1 and 4-2) which are -1.45 and -1.22 kcal $mol^{-1}K^{-1}$ for Dpo1 and Dpo4 , respectively. However, we derived ΔC_p values assuming they were temperature independent. In this chapter, our results from ITC are more complicated with a temperature dependency of ΔC_p, which comes from coupled equilibria between the individual monomeric and oligomeric complexes. For example, in the forward ITC, DNA is initially titrated into excess of protein resulting in a mixture of oligomeric complexes with DNA, trimer and monomer complexes for Dpo1; tetramer, dimer, and monomer complexes for Dpo4. The individual complex can couple with one another and thus move the intrinsic equilibria between different complexes. Observed ΔC^{o}_{p} can be thought of as the summation of an intrinsic $\Delta C_{p,intrin}$ and a temperature-dependent coupling $\Delta C_{p,coupl}$ according to the following equation:

$$\Delta C^{o}_{p} = \Delta C_{p,intrin} + \Delta C_{p,coupl} \qquad \text{(Equation 4-15).}$$

If the observed ΔC^{o}_{p} is temperature dependent relative to T_H, Equation 4-15 can be rewritten as:

$$\Delta C^{o}_{p} = \Delta C_{p,intrin} + \Delta\Delta C_{p} (T-T_H) \qquad \text{(Equation 4-16).}$$

The overall $\Delta C_{p,intrin}$ for trimeric Dpo1 and dimeric Dpo4 reported in Chapter 3 are 1.45 and 1.22 kacl mol^{-1} K^{-1}, respectively. We can then calculate $\Delta C_{p,coupl}$ at each temperature using equation 4-15 and plotted the results in Figure 4-18. Note that a positive $\Delta C_{p, coupl}$ corresponds to a shift in the equilibria from oligomeric to monomeric species, while a negative $\Delta C_{p, coupl}$ corresponds to an opposite equilibria shift over the experimental temperature range. Most of $\Delta C_{p, coupl}$ values for ITC are positive except for values from the forward ITC of Dpo1 above ~45^{o}C. This mass action shifts from oligomeric to monomeric species is more prominent at lower temperatures and is gradually alleviated with increasing temperature. The trend of $\Delta C_{p, coupl}$ is also supported in the EMSA studies, where monomeric species persist longer in the titration course at 22 ^{o}C than at 50 ^{o}C. (more lanes containing monomeric species in Figure 4-8 than in Figure 4-9). This $\Delta C_{p, coupl}$ may also be the result of an equilibrium in which the polymerase can complex themselves in the absence of DNA. (*174*) However, we are not able to detect the stable association of polymerase without DNA in any of our previous assays (Chapters 2 or 3).

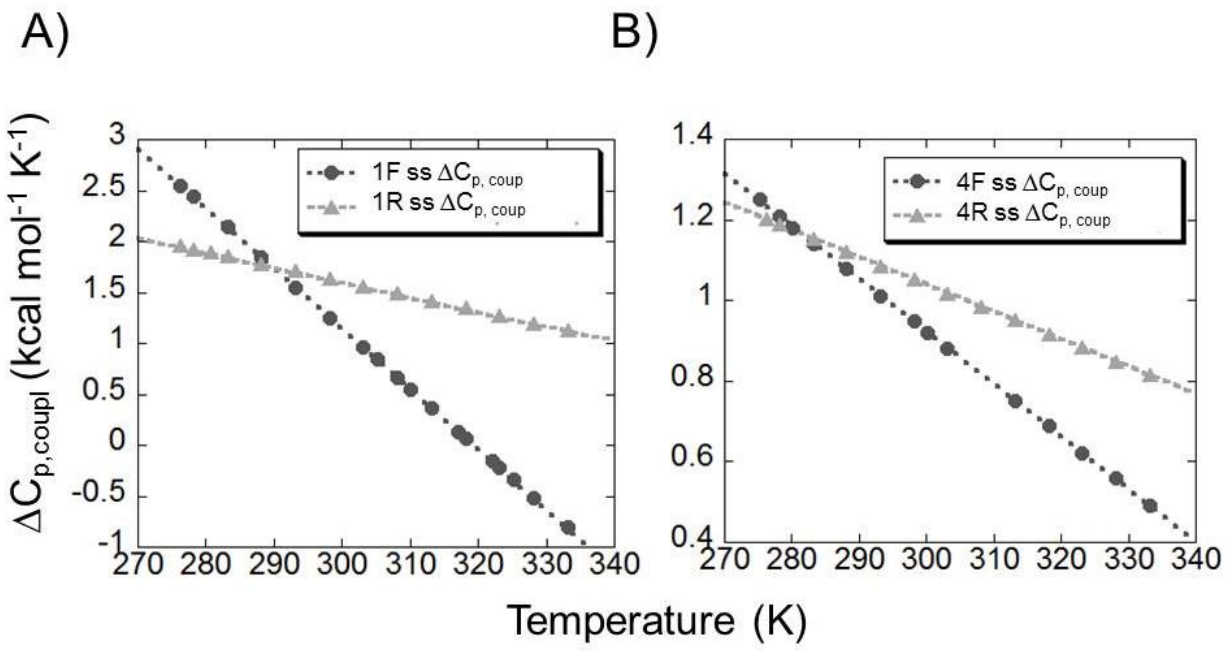

Figure 4-18. The temperature dependency of $\Delta C_{p,coupl}$ in different ITC titrations. $\Delta C_{p,coupl}$ were calculated from equation 4-15. A) $\Delta_{Cp, coupl}$ fore Dpo1 measured in forward ITC (1Fss $\Delta C_{p,coup}$) and reverse ITC (1R ss $\Delta C_{p,coup}$). B) $\Delta C_{p, coupl}$ fore Dpo4 measured in forward ITC (4Fss $\Delta C_{p, coup}$) and reverse ITC (4R ss $\Delta C_{p, coup}$). The slopes of the lines report the $\Delta\Delta C_p^o$ values.

Instead, if we consider Equation 4-16 for Dpo1, for which T_H is around 48 ^oC by forward ITC, the temperature dependent term equals to zero at T_H, and the intrinsic ΔC_p (around -1.6 kcal mol^{-1} K^{-1}) dominates at temperatures greater than T_H (Figure 4-19). This value is consistent with the intrinsic ΔC_p from fluorescence anisotropy study (-1.45 kcal mol^{-1} K^{-1}) suggesting coupled equilibrium may diminish at higher temperatures for Dpo1. However, for Dpo4, the value of intrinsic ΔC_p from fluorescence anisotropy is -1.22 kcal mol^{-1}K^{-1} which does not lie in the experimental ΔC^o_p range (0.02~-0.73 kcal mol^{-1}K^{-1}) obtained from forward ITC, suggesting a negative $\Delta\Delta C^o_p$ for Dpo4 still exists at higher temperatures. In support, we find that Dpo4's oligomerization is not stimulated by DNA in our cross-linking assays (Chapter 3), indicating that Dpo4 has a significantly more complicated equilibria profile with monomer-dimer-tetramer complexes existing off DNA resulting in a negative $\Delta\Delta C^o_p$ contribution.

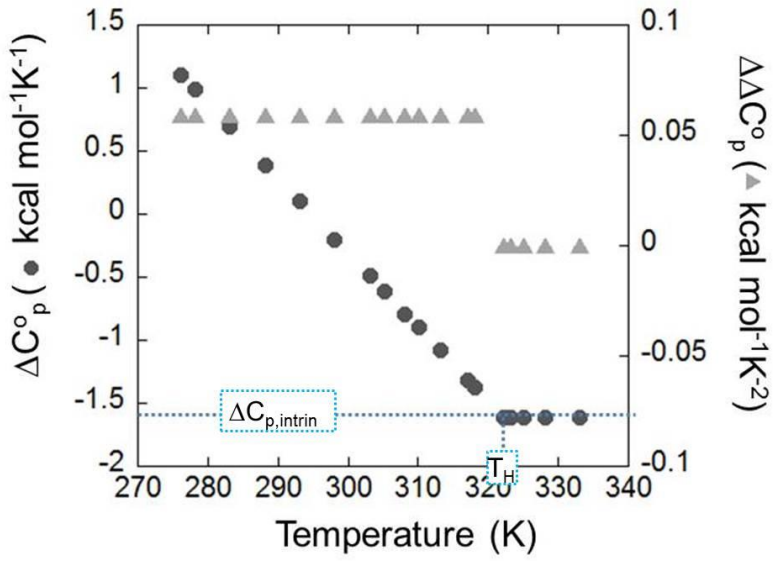

Figure 4-19. Temperature dependency of observed ΔC^{o}_{p} (●) for the binding of Dpo1 and DNA detected by forward ITC, assuming $\Delta\Delta C_{p,coupl}$ (▲) has no contribution above the T_H (321 K) (vertical dashed line). Below T_H, there is constant $\Delta\Delta C_{p,coupl}$ (0.059 kcal mol^{-1} K^{-1}). Horizontal dotted line indicates where intrinsic DC_p becomes temperature independent.

4.3.3 Mechanism for Replication or Repair DNA Polymerase Binding Specificity

The association constants as measured in the forward ITC experiments for Dpo1 and Dpo4 are very similar and parallel across a broad range of temperatures. The values suggest that at lower temp, Dpo4 generally has a higher binding affinity than Dpo1, but with increasing temperature, the affinities for Dpo1 and Dpo4 become more similar. In addition, Dpo1 has higher affinity at higher temperatures (>60 ^{o}C), but Dpo4 has its greatest affinity around 30^{o}C. As the temperature approaches physiological (70 ^{o}C), the free energy of Dpo1 binding to DNA equals or surpasses that for Dpo4, especially when comparing a Dpo1 trimer to a Dpo4 dimer (Chapter 3). If the local concentrations at the replication fork are low (< 250 nM), then the specificities of binding individual molecules of either polymerase to DNA will depend primarily on the monomeric binding affinities for DNA and other accessory proteins. At higher local

concentrations, coupling between monomeric and oligomeric DNA polymerase equilibria would dominate and the lower total free energy for trimeric Dpo1 would provide thermodynamic selection.(*208*) Recently, quantification of the mRNA and protein levels in *Sso* have noted that Dpo1 is expressed at least an order of magnitude greater than Dpo4.(*104*) It was noted previously, that even under DNA damaging conditions, the concentrations of Dpo4 are stable.(*194, 195*) Therefore, higher concentrations of Dpo1 in the cell would thermodynamically favor binding of this polymerase over Dpo4 in spite of similar binding affinities.

The small differences in oligomeric association constants between Dpo1 and Dpo4 would also allow for a mechanism of dynamic exchange of DNA polymerases at the replication fork for uninterrupted and coordinated DNA replication and lesion bypass processing. The coupled equilibria between monomer and trimer Dpo1 and monomer and oligomeric Dpo4 for binding DNA will compete. Subtle changes in protein levels will direct DNA binding of either DNA polymerase under the appropriate cellular conditions. Stalling at sites of damage (shuttling between polymerase and exonuclease active sites) will also destabilize Dpo1 binding in favor of lesion bypass ability of Dpo4. Dpo1 and Dpo4 are also known to interact directly in solution possibly providing for a mechanism of direct exchange.(*34*) The oligomeric nature of each DNA polymerase provides for a plausible mechanism of active site exchange within a heteroligomeric (Dpo1-Dpo4) complex depending on the type of DNA substrate (damaged or undamaged). It is proposed in *E. coli* or yeast that both polymerases are held at the replication fork and exchanged on the DNA template through interactions with the processivity factor.(*227*) This is also proposed for *Sso*, where specific contacts of Dpo1 with PCNA2 and Dpo4 with PCNA1 within the heterotrimeric PCNA123 complex may provide for close directed polymerase engagement of the DNA template.(*192, 228*) The regulation of these oligomeric polymerase complexes on DNA

as well as with interacting proteins including PCNA are influenced by small thermodynamic differences, coupled equilibrium processes, and cellular concentrations to direct efficient DNA replication or repair.

4.4 CONCLUSION

In Chapter 3, we found that for both Dpo1 and Dpo4, the binding between polymerases and DNA consists of an initial high-affinity binding site followed by a sequential lower-affinity binding, whose affinities are dependent on temperature. We derived the intrinsic heat capacity changes for the formation of the monomeric and oligomeric complexes. In this chapter, we examined more specifically the thermodynamics for this stepwise process using ITC and found that the true binding equilibria processes are more complicated. Most notably, we are surprised to find that the heat capacity changes for Dpo1 and Dpo4 are temperature dependent. We used several techniques to decipher the molecular factors affecting the heat capacity changes, and the cumulative results suggest that the temperature dependence results from the coupled equilibria between the monomeric and oligomeric polymerase-DNA complex. The complete coupled equilibria can alter the population of different complex states both in the presence and absence of DNA (Figure 4-20).(*39, 174*) Evidence for a polymerase equilibrium complex off DNA comes primarily from cross-linking assays (Chapter 2 and Chapter 3). However, this oligomerization was not detected by analytical ultracentrifugation (Chapter 3) or gel filtration assays (Chapter 2) suggesting that these individual equilibria (K_A, K_B, K_C, and K_D) are not strong compared to when DNA is present.

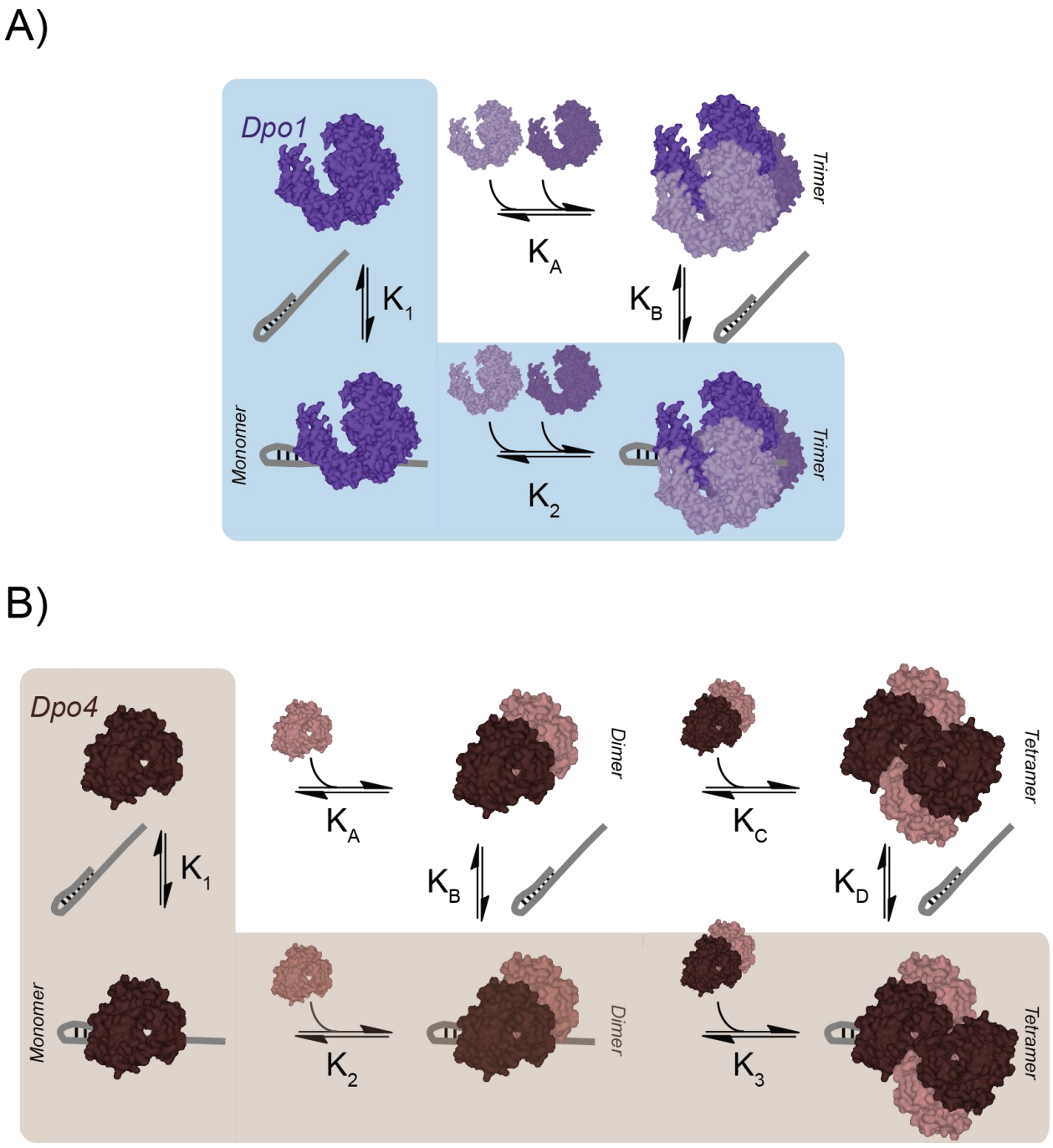

Figure 4-20. Complete equilibria profiles for oligomeric A) Dpo1 or B) Dpo4 biding to DNA. In addition to stepwise binding of polymerase to DNA in Schemes 4-1 and 4-2 and shaded here, polymerases may also associate off DNA with associated equilibrium constants K_A, K_B, K_C, and K_D.

5.0 SUMMARY AND FUTURE DIRECTIONS

5.1 STRUCTURED CROWDING AND OLIGOMERIZATION OF DNA REPLICATION POLYMERASES

The cellular environment is crowed with high concentrations of proteins, enzymes, substrates, and electrolytes. Twenty percent of the cellular mass comes from protein. (*103*) Molecular crowding decreases the diffusion rate, fluctuates equilibrium between protein and substrates, and affects the catalysis of enzymes, yet in most cases the metabolic processes proceed unencumbered. There are two types of crowding: uniform crowding and structured crowding. The latter refers to a highly coordinated cellular environment, where enzymes and other structural factors are clustered and organized, and are able to modulate physiological function effectively and dynamically. (*229*) In this work, we found that *Sso* DNA polymerases, Dpo1 and Dpo4, form oligomeric complexes with DNA. The detected oligomerization further increases the structured crowding to coordinate concerted actions within the DNA replication holoenzyme. In addition, this oligomerization can enhance the thermostability of Dpo1 (Chapter 3) and DNA (Chapter 2) and physiological activities of polymerases (Chapter 2 and Chapter 3) in organisms that thrive at high temperatures.

5.2 TEMPERATURE-DEPENDENT DIFFERENTIATION BETWEEN DNA BINDING TO DPO1 AND DPO4

Furthermore, we examined the mechanistic strategy to enhance physiological efficiency and replication fidelity through DNA polymerase oligomerization. We found that the oligomerization is stepwise for both Dpo1 and Dpo4, comprising an initial high-affinity binding step followed by a sequential weaker-affinity binding step. In the *Sso* cell, 2.2 μM Dpo1 will promote the formation of trimeric Dpo1-DNA complexed at the 3'OH of the few primer strands available during DNA replication, while Dpo4 at a cellular concentration of 150 nM will be thermodynamically blocked from binding DNA and limited to monomeric binding only when a lesion is present and Dpo1 is destabilized. The temperature range where the maximum affinities of the protein-protein interactions (oligomerization) are different for Dpo1 (60~70 ^{o}C) and Dpo4 (50 ~60 ^{o}C). Therefore, at *Sso*'s physiological temperature (75 ^{o}C), trimeric Dpo1 will primarily bind and synthesize DNA, while Dpo4 will bind and act only in certain instances such as at lesions where Dpo1 is destabilized from DNA. However, Dpo4 may also use oligomerization to increase the local availability around the replication fork, especially when DNA damage is abundant or promote heteroligomeric complexes with Dpo1 to coordinate polymerase exchange events.

In addition to temperature-dependent binding affinities, we also found that both binding enthalpies and entropies are temperature-dependent, giving fascinating temperature dependent changes in heat capacity. We examined the molecular factors that vary heat capacity changes using a variety of biophysical techniques, and conclude that contributions from temperature dependent changes in coupled equilibria are the primary factors causing these temperature-

dependent heat capacity changes. This coupled equilibrium may result from a complicated binding mechanism (*174*) or fluctuation between different binding states as shown in Equation 5-1:(*39*)

$$C_p = \Delta U^2/kT^2\ P_0P_1 \qquad \text{(Equation 5-1)}$$

where ΔU is the energy difference between two binding states, P_0 and P_1. Thus, the coexistence of two or more binding states can increase the coupled heat capacity (Equation 5-1). This contribution is more extreme at lower temperatures where the curvature in the Gibbs-Helmholtz plots for Dpo1 and Dpo4 are greater. The $\Delta\Delta Cp$ remains relatively constant over the lower temperature range (5~45 ^oC). However, at higher temperatures (>45 ^oC), less population of the monomeric state of Dpo1-DNA diminishes the coupled equilibria effect in C_P. Note that at T_H for Dpo1 (48 ^oC), the coupled heat capacity change is close to zero and contributes little to Cp. Interestingly, T_H has been recently suggested to be the starting point for physiological activity.(*1*) It is possible that the coupled equilibrium noted here for Dpo1 and Dpo4, i.e. moving the oligomeric state towards monomeric state, is responsible for reduced physiological activity at lower temperatures.

5.3 FUTURE DIRECTIONS

There are several thermodynamic and kinetic details within the DNA replication mechanism that are still unclear, including binding of polymerases to damaged DNA and how PCNA, the replication clamp, coordinates with Dpo1 and Dpo4 for uninterrupted DNA synthesis in the presence of lesions. I would predict that for damaged templates, Dpo4 would have higher binding affinity than Dpo1 for both monomeric and oligomeric forms, with a different

thermodynamic binding profile than with undamaged substrates, and $T_{H,Dpo4}$ may increase. DNA replication polymerases from thermodynamic organisms including *Sso* are one of a few systems allowing a thorough examination of the relationship between oligomerization, thermodynamics, and kinetics providing a preliminary model for other replication systems and similar multiequilibria protein binding mechanisms.

BIBLIOGRAPHY

1. Brown, H. S., and Licata, V. J. (2013) Enthalpic switch-points and temperature dependencies of DNA binding and nucleotide incorporation by Pol I DNA polymerases.
2. Watson, J. D., and Crick, F. H. (1953) Molecular structure of nucleic acids; a structure for deoxyribose nucleic acid, *171*, 737-738.
3. Meselson, M., and Stahl, F. W. (1958) THE REPLICATION OF DNA IN ESCHERICHIA COLI, *44*, 671-682.
4. Marians, K. J. (1992) Prokaryotic DNA replication, *61*, 673-719.
5. Woese, C. R., Kandler, O., and Wheelis, M. L. (1990) Towards a natural system of organisms: proposal for the domains Archaea, Bacteria, and Eucarya, *87*, 4576-4579.
6. Liu, L., Komori, K., Ishino, S., Bocquier, A. A., Cann, I. K., Kohda, D., and Ishino, Y. (2001) The archaeal DNA primase: biochemical characterization of the p41-p46 complex from Pyrococcus furiosus, *276*, 45484-45490.
7. Bocquier, A. A., Liu, L., Cann, I. K., Komori, K., Kohda, D., and Ishino, Y. (2001) Archaeal primase: bridging the gap between RNA and DNA polymerases, *11*, 452-456.
8. Le Breton, M., Henneke, G., Norais, C., Flament, D., Myllykallio, H., Querellou, J., and Raffin, J. P. (2007) The heterodimeric primase from the euryarchaeon Pyrococcus abyssi: a multifunctional enzyme for initiation and repair?, *374*, 1172-1185.
9. Xing, G., Kirouac, K., Shin, Y. J., Bell, S. D., and Ling, H. (2009) Structural insight into recruitment of translesion DNA polymerase Dpo4 to sliding clamp PCNA, *71*, 678-691.
10. Dionne, I. (2003) A heterotrimeric PCNA in the hyperthermophilic archaeon Sulfolobus solfataricus, *Molecular Cell 11*, 275-282.
11. Dionne, I. (2005) Characterization of an archaeal family 4 uracil DNA glycosylase and its interaction with PCNA and chromatin proteins, *Biochemical Journal 387*, 859-863.
12. Dore, A. S. (2006) Structure of an archaeal PCNA1-PCNA2-FEN1 complex: elucidating PCNA subunit and client enzyme specificity, *Nucleic Acids Research 34*, 4515-4526.
13. Pascal, J. M. (2006) A flexible interface between DNA ligase and PCNA supports conformational switching and efficient ligation of DNA, *Molecular Cell 24*, 279-291.
14. Roberts, J. A. (2003) An archaeal XPF repair endonuclease dependent on a heterotrimeric PCNA, *Molecular Microbiology 48*, 361-371.
15. Bowman, G. D. (2004) Structural analysis of a eukaryotic sliding DNA clamp-clamp loader complex, *Nature 429*, 724-730.
16. Stewart, J. (2001) Mechanism of beta clamp opening by the delta subunit of Escherichia coli DNA polymerase III holoenzyme, *Journal of Biological Chemistry 276*, 19182-19189.

17. Williams, G. J. (2006) Structure of the heterotrimeric PCNA from Sulfolobus solfataricus, *Acta Crystallographica Section F-Structural Biology and Crystallization Communications 62*, 944-948.
18. Imamura, K. (2007) Specific interactions of three proliferating cell nuclear antigens with replication-related proteins in Aeropyrum pernix, *Molecular Microbiology 64*, 308-318.
19. Dionne, I. (2008) On the mechanism of loading the PCNA sliding clamp by RFC, *Molecular Microbiology 68*, 216-222.
20. Indiani, C. (2006) The replication clamp-loading machine at work in the three domains of life, *Nature Reviews Molecular Cell Biology 7*, 751-761.
21. Ito, J., and Braithwaite, D. K. (1991) Compilation and alignment of DNA polymerase sequences, *Nucleic Acids Res 19*, 4045-4057.
22. Filee, J., Forterre, P., Sen-Lin, T., and Laurent, J. (2002) Evolution of DNA polymerase families: evidences for multiple gene exchange between cellular and viral proteins, *J Mol Evol 54*, 763-773.
23. Kozlov, A. G., and Lohman, T. M. (2000) Large contributions of coupled protonation equilibria to the observed enthalpy and heat capacity changes for ssDNA binding to Escherichia coli SSB protein, *Suppl 4*, 8-22.
24. Edgell, D. R., Klenk, H. P., and Doolittle, W. F. (1997) Gene duplications in evolution of archaeal family B DNA polymerases, *Journal of Bacteriology 179*, 2632-2640.
25. She, Q., Singh, R. K., Confalonieri, F., Zivanovic, Y., Allard, G., Awayez, M. J., Chan-Weiher, C. C. Y., Clausen, I. G., Curtis, B. A., De Moors, A., Erauso, G., Fletcher, C., Gordon, P. M. K., Heikamp-de Jong, I., Jeffries, A. C., Kozera, C. J., Medina, N., Peng, X., Thi-Ngoc, H. P., Redder, P., Schenk, M. E., Theriault, C., Tolstrup, N., Charlebois, R. L., Doolittle, W. F., Duguet, M., Gaasterland, T., Garrett, R. A., Ragan, M. A., Sensen, C. W., and Van der Oost, J. (2001) The complete genome of the crenarchaeon Sulfolobus solfataricus P2, *Proceedings of the National Academy of Sciences of the United States of America 98*, 7835-7840.
26. Joyce, C. M., and Steitz, T. A. (1994) Function and Structure Relationships in DNA-Polymerases, *Annual Review of Biochemistry 63*, 777-822.
27. Lou, H., Duan, Z., Huo, X., and Huang, L. (2004) Modulation of hyperthermophilic DNA polymerase activity by archaeal chromatin proteins, *J Biol Chem 279*, 127-132.
28. Lou, H., Duan, Z., Sun, T., and Huang, L. (2004) Cleavage of double-stranded DNA by the intrinsic 3'-5' exonuclease activity of DNA polymerase B1 from the hyperthermophilic archaeon Sulfolobus solfataricus at high temperature, *FEMS Microbiol Lett 231*, 111-117.
29. Pisani, F. M., De Felice, M., Manco, G., and Rossi, M. (1998) Domain organization and biochemical features of Sulfolobus solfataricus DNA polymerase, *Extremophiles 2*, 171-177.
30. Pisani, F. M., De Felice, M., and Rossi, M. (1998) Amino acid residues involved in determining the processivity of the 3'-5' exonuclease activity in a family B DNA polymerase from the thermoacidophilic archaeon Sulfolobus solfataricus, *Biochemistry 37*, 15005-15012.
31. Pisani, F. M., De Martino, C., and Rossi, M. (1992) A DNA polymerase from the archaeon Sulfolobus solfataricus shows sequence similarity to family B DNA polymerases, *Nucleic Acids Res 20*, 2711-2716.

32. Rella, R., Raia, C. A., Pisani, F. M., D'Auria, S., Nucci, R., Gambacorta, A., De Rosa, M., and Rossi, M. (1990) Purification and properties of a thermophilic and thermostable DNA polymerase from the archaebacterium Sulfolobus solfataricus, *Ital J Biochem 39*, 83-99.
33. Savino, C., Federici, L., Johnson, K. A., Vallone, B., Nastopoulos, V., Rossi, M., Pisani, F. M., and Tsernoglou, D. (2004) Insights into DNA replication: the crystal structure of DNA polymerase B1 from the archaeon *Sulfolobus solfataricus*, *Structure 12*, 2001-2008.
34. De Felice, M., Medagli, B., Esposito, L., De Falco, M., Pucci, B., Rossi, M., Gruz, P., Nohmi, T., and Pisani, F. M. (2007) Biochemical evidence of a physical interaction between *Sulfolobus solfataricus* B-family and Y-family DNA polymerases, *Extremophiles 11*, 277-282.
35. Alley, S. C. (2001) Building a replisome solution structure by elucidation of protein-protein interactions in the bacteriophage T4 DNA polymerise holoenzyme, *Journal of Biological Chemistry 276*, 39340-39349.
36. Trakselis, M. A. (2001) Creating a dynamic picture of the sliding clamp during T4 DNA polymerase holoenzyme assembly by using fluorescence resonance energy transfer, *Proceedings of the National Academy of Sciences of the United States of America 98*, 8368-8375.
37. Trakselis, M. A. (2003) Examination of the role of the clamp-loader and ATP hydrolysis in the formation of the bacteriophage T4 polymerase holoenzyme, *Journal of Molecular Biology 326*, 435-451.
38. Liu, C. C., Richard, A. J., Datta, K., and LiCata, V. J. (2008) Prevalence of temperature-dependent heat capacity changes in protein-DNA interactions, *94*, 3258-3265.
39. Prabhu, N. V., and Sharp, K. A. (2005) Heat capacity in proteins, *56*, 521-548.
40. Indiani, C., McInerney, P., Georgescu, R., Goodman, M. F., and O'Donnell, M. (2005) A sliding-clamp toolbelt binds high- and low-fidelity DNA polymerases simultaneously, *Mol Cell 19*, 805-815.
41. Moldovan, G. L., Pfander, B., and Jentsch, S. (2007) PCNA, the maestro of the replication fork, *Cell 129*, 665-679.
42. Savino, C., Federici, L., Johnson, K. A., Vallone, B., Nastopoulos, V., Rossi, M., Pisani, F. M., and Tsernoglou, D. (2004) Insights into DNA replication: the crystal structure of DNA polymerase B1 from the archaeon Sulfolobus solfataricus, *12*, 2001-2008.
43. Ling, H., Boudsocq, F., Woodgate, R., and Yang, W. (2001) Crystal structure of a Y-family DNA polymerase in action: a mechanism for error-prone and lesion-bypass replication, *107*, 91-102.
44. Ali, M. H., and Imperiali, B. (2005) Protein oligomerization: how and why, *13*, 5013-5020.
45. Koonin, E. V., Mushegian, A. R., Galperin, M. Y., and Walker, D. R. (1997) Comparison of archaeal and bacterial genomes: computer analysis of protein sequences predicts novel functions and suggests a chimeric origin for the archaea, *25*, 619-637.
46. Barry, E. R., and Bell, S. D. (2006) DNA replication in the archaea, *70*, 876-887.
47. Tahirov, T. H., Makarova, K. S., Rogozin, I. B., Pavlov, Y. I., and Koonin, E. V. (2009) Evolution of DNA polymerases: an inactivated polymerase-exonuclease module in Pol epsilon and a chimeric origin of eukaryotic polymerases from two classes of archaeal ancestors, *4*, 11.

48. Ishmael, F. T., Trakselis, M. A., and Benkovic, S. J. (2003) Protein-protein interactions in the bacteriophage T4 replisome. The leading strand holoenzyme is physically linked to the lagging strand holoenzyme and the primosome, *J. Biol. Chem. 278*, 3145-3152.
49. Yang, J., Zhuang, Z., Roccasecca, R. M., Trakselis, M. A., and Benkovic, S. J. (2004) The dynamic processivity of the T4 DNA polymerase during replication, *Proc. Natl. Acad. Sci. U. S. A. 101*, 8289-8294.
50. Kim, S., Dallmann, H. G., McHenry, C. S., and Marians, K. J. (1996) tau couples the leading- and lagging-strand polymerases at the Escherichia coli DNA replication fork, *271*, 21406-21412.
51. Purohit, V., Grindley, N. D., and Joyce, C. M. (2003) Use of 2-aminopurine fluorescence to examine conformational changes during nucleotide incorporation by DNA polymerase I (Klenow fragment), *Biochemistry 42*, 10200-10211.
52. Jezewska, M. J., Rajendran, S., and Bujalowski, W. (1998) Transition between different binding modes in rat DNA polymerase beta- ssDNA complexes, *J. Mol. Biol. 284*, 1113-1131.
53. Jezewska, M. J., Bujalowski, P. J., and Bujalowski, W. (2007) Interactions of the DNA polymerase X from African swine fever virus with gapped DNA substrates. Quantitative analysis of functional structures of the formed complexes, *Biochemistry 46*, 12909-12924.
54. Choi, J. Y., Eoff, R. L., Pence, M. G., Wang, J., Martin, M. V., Kim, E. J., Folkmann, L. M., and Guengerich, F. P. (2011) Roles of the four DNA polymerases of the crenarchaeon Sulfolobus solfataricus and accessory proteins in DNA replication, *286*, 31180-31193.
55. Steitz, T. A. (1999) DNA polymerases: structural diversity and common mechanisms, *274*, 17395-17398.
56. Kunkel, T. A. (2004) DNA replication fidelity, *279*, 16895-16898.
57. Prakash, S., Johnson, R. E., and Prakash, L. (2005) Eukaryotic translesion synthesis DNA polymerases: specificity of structure and function, *74*, 317-353.
58. Braithwaite, D. K., and Ito, J. (1993) Compilation, alignment, and phylogenetic relationships of DNA polymerases, *21*, 787-802.
59. Burgers, P. M., Koonin, E. V., Bruford, E., Blanco, L., Burtis, K. C., Christman, M. F., Copeland, W. C., Friedberg, E. C., Hanaoka, F., Hinkle, D. C., Lawrence, C. W., Nakanishi, M., Ohmori, H., Prakash, L., Prakash, S., Reynaud, C. A., Sugino, A., Todo, T., Wang, Z., Weill, J. C., and Woodgate, R. (2001) Eukaryotic DNA polymerases: proposal for a revised nomenclature, *276*, 43487-43490.
60. Rogozin, I. B., Makarova, K. S., Pavlov, Y. I., and Koonin, E. V. (2008) A highly conserved family of inactivated archaeal B family DNA polymerases, *3*, 32.
61. Pisani, F. M., De Felice, M., Manco, G., and Rossi, M. (1998) Domain organization and biochemical features of Sulfolobus solfataricus DNA polymerase, *2*, 171-177.
62. Pisani, F. M., De Felice, M., and Rossi, M. (1998) Amino acid residues involved in determining the processivity of the 3'-5' exonuclease activity in a family B DNA polymerase from the thermoacidophilic archaeon Sulfolobus solfataricus, *37*, 15005-15012.
63. Pisani, F. M., De Martino, C., and Rossi, M. (1992) A DNA polymerase from the archaeon Sulfolobus solfataricus shows sequence similarity to family B DNA polymerases, *20*, 2711-2716.

64. Rella, R., Raia, C. A., Pisani, F. M., D'Auria, S., Nucci, R., Gambacorta, A., De Rosa, M., and Rossi, M. (1990) Purification and properties of a thermophilic and thermostable DNA polymerase from the archaebacterium Sulfolobus solfataricus, *39*, 83-99.
65. Lou, H., Duan, Z., Sun, T., and Huang, L. (2004) Cleavage of double-stranded DNA by the intrinsic 3'-5' exonuclease activity of DNA polymerase B1 from the hyperthermophilic archaeon Sulfolobus solfataricus at high temperature, *231*, 111-117.
66. Lou, H., Duan, Z., Huo, X., and Huang, L. (2004) Modulation of hyperthermophilic DNA polymerase activity by archaeal chromatin proteins, *279*, 127-132.
67. Dionne, I., Brown, N. J., Woodgate, R., and Bell, S. D. (2008) On the mechanism of loading the PCNA sliding clamp by RFC, *68*, 216-222.
68. Dionne, I., Nookala, R. K., Jackson, S. P., Doherty, A. J., and Bell, S. D. (2003) A heterotrimeric PCNA in the hyperthermophilic archaeon Sulfolobus solfataricus, *11*, 275-282.
69. Von Hippel, P. H., Fairfield, F. R., and Dolejsi, M. K. (1994) On the processivity of polymerases, *726*, 118-131.
70. De Felice, M., Medagli, B., Esposito, L., De Falco, M., Pucci, B., Rossi, M., Gruz, P., Nohmi, T., and Pisani, F. M. (2007) Biochemical evidence of a physical interaction between Sulfolobus solfataricus B-family and Y-family DNA polymerases, *11*, 277-282.
71. Indiani, C., McInerney, P., Georgescu, R., Goodman, M. F., and O'Donnell, M. (2005) A sliding-clamp toolbelt binds high- and low-fidelity DNA polymerases simultaneously, *19*, 805-815.
72. Moldovan, G. L., Pfander, B., and Jentsch, S. (2007) PCNA, the maestro of the replication fork, *129*, 665-679.
73. Ishmael, F. T., Trakselis, M. A., and Benkovic, S. J. (2003) Protein-protein interactions in the bacteriophage T4 replisome. The leading strand holoenzyme is physically linked to the lagging strand holoenzyme and the primosome, *278*, 3145-3152.
74. Yang, J., Zhuang, Z., Roccasecca, R. M., Trakselis, M. A., and Benkovic, S. J. (2004) The dynamic processivity of the T4 DNA polymerase during replication, *101*, 8289-8294.
75. McInerney, P., Johnson, A., Katz, F., and O'Donnell, M. (2007) Characterization of a triple DNA polymerase replisome, *27*, 527-538.
76. Nick McElhinny, S. A., Gordenin, D. A., Stith, C. M., Burgers, P. M., and Kunkel, T. A. (2008) Division of labor at the eukaryotic replication fork, *30*, 137-144.
77. Kunkel, T. A., and Burgers, P. M. (2008) Dividing the workload at a eukaryotic replication fork, *18*, 521-527.
78. Li, Y., Kong, Y., Korolev, S., and Waksman, G. (1998) Crystal structures of the Klenow fragment of Thermus aquaticus DNA polymerase I complexed with deoxyribonucleoside triphosphates, *7*, 1116-1123.
79. Beese, L. S., Friedman, J. M., and Steitz, T. A. (1993) Crystal structures of the Klenow fragment of DNA polymerase I complexed with deoxynucleoside triphosphate and pyrophosphate, *32*, 14095-14101.
80. Beese, L. S., Derbyshire, V., and Steitz, T. A. (1993) Structure of DNA polymerase I Klenow fragment bound to duplex DNA, *260*, 352-355.
81. Bailey, M. F., Van der Schans, E. J., and Millar, D. P. (2007) Dimerization of the Klenow fragment of Escherichia coli DNA polymerase I is linked to its mode of DNA binding, *46*, 8085-8099.

82. Trakselis, M. A., Alley, S. C., Abel-Santos, E., and Benkovic, S. J. (2001) Creating a dynamic picture of the sliding clamp during T4 DNA polymerase holoenzyme assembly by using fluorescence resonance energy transfer, *98*, 8368-8375.
83. Gill, S. C., and von Hippel, P. H. (1989) Calculation of protein extinction coefficients from amino acid sequence data, *182*, 319-326.
84. Shuttleworth, G., Fogg, M. J., Kurpiewski, M. R., Jen-Jacobson, L., and Connolly, B. A. (2004) Recognition of the pro-mutagenic base uracil by family B DNA polymerases from archaea, *337*, 621-634.
85. Pierce, M. M., Raman, C. S., and Nall, B. T. (1999) Isothermal titration calorimetry of protein-protein interactions, *19*, 213-221.
86. Eom, S. H., Wang, J., and Steitz, T. A. (1996) Structure of Taq polymerase with DNA at the polymerase active site, *382*, 278-281.
87. Datta, K., and LiCata, V. J. (2003) Thermodynamics of the binding of Thermus aquaticus DNA polymerase to primed-template DNA, *31*, 5590-5597.
88. Trakselis, M. A., Alley, S. C., and Ishmael, F. T. (2005) Identification and mapping of protein-protein interactions by a combination of cross-linking, cleavage, and proteomics, *16*, 741-750.
89. Tabor, S., Huber, H. E., and Richardson, C. C. (1987) Escherichia coli thioredoxin confers processivity on the DNA polymerase activity of the gene 5 protein of bacteriophage T7, *262*, 16212-16223.
90. Jarvis, T. C., Newport, J. W., and von Hippel, P. H. (1991) Stimulation of the processivity of the DNA polymerase of bacteriophage T4 by the polymerase accessory proteins. The role of ATP hydrolysis, *266*, 1830-1840.
91. Merkens, L. S., Bryan, S. K., and Moses, R. E. (1995) Inactivation of the 5'-3' exonuclease of Thermus aquaticus DNA polymerase, *1264*, 243-248.
92. Greagg, M. A., Fogg, M. J., Panayotou, G., Evans, S. J., Connolly, B. A., and Pearl, L. H. (1999) A read-ahead function in archaeal DNA polymerases detects promutagenic template-strand uracil, *96*, 9045-9050.
93. Gruz, P., Shimizu, M., Pisani, F. M., De Felice, M., Kanke, Y., and Nohmi, T. (2003) Processing of DNA lesions by archaeal DNA polymerases from Sulfolobus solfataricus, *31*, 4024-4030.
94. Lone, S., Townson, S. A., Uljon, S. N., Johnson, R. E., Brahma, A., Nair, D. T., Prakash, S., Prakash, L., and Aggarwal, A. K. (2007) Human DNA polymerase kappa encircles DNA: implications for mismatch extension and lesion bypass, *25*, 601-614.
95. Naktinis, V., Turner, J., and O'Donnell, M. (1996) A molecular switch in a replication machine defined by an internal competition for protein rings, *84*, 137-145.
96. Zhang, L., Liu, Y., Yang, S., Gao, C., Gong, H., Feng, Y., and He, Z. G. (2009) Archaeal eukaryote-like Orc1/Cdc6 initiators physically interact with DNA polymerase B1 and regulate its functions, *106*, 7792-7797.
97. Trakselis, M. A., and Benkovic, S. J. (2001) Intricacies in ATP-dependent clamp loading: variations across replication systems, *9*, 999-1004.
98. Yang, J., Trakselis, M. A., Roccasecca, R. M., and Benkovic, S. J. (2003) The application of a minicircle substrate in the study of the coordinated T4 DNA replication, *278*, 49828-49838.

99. LaDuca, R. J., Fay, P. J., Chuang, C., McHenry, C. S., and Bambara, R. A. (1983) Site-specific pausing of deoxyribonucleic acid synthesis catalyzed by four forms of Escherichia coli DNA polymerase III, *22*, 5177-5188.
100. Donlin, M. J., Patel, S. S., and Johnson, K. A. (1991) Kinetic partitioning between the exonuclease and polymerase sites in DNA error correction, *30*, 538-546.
101. Jezewska, M. J., Rajendran, S., and Bujalowski, W. (2001) Energetics and specificity of Rat DNA polymerase beta interactions with template-primer and gapped DNA substrates, *276*, 16123-16136.
102. Zuo, Z., Lin, H. K., and Trakselis, M. A. (2011) Strand annealing and terminal transferase activities of a B-family DNA polymerase, *50*, 5379-5390.
103. Lodish, H., Berk, A., Zipursky, S. L., Matsudaira, P., Baltimore, D., and Darnell, J. (2000) *Molecular Cell Biology*, *4th edition*, New York: W. H. Freeman.
104. Choi, J. Y., Eoff, R. L., Pence, M. G., Wang, J., Martin, M. V., Kim, E. J., Folkmann, L. M., and Guengerich, F. P. (2011) Roles of the four DNA polymerases of the crenarchaeon *Sulfolobus solfataricus* and accessory proteins in DNA replication, *J. Biol. Chem. 286*, 31180-31193.
105. Burgers, P. M., Koonin, E. V., Bruford, E., Blanco, L., Burtis, K. C., Christman, M. F., Copeland, W. C., Friedberg, E. C., Hanaoka, F., Hinkle, D. C., Lawrence, C. W., Nakanishi, M., Ohmori, H., Prakash, L., Prakash, S., Reynaud, C. A., Sugino, A., Todo, T., Wang, Z., Weill, J. C., and Woodgate, R. (2001) Eukaryotic DNA polymerases: Proposal for a revised nomenclature, *J. Biol. Chem. 276*, 43487-43490.
106. Lange, S. S., Takata, K., and Wood, R. D. (2011) DNA polymerases and cancer, *Nat. Rev. Cancer 11*, 96-110.
107. Nishida, H., Mayanagi, K., Kiyonari, S., Sato, Y., Oyama, T., Ishino, Y., and Morikawa, K. (2009) Structural determinant for switching between the polymerase and exonuclease modes in the PCNA-replicative DNA polymerase complex, *Proc. Natl. Acad. Sci. U.S.A. 106*, 20693-20698.
108. Jezewska, M. J., Rajendran, S., and Bujalowski, W. (1998) Transition between different binding modes in rat DNA polymerase β-ssDNA complexes, *J. Mol. Biol. 284*, 1113-1131.
109. Tang, K. H., Niebuhr, M., Aulabaugh, A., and Tsai, M. D. (2008) Solution structures of 2:1 and 1:1 DNA polymerase-DNA complexes probed by ultracentrifugation and small-angle X-ray scattering, *Nucleic Acids Res. 36*, 849-860.
110. Tang, K. H., and Tsai, M. D. (2008) Structure and function of 2:1 DNA polymerase.DNA complexes, *J. Cell. Physiol. 216*, 315-320.
111. McInerney, P., Johnson, A., Katz, F., and O'Donnell, M. (2007) Characterization of a triple DNA polymerase replisome, *Mol. Cell 27*, 527-538.
112. Yang, J., Zhuang, Z., Roccasecca, R. M., Trakselis, M. A., and Benkovic, S. J. (2004) The dynamic processivity of the T4 DNA polymerase during replication, *Proc. Natl. Acad. Sci. U.S.A. 101*, 8289-8294.
113. Loparo, J. J., Kulczyk, A. W., Richardson, C. C., and van Oijen, A. M. (2011) Simultaneous single-molecule measurements of phage T7 replisome composition and function reveal the mechanism of polymerase exchange, *Proc. Natl. Acad. Sci. U.S.A. 108*, 3584-3589.

114. Koonin, E. V., Mushegian, A. R., Galperin, M. Y., and Walker, D. R. (1997) Comparison of archaeal and bacterial genomes: Computer analysis of protein sequences predicts novel functions and suggests a chimeric origin for the archaea, *Mol. Microbiol. 25*, 619-637.
115. Barry, E. R., and Bell, S. D. (2006) DNA replication in the archaea, *Microbiol. Mol. Biol. Rev. 70*, 876-887.
116. Tahirov, T. H., Makarova, K. S., Rogozin, I. B., Pavlov, Y. I., and Koonin, E. V. (2009) Evolution of DNA polymerases: An inactivated polymerase-exonuclease module in Pol ε and a chimeric origin of eukaryotic polymerases from two classes of archaeal ancestors, *Biol. Direct 4*, 11.
117. Boudsocq, F., Iwai, S., Hanaoka, F., and Woodgate, R. (2001) *Sulfolobus solfataricus* P2 DNA polymerase IV (Dpo4): an archaeal DinB-like DNA polymerase with lesion-bypass properties akin to eukaryotic poleta, *Nucleic Acids Res. 29*, 4607-4616.
118. Ling, H., Boudsocq, F., Woodgate, R., and Yang, W. (2001) Crystal structure of a Y-family DNA polymerase in action: a mechanism for error-prone and lesion-bypass replication, *Cell 107*, 91-102.
119. Kokoska, R. J., Bebenek, K., Boudsocq, F., Woodgate, R., and Kunkel, T. A. (2002) Low fidelity DNA synthesis by a Y-family DNA polymerase due to misalignment in the active site, *J. Biol. Chem. 277*, 19633-19638.
120. Mikheikin, A. L., Lin, H. K., Mehta, P., Jen-Jacobson, L., and Trakselis, M. A. (2009) A trimeric DNA polymerase complex increases the native replication processivity, *Nucleic Acids Res. 37*, 7194-7205.
121. Brown, J. A., and Suo, Z. (2009) Elucidating the kinetic mechanism of DNA polymerization catalyzed by *Sulfolobus solfataricus* P2 DNA polymerase B1, *Biochemistry 48*, 7502-7511.
122. Fiala, K. A., Hypes, C. D., and Suo, Z. (2007) Mechanism of abasic lesion bypass catalyzed by a Y-family DNA polymerase, *J. Biol. Chem. 282*, 8188-8198.
123. Fiala, K. A., and Suo, Z. (2004) Mechanism of DNA polymerization catalyzed by *Sulfolobus solfataricus* P2 DNA polymerase IV, *Biochemistry 43*, 2116-2125.
124. Fiala, K. A., and Suo, Z. (2004) Pre-steady-state kinetic studies of the fidelity of *Sulfolobus solfataricus* P2 DNA polymerase IV, *Biochemistry 43*, 2106-2115.
125. Zang, H., Irimia, A., Choi, J. Y., Angel, K. C., Loukachevitch, L. V., Egli, M., and Guengerich, F. P. (2006) Efficient and high fidelity incorporation of dCTP opposite 7,8-dihydro-8-oxodeoxyguanosine by *Sulfolobus solfataricus* DNA polymerase Dpo4, *J. Biol. Chem. 281*, 2358-2372.
126. Zang, H., Goodenough, A. K., Choi, J. Y., Irimia, A., Loukachevitch, L. V., Kozekov, I. D., Angel, K. C., Rizzo, C. J., Egli, M., and Guengerich, F. P. (2005) DNA adduct bypass polymerization by *Sulfolobus solfataricus* DNA polymerase Dpo4: analysis and crystal structures of multiple base pair substitution and frameshift products with the adduct 1,N2-ethenoguanine, *J. Biol. Chem. 280*, 29750-29764.
127. Sakofsky, C. J., Foster, P. L., and Grogan, D. W. (2012) Roles of the Y-family DNA polymerase Dbh in accurate replication of the *Sulfolobus* genome at high temperature, *DNA Repair (Amst) 11*, 391-400.
128. Jen-Jacobson, L., Engler, L. E., and Jacobson, L. A. (2000) Structural and thermodynamic strategies for site-specific DNA binding proteins, *Structure. 8*, 1015-1023.

129. Jen-Jacobson, L., Engler, L. E., Ames, J. T., Kurpiewski, M. R., and Grigorescu, A. (2000) Thermodynamic parameters of specific and nonspecific protein-DNA binding, *Supramol. Chem. 12*, 143-160.
130. Datta, K., and LiCata, V. J. (2003) Thermodynamics of the binding of *Thermus aquaticus* DNA polymerase to primed-template DNA, *Nucleic Acids Res. 31*, 5590-5597.
131. Datta, K., Wowor, A. J., Richard, A. J., and LiCata, V. J. (2006) Temperature dependence and thermodynamics of Klenow polymerase binding to primed-template DNA, *Biophys. J. 90*, 1739-1751.
132. Takeda, Y., Ross, P. D., and Mudd, C. P. (1992) Thermodynamics of Cro protein-DNA interactions, *Proc. Natl. Acad. Sci. U.S.A. 89*, 8180-8184.
133. Lundback, T., Hansson, H., Knapp, S., Ladenstein, R., and Hard, T. (1998) Thermodynamic characterization of non-sequence-specific DNA-binding by the Sso7d protein from *Sulfolobus solfataricus*, *J. Mol. Biol. 276*, 775-786.
134. Ladbury, J. E., Wright, J. G., Sturtevant, J. M., and Sigler, P. B. (1994) A thermodynamic study of the trp repressor-operator interaction, *J. Mol. Biol. 238*, 669-681.
135. Eom, S. H., Wang, J., and Steitz, T. A. (1996) Structure of *Taq* polymerase with DNA at the polymerase active site, *Nature 382*, 278-281.
136. Beese, L. S., Derbyshire, V., and Steitz, T. A. (1993) Structure of DNA polymerase I Klenow fragment bound to duplex DNA, *Science 260*, 352-355.
137. Studier, F. W. (2005) Protein production by auto-induction in high density shaking cultures, *Protein Expression Purif. 41*, 207-234.
138. Pierce, M. M., Raman, C. S., and Nall, B. T. (1999) Isothermal titration calorimetry of protein-protein interactions, *Methods 19*, 213-221.
139. Schuck, P. (2000) Size-distribution analysis of macromolecules by sedimentation velocity ultracentrifugation and lamm equation modeling, *Biophys. J. 78*, 1606-1619.
140. Laue, T. M., Saha, B. D., Ridgeway, T. M., and Pellettier, S. L. (1992) Computer-aided interpretation of analytical sedimentation data for proteins, In *Analytical Ultracentrifugation in Biochemistry and Polymer Science* (Harding, S. E., Ed.), pp 90-125, Royal Society of Chemistry, Cambridge, UK.
141. Schuck, P. (2003) On the analysis of protein self-association by sedimentation velocity analytical ultracentrifugation, *Anal. Biochem. 320*, 104-124.
142. Marras, S. A. (2006) Selection of fluorophore and quencher pairs for fluorescent nucleic acid hybridization probes, *Methods Mol. Biol. 335*, 3-16.
143. Wong, J. H., Fiala, K. A., Suo, Z., and Ling, H. (2008) Snapshots of a Y-family DNA polymerase in replication: Substrate-induced conformational transitions and implications for fidelity of Dpo4, *J. Mol. Biol. 379*, 317-330.
144. Sanner, M. F., Olson, A. J., and Spehner, J. C. (1996) Reduced surface: An efficient way to compute molecular surfaces, *Biopolymers 38*, 305-320.
145. Spolar, R. S., Livingstone, J. R., and Record, M. T. (1992) Use of liquid hydrocarbon and amide transfer data to estimate contributions to thermodynamic functions of protein folding from the removal of nonpolar and polar surface from water, *Biochemistry 31*, 3947-3955.
146. Zhang, H., Eoff, R. L., Kozekov, I. D., Rizzo, C. J., Egli, M., and Guengerich, F. P. (2009) Structure-function relationships in miscoding by *Sulfolobus solfataricus* DNA polymerase Dpo4: guanine N2,N2-dimethyl substitution produces inactive and miscoding polymerase complexes, *J. Biol. Chem. 284*, 17687-17699.

147. Kingsbury, J. S., and Laue, T. M. (2011) Fluorescence-detected sedimentation in dilute and highly concentrated solutions, *Methods Enzymol. 492*, 283-304.
148. Ha, J. H., Spolar, R. S., and Record, M. T., Jr. (1989) Role of the hydrophobic effect in stability of site-specific protein-DNA complexes, *J. Mol. Biol. 209*, 801-816.
149. Spolar, R. S., and Record, M. T., Jr. (1994) Coupling of local folding to site-specific binding of proteins to DNA, *Science 263*, 777-784.
150. Lazaridis, T., and Karplus, M. (1999) Heat capacity and compactness of denatured proteins, *Biophys. Chem. 78*, 207-217.
151. Petri, V., Hsieh, M., and Brenowitz, M. (1995) Thermodynamic and kinetic characterization of the binding of the TATA binding protein to the adenovirus E4 promoter, *Biochemistry 34*, 9977-9984.
152. Berger, C., Jelesarov, I., and Bosshard, H. R. (1996) Coupled folding and site-specific binding of the GCN4-bZIP transcription factor to the AP-1 and ATF/CREB DNA sites studied by microcalorimetry, *Biochemistry 35*, 14984-14991.
153. Lundback, T., Cairns, C., Gustafsson, J. A., Carlstedt-Duke, J., and Hard, T. (1993) Thermodynamics of the glucocorticoid receptor-DNA interaction: binding of wild-type GR DBD to different response elements, *Biochemistry 32*, 5074-5082.
154. Morton, C. J., and Ladbury, J. E. (1996) Water-mediated protein-DNA interactions: The relationship of thermodynamics to structural detail, *Protein Science 5*, 2115-2118.
155. Jen-Jacobson, L., and Jacobson, L. A. (2008) Chapter 2 Role of Water and Effects of Small Ions in Site-specific Protein-DNA Interactions, In *Protein-Nucleic Acid Interactions: Structural Biology*, pp 13-46, The Royal Society of Chemistry.
156. Fairfield, F. R., Newport, J. W., Dolejsi, M. K., and von Hippel, P. H. (1983) On the processivity of DNA replication, *J. Biomol. Struct. Dyn. 1*, 715-727.
157. Eoff, R. L., Sanchez-Ponce, R., and Guengerich, F. P. (2009) Conformational changes during nucleotide selection by Sulfolobus solfataricus DNA polymerase Dpo4, *J. Biol. Chem. 284*, 21090-21099.
158. Fiala, K. A., Sherrer, S. M., Brown, J. A., and Suo, Z. (2008) Mechanistic consequences of temperature on DNA polymerization catalyzed by a Y-family DNA polymerase, *Nucleic Acids Res 36*, 1990-2001.
159. Fiala, K. A., and Suo, Z. (2007) Sloppy bypass of an abasic lesion catalyzed by a Y-family DNA polymerase, *J. Biol. Chem. 282*, 8199-8206.
160. Vaisman, A., Ling, H., Woodgate, R., and Yang, W. (2005) Fidelity of Dpo4: Effect of metal ions, nucleotide selection and pyrophosphorolysis, *EMBO J. 24*, 2957-2967.
161. Ling, H., Boudsocq, F., Woodgate, R., and Yang, W. (2004) Snapshots of replication through an abasic lesion; structural basis for base substitutions and frameshifts, *Mol. Cell 13*, 751-762.
162. Sherrer, S. M., Brown, J. A., Pack, L. R., Jasti, V. P., Fowler, J. D., Basu, A. K., and Suo, Z. (2009) Mechanistic studies of the bypass of a bulky single-base lesion catalyzed by a Y-family DNA polymerase, *J. Biol. Chem. 284*, 6379-6388.
163. Fiala, K. A., Brown, J. A., Ling, H., Kshetry, A. K., Zhang, J., Taylor, J. S., Yang, W., and Suo, Z. (2007) Mechanism of template-independent nucleotide incorporation catalyzed by a template-dependent DNA polymerase, *J. Mol. Biol. 365*, 590-602.
164. Eoff, R. L., Stafford, J. B., Szekely, J., Rizzo, C. J., Egli, M., Guengerich, F. P., and Marnett, L. J. (2009) Structural and functional analysis of Sulfolobus solfataricus Y-

family DNA polymerase Dpo4-catalyzed bypass of the malondialdehyde-deoxyguanosine adduct, *Biochemistry 48*, 7079-7088.
165. Irimia, A., Eoff, R. L., Pallan, P. S., Guengerich, F. P., and Egli, M. (2007) Structure and activity of Y-class DNA polymerase Dpo4 from *Sulfolobus solfataricus* with templates containing the hydrophobic thymine analog 2,4-difluorotoluene, *J. Biol. Chem. 282*, 36421-36433.
166. Silvian, L. F., Toth, E. A., Pham, P., Goodman, M. F., and Ellenberger, T. (2001) Crystal structure of a DinB family error-prone DNA polymerase from *Sulfolobus solfataricus*, *Nat. Struct. Biol. 8*, 984-989.
167. Wilson, R. C., and Pata, J. D. (2008) Structural insights into the generation of single-base deletions by the Y family DNA polymerase dbh, *Mol. Cell 29*, 767-779.
168. Pata, J. D. (2010) Structural diversity of the Y-family DNA polymerases, *Biochim. Biophys. Acta 1804*, 1124-1135.
169. Gruz, P., Shimizu, M., Pisani, F. M., De, F. M., Kanke, Y., and Nohmi, T. (2003) Processing of DNA lesions by archaeal DNA polymerases from *Sulfolobus solfataricus*, *Nucleic Acids Res. 31*, 4024-4030.
170. Xu, C., Maxwell, B. A., Brown, J. A., Zhang, L., and Suo, Z. (2009) Global conformational dynamics of a Y-family DNA polymerase during catalysis, *PLoS Biol. 7*, e1000225.
171. Boudsocq, F., Kokoska, R. J., Plosky, B. S., Vaisman, A., Ling, H., Kunkel, T. A., Yang, W., and Woodgate, R. (2004) Investigating the role of the little finger domain of Y-family DNA polymerases in low fidelity synthesis and translesion replication, *J. Biol. Chem. 279*, 32932-32940.
172. Zuo, Z., Lin, H. K., and Trakselis, M. A. (2011) Strand annealing and terminal transferase activities of a B-family DNA polymerase, *Biochemistry 50*, 5379-5390.
173. Sturtevant, J. M. (1977) Heat capacity and entropy changes in processes involving proteins, *Proc. Natl. Acad. Sci. U. S. A. 74*, 2236-2240.
174. Eftink, M. R., Anusiem, A. C., and Biltonen, R. L. (1983) Enthalpy-entropy compensation and heat capacity changes for protein-ligand interactions: general thermodynamic models and data for the binding of nucleotides to ribonuclease A, *Biochemistry 22*, 3884-3896.
175. Peters, W. B., Edmondson, S. P., and Shriver, J. W. (2005) Effect of mutation of the Sac7d intercalating residues on the temperature dependence of DNA distortion and binding thermodynamics, *Biochemistry 44*, 4794-4804.
176. Kozlov, A. G., and Lohman, T. M. (2011) *E. coli* SSB tetramer binds the first and second molecules of (dT)(35) with heat capacities of opposite sign, *Biophys. Chem. 159*, 48-57.
177. Kozlov, A. G., and Lohman, T. M. (2006) Effects of monovalent anions on a temperature-dependent heat capacity change for *Escherichia coli* SSB tetramer binding to single-stranded DNA, *Biochemistry 45*, 5190-5205.
178. Kozlov, A. G., and Lohman, T. M. (2000) Large contributions of coupled protonation equilibria to the observed enthalpy and heat capacity changes for ssDNA binding to *Escherichia coli* SSB protein, *Proteins Suppl 4*, 8-22.
179. Holbrook, J. A., Tsodikov, O. V., Saecker, R. M., and Record, M. T., Jr. (2001) Specific and non-specific interactions of integration host factor with DNA: Thermodynamic evidence for disruption of multiple IHF surface salt-bridges coupled to DNA binding, *J. Mol. Biol. 310*, 379-401.

180. Bergqvist, S., Williams, M. A., O'Brien, R., and Ladbury, J. E. (2004) Heat capacity effects of water molecules and ions at a protein-DNA interface, *J. Mol. Biol. 336*, 829-842.
181. Yang, Y., and LiCata, V. J. (2011) Interactions of replication versus repair DNA substrates with the Pol I DNA polymerases from *Escherichia coli* and *Thermus aquaticus*, *Biophys. Chem. 159*, 188-193.
182. Datta, K., Johnson, N. P., LiCata, V. J., and von Hippel, P. H. (2009) Local conformations and competitive binding affinities of single- and double-stranded primer-template DNA at the polymerization and editing active sites of DNA polymerases, *J. Biol. Chem. 284*, 17180-17193.
183. Filfil, R., and Chalikian, T. V. (2003) The thermodynamics of protein-protein recognition as characterized by a combination of volumetric and calorimetric techniques: The binding of turkey ovomucoid third domain to alpha-chymotrypsin, *J. Mol. Biol. 326*, 1271-1288.
184. Baker, B. M., and Murphy, K. P. (1997) Dissecting the energetics of a protein-protein interaction: The binding of ovomucoid third domain to elastase, *J. Mol. Biol. 268*, 557-569.
185. Armstrong, K. M., Insaidoo, F. K., and Baker, B. M. (2008) Thermodynamics of T-cell receptor-peptide/MHC interactions: Progress and opportunities, *J. Mol. Recognit. 21*, 275-287.
186. Frisch, C., Schreiber, G., Johnson, C. M., and Fersht, A. R. (1997) Thermodynamics of the interaction of barnase and barstar: Changes in free energy versus changes in enthalpy on mutation, *J. Mol. Biol. 267*, 696-706.
187. Sun, D., Lopez-Guajardo, C. C., Quada, J., Hurley, L. H., and Von Hoff, D. D. (1999) Regulation of Catalytic Activity and Processivity of Human Telomerase, *Biochemistry 38*, 4037-4044.
188. Trakselis, M. A., and Benkovic, S. J. (2001) Intricacies in ATP-dependent clamp loading: variations across replication systems, *Structure 9*, 999-1004.
189. Kamtekar, S., Berman, A. J., Wang, J., Lazaro, J. M., de, V. M., Blanco, L., Salas, M., and Steitz, T. A. (2006) The phi29 DNA polymerase: Protein-primer structure suggests a model for the initiation to elongation transition, *EMBO J. 25*, 1335-1343.
190. Blanco, L., Bernad, A., Lazaro, J. M., Martin, G., Garmendia, C., and Salas, M. (1989) Highly efficient DNA synthesis by the phage phi 29 DNA polymerase. Symmetrical mode of DNA replication, *J. Biol. Chem. 264*, 8935-8940.
191. Beckman, J. W., Wang, Q., and Guengerich, F. P. (2008) Kinetic analysis of correct nucleotide insertion by a Y-family DNA polymerase reveals conformational changes both prior to and following phosphodiester bond formation as detected by tryptophan fluorescence, *J. Biol. Chem. 283*, 36711-36723.
192. Dionne, I., Nookala, R. K., Jackson, S. P., Doherty, A. J., and Bell, S. D. (2003) A heterotrimeric PCNA in the hyperthermophilic archaeon *Sulfolobus solfataricus*, *Mol. Cell 11*, 275-282.
193. Dionne, I., Brown, N. J., Woodgate, R., and Bell, S. D. (2008) On the mechanism of loading the PCNA sliding clamp by RFC, *Mol. Microbiol. 68*, 216-222.
194. Gotz, D., Paytubi, S., Munro, S., Lundgren, M., Bernander, R., and White, M. F. (2007) Responses of hyperthermophilic crenarchaea to UV irradiation, *Genome Biol. 8*, R220.

195. Frols, S., Gordon, P. M., Panlilio, M. A., Duggin, I. G., Bell, S. D., Sensen, C. W., and Schleper, C. (2007) Response of the hyperthermophilic archaeon *Sulfolobus solfataricus* to UV damage, *J. Bacteriol. 189*, 8708-8718.
196. Lovett, S. T. (2007) Polymerase switching in DNA replication, *Mol. Cell 27*, 523-526.
197. Prakash, S., Johnson, R. E., and Prakash, L. (2005) Eukaryotic translesion synthesis DNA polymerases: Specificity of structure and function, *Annu. Rev. Biochem. 74*, 317-353.
198. Zhuang, Z., Johnson, R. E., Haracska, L., Prakash, L., Prakash, S., and Benkovic, S. J. (2008) Regulation of polymerase exchange between Poleta and Poldelta by monoubiquitination of PCNA and the movement of DNA polymerase holoenzyme, *Proc. Natl. Acad. Sci.U.S.A. 105*, 5361-5366.
199. Moldovan, G. L., Pfander, B., and Jentsch, S. (2007) PCNA, the maestro of the replication fork, *Cell 129*, 665-679.
200. Hoege, C., Pfander, B., Moldovan, G. L., Pyrowolakis, G., and Jentsch, S. (2002) RAD6-dependent DNA repair is linked to modification of PCNA by ubiquitin and SUMO, *Nature 419*, 135-141.
201. Stelter, P., and Ulrich, H. D. (2003) Control of spontaneous and damage-induced mutagenesis by SUMO and ubiquitin conjugation, *Nature 425*, 188-191.
202. Heltzel, J. M., Maul, R. W., Scouten Ponticelli, S. K., and Sutton, M. D. (2009) A model for DNA polymerase switching involving a single cleft and the rim of the sliding clamp, *Proc. Natl. Acad. Sci. U.S.A. 106*, 12664-12669.
203. Milev, S., Gorfe, A. A., Karshikoff, A., Clubb, R. T., Bosshard, H. R., and Jelesarov, I. (2003) Energetics of sequence-specific protein-DNA association: Binding of integrase Tn916 to its target DNA, *Biochemistry 42*, 3481-3491.
204. Jen-Jacobson, L., and Jacobson, L. A. (2008) Role of Water and Effects of Small Ions in Site-specific Protein-DNA Interactions, In *Protein-Nucleic Acid Interactions: Structural Biology*, pp 13-46, The Royal Society of Chemistry, Cambridge, U.K.
205. Sapienza, P. J., Rosenberg, J. M., and Jen-Jacobson, L. (2007) Structural and thermodynamic basis for enhanced DNA binding by a promiscuous mutant *EcoRI* endonuclease, *Structure 15*, 1368-1382.
206. Engler, L. E., Sapienza, P., Dorner, L. F., Kucera, R., Schildkraut, I., and Jen-Jacobson, L. (2001) The energetics of the interaction of BamHI endonuclease with its recognition site GGATCC, *J. Mol. Biol. 307*, 619-636.
207. Datta, K., and LiCata, V. J. (2003) Salt dependence of DNA binding by *Thermus aquaticus* and *Escherichia coli* DNA polymerases, *J.Biol.Chem. 278*, 5694-5701.
208. Lin, H. K., Chase, S. F., Laue, T. M., Jen-Jacobson, L., and Trakselis, M. A. (2012) Differential temperature-dependent multimeric assemblies of replication and repair polymerases on DNA increase processivity, *Biochemistry 51*, 7367-7382.
209. Adamson, N. J., and Reynolds, E. C. (1997) Rules relating electrophoretic mobility, charge and molecular size of peptides and proteins, *J Chromatogr B Biomed Sci Appl 699*, 133-147.
210. Brummitt, R. K., Nesta, D. P., Chang, L., Chase, S. F., Laue, T. M., and Roberts, C. J. (2011) Nonnative aggregation of an IgG1 antibody in acidic conditions: part 1. Unfolding, colloidal interactions, and formation of high-molecular-weight aggregates, *J. Pharm. Sci. 100*, 2087-2103.
211. Chase, S. F., and Laue, T. M. (2008) The determiniation of protein valence by capillary electrophoresis, *Beckman Coulter P/ACE Setter 12*, 1-5.

212. Marky, L. A., and Breslauer, K. J. (1987) Calculating thermodynamic data for transitions of any molecularity from equilibrium melting curves, *Biopolymers 26*, 1601-1620.
213. Fukada, H., and Takahashi, K. (1998) Enthalpy and heat capacity changes for the proton dissociation of various buffer components in 0.1 M potassium chloride, *Proteins-Structure Function and Genetics 33*, 159-166.
214. Baker, B. M., and Murphy, K. P. (1996) Evaluation of linked protonation effects in protein binding reactions using isothermal titration calorimetry, *Biophys. J. 71*, 2049-2055.
215. Kozlov, A. G., and Lohman, T. M. (2000) Large contributions of coupled protonation equilibria to the observed enthalpy and heat capacity changes for ssDNA binding to *Escherichia coli* SSB protein, *Proteins 4*, 8-22.
216. Moody, T. P., Kingsbury, J. S., Durant, J. A., Wilson, T. J., Chase, S. F., and Laue, T. M. (2005) Valence and anion binding of bovine ribonuclease A between pH 6 and 8, *Anal. Biochem. 336*, 243-252.
217. Dill, K. A., and Bromberg, S. (2003) *Molecular Driving Forces*, Garland Science, New York.
218. Liu, C. C., Richard, A. J., Datta, K., and LiCata, V. J. (2008) Prevalence of temperature-dependent heat capacity changes in protein-DNA interactions, *Biophys. J. 94*, 3258-3265.
219. Gallagher, K., and Sharp, K. (1998) Electrostatic contributions to heat capacity changes of DNA-ligand binding, *Biophys. J. 75*, 769-776.
220. Prabhu, N. V., and Sharp, K. A. (2005) Heat capacity in proteins, *Annu. Rev. Phys. Chem. 56*, 521-548.
221. Holbrook, J. A., Capp, M. W., Saecker, R. M., and Record, M. T., Jr. (1999) Enthalpy and heat capacity changes for formation of an oligomeric DNA duplex: interpretation in terms of coupled processes of formation and association of single-stranded helices, *Biochemistry 38*, 8409-8422.
222. Shuttleworth, G., Fogg, M. J., Kurpiewski, M. R., Jen-Jacobson, L., and Connolly, B. A. (2004) Recognition of the pro-mutagenic base uracil by family B DNA polymerases from archaea, *J. Mol. Biol. 337*, 621-634.
223. Turner, R. M., Jr., Grindley, N. D., and Joyce, C. M. (2003) Interaction of DNA polymerase I (Klenow fragment) with the single-stranded template beyond the site of synthesis, *Biochemistry 42*, 2373-2385.
224. Delagoutte, E., and von Hippel, P. H. (2003) Function and assembly of the bacteriophage T4 DNA replication complex: interactions of the T4 polymerase with various model DNA constructs, *J. Biol. Chem. 278*, 25435-25447.
225. Kozlov, A. G., and Lohman, T. M. (2011) *E. coli* SSB tetramer binds the first and second molecules of $(dT)_{35}$ with heat capacities of opposite sign, *Biophys. Chem. 159*, 48-57.
226. Peters, W. B., Edmondson, S. P., and Shriver, J. W. (2004) Thermodynamics of DNA binding and distortion by the hyperthermophile chromatin protein *Sac*7d, *J Mol Biol 343*, 339-360.
227. Heltzel, J. M., Scouten Ponticelli, S. K., Sanders, L. H., Duzen, J. M., Cody, V., Pace, J., Snell, E. H., and Sutton, M. D. (2009) Sliding clamp-DNA interactions are required for viability and contribute to DNA polymerase management in *Escherichia coli*, *J. Mol. Biol. 387*, 74-91.
228. Dionne, I., Brown, N. J., Woodgate, R., and Bell, S. D. (2008) On the mechanism of loading the PCNA sliding clamp by RFC, *Mol. Microbiol. 68*, 216-222.

229. Ma, B., and Nussinov, R. (2013) Structured crowding and its effects on enzyme catalysis, *337*, 123-137.